MOLECULAR MECHANISMS OF LAMINAR CIRCUIT FORMATION IN VISUAL CORTEX

by

JOHANNA ELIZABETH TOMORSKY

A DISSERTATION

Presented to the Department of Biology
and the Graduate School of the University of Oregon
in partial fulfillment of the requirements
for the degree of
Doctor of Philosophy

December 2018

DISSERTATION APPROVAL PAGE

Student: Johanna Elizabeth Tomorsky

Title: Molecular Mechanisms of Laminar Circuit Formation in Visual Cortex

This dissertation has been accepted and approved in partial fulfillment of the requirements for the Doctor of Philosophy degree in the Department of Biology by:

John Postlethwait	Chairperson
Cris Niell	Advisor
Chris Doe	Advisor
Kryn Stankunas	Core Member
Mike Wehr	Institutional Representative

and

Janet Woodruff-Borden	Vice Provost and Dean of the Graduate School

Original approval signatures are on file with the University of Oregon Graduate School.

Degree awarded December 2018

DISSERTATION ABSTRACT

Johanna Elizabeth Tomorsky

Doctor of Philosophy

Department of Biology

December 2018

Title: Molecular Mechanisms of Laminar Circuit Formation in Visual Cortex

The mammalian visual system develops to perform many complex tasks that allow us to perceive the natural world. These tasks rely on a dense network of synaptic connections transporting visual information both to and within visual cortex (V1). The laminar organization and functional properties of visual cortical neurons are largely conserved across mammals, and the mouse has been adopted as a model organism to study the development of this cortical circuit. Neurons in each cortical layer must find the correct synaptic partners for the optimal receipt, transfer, and processing of information. The molecular cues guiding the development of these connections, however, are largely unknown.

In this thesis, I identify and then examine the role of molecular factors important for synapse formation in layer 2/3 (L2/3) of visual cortex. L2/3 neurons are highly interconnected and fire selectively to a refined set of visual stimuli. The developmental refinement of these visual preferences has been shown to occur in the week following eye opening, corresponding with a period of intense synapse formation and dynamic gene expression in mouse V1. In Chapters II–IV, I use the TU-tagging technique to identify molecular factors enriched L2/3 neurons before and after eye opening and identify several candidate genes with potential functions in synapse formation.

In Chapter V, I examine the function of cell adhesion molecules nectin-1 and nectin-3, identified here as enriched in L2/3 visual cortex at eye opening, and previously shown to interact across synaptic junctions. I focus mainly on the effect of nectin-3 (having post-synaptic localization in hippocampus) on post-synaptic dendritic spine densities in developing L2/3 cortical neurons. I show that nectin-3 knockdown further increases spine densities after eye opening, while overexpressing a full length or truncated nectin-3 protein reduces spine densities. I conclude that nectin-3 may have a role in synapse formation following eye opening, and propose a mechanism describing the effects observed. Here, I describe a unique approach for understanding how cell-type specific connections are formed in visual cortex, beginning with the spatiotemporal examination gene expression and followed by the spatiotemporal manipulation of a single gene.

This dissertation includes previously published co-authored material.

CURRICULUM VITAE

NAME OF AUTHOR: Johanna Elizabeth Tomorsky

GRADUATE AND UNDERGRADUATE SCHOOLS ATTENDED:

University of Oregon, Eugene
University of Wisconsin-Milwaukee
University of Utah, Salt Lake City

DEGREES AWARDED:

Doctor of Philosophy, 2018, University of Oregon
Certificate of Major in Biology and Minor in Chemistry, 2009, University of Wisconsin-Milwaukee
Bachelor of Fine Arts, Ballet Performance, 2006, University of Utah

AREAS OF SPECIAL INTEREST:

Neurobiology
Development

PROFESSIONAL EXPERIENCE:

Behavior Technician, Medical College of Wisconsin, Neuroscience Research Center, 11/2011–06/2012

Butterfly Technician, Milwaukee County Zoo, 07/2011–09/2011

Research Assistant, University of Auckland, 05/2010–11/2010

Undergraduate Research Assistant, University of Wisconsin-Milwaukee, 01/2008–09/2009

GRANTS, AWARDS, AND HONORS:

College of Arts and Sciences Dissertation Research Fellowship, Molecular mechanisms of laminar circuit formation in visual cortex, University of Oregon, 2017–2018

Development of Biology Training Grant, National Institute of Health, Identification of the genetic factors underlying the functional development of visual cortex, University of Oregon, 2013–2016

Office of Undergraduate Research Stipend for Undergraduate Research Fellows, Effect of prolactin on the parenting behavior of ring-necked doves, University of Wisconsin-Milwaukee, 2009

Best Oral Presentation (Biological Sciences Research Symposium), Taxonomic classification of a bioluminescent bacterium through environmental cultivation and sequencing of the lux operon, University of Wisconsin-Milwaukee, 2009

Center of International Education and Office of Undergraduate Research Grant, Effects of topography on liana distribution and size in tropical rain forests, University of Wisconsin-Milwaukee, 2009

Center for Latin American and Caribbean Studies Graduate Student / Advanced Undergraduate Travel Award, Effects of topography on liana distribution and size in tropical rain forests, University of Wisconsin-Milwaukee, 2009

Graduation with Honors Magna Cum Laude, University of Utah, 2006

PUBLICATIONS:

J. Tomorsky, L. DeBlander, C.G. Kentros, C.Q. Doe, and C.M. Niell. TU-Tagging: A Method for Identifying Layer-Enriched Neuronal Genes in Developing Mouse Visual Cortex. *eNeuro*, 2017.

ACKNOWLEDGMENTS

I would like to thank Chris Doe and Cris Niell for taking me on as a joint graduate student and guiding me through my PhD. I was extremely fortunate to be a part of not one, but two extraordinary labs during my time at UO, and have learned and grown immensely as a result of my unique experience as a co-advised graduate student. I am so happy to have had two academic families at UO, and am grateful to large number of lab members who provided ideas and support throughout my PhD.

In the Niell lab, I would like to thank Phil Parker for being a great source or support, helping with all the electroporations and offering advice on projects and career options. Denise Niell and Jen Hoy, for offering support and advice on all things mouse molecular and developmental. Judit Pungor, for always being kind, compassionate, and helpful. Mandi Severson, for helping with various aspects of the nectin project, including imaging a large number of neurons and dendrites. And finally, Angie Michaiel, Hannah Bishop, Joe Wekselblatt and other members of the Niell lab both past and present, you have all played unique roles in my PhD experience, and I have thoroughly enjoyed being a part of this group.

In the Doe lab, I want to give a special thanks to Leslie Gay for teaching me the TU-tagging technique. Also, to my close friend, Kate Walsh, thank you for supporting me through all the ups and downs of a PhD. I am also grateful to other members of the Doe lab, both past and present, including but not limited to: Emily Sales, Luis Sullivan, Brandon Mark, Austin Seroka, Emily Heckman, Keiko Hirono, Sen-Lin Lai, Janet Hanawalt, Laurina Manning, and Syed, Mübarak Hüssain. You have all provided support,

ideas and guidance, and I am so happy to have been an adopted as the mouse researcher in this *Drosophila* development lab.

I would also like to thank Peter Batzel who helped advise in the bioinformatic processing of sequence data, and Dr. Clay Small for statistical advice on the TU-tagging project.

I am also grateful to my Dissertation Advisory Committee members: Mike Wehr, John Postlethwait, and Kryn Stankunas for guiding my scientific development.

I also need to thank my parents, Betty and Dennis Tomorsky, for always supporting and loving me. And my sister, Jessica Marrero and niece, Lana Marrero, for always being a joy to come home to.

Finally, I have to thank my partner, Kyle Meyer, for offering constant love and support as I worked my way through this PhD. I am always amazed by your drive and adventurous spirit, and am excited to continue to grow with you in our next chapter together.

This study was supported in part by an Institutional Developmental Training Grant through the department of Biology, NIH T32-HD007348, and by a University of Oregon CAS Dissertation Research Fellowship.

TABLE OF CONTENTS

LIST OF FIGURES

LIST OF TABLES

CHAPTER I

INTRODUCTION

Brain development requires the coordinated maturation of a variety of cell types with different morphological and physiological characteristics, organized and connected in specific ways to produce specialized functional regions (Miterko, Lackey, Heck, & Sillitoe, 2018). Neocortex is thought to be the brain structure that gives humans their unique cognitive function, since human cortex is larger and more complex than that of other mammals (Azzarelli, Kerloch, & Pacary, 2014; Mitchell & Silver, 2018). However, many functional and morphological cortical features are conserved across mammalian species, and much can be learned about cortical development using small mammalian model organisms (Balaram & Kaas, 2014; Kaas, 2011; Niell & Stryker, 2008). As with other brain regions, strictly regulated genetic programs guide the differentiation, migration, and connectivity of various neuronal and non-neuronal cell types during cortical development, the disturbance of which can lead to cortical deficits (Manzini & Walsh, 2011). The formation of synapses, distinct structures of cell contact and neurotransmission between neurons, is crucial for cortical development and is regulated by activity dependent and independent molecular signaling pathways (Lu, Wang, & Nose, 2009). Developing neurons must first identify the correct synaptic partners, then modify the strength of individual synapses depending on functional requirements, all while maintaining activity levels within a working range (Desai, Cudmore, Nelson, & Turrigiano, 2002; Lu et al., 2009; Lyckman et al., 2008; Tien & Kerschensteiner, 2018).

All of these processes require the highly regulated expression of a complex system of genes and the proteins they encode over development (Hackett et al., 2015).

Primary visual cortex (V1) receives and processes visual information originating from retinal ganglion cells in the eye and relayed through the lateral geniculate nucleus (LGN) of the thalamus (Erskine & Herrera, 2014). Recently, mouse has been adopted as a model organism to study the circuit mechanisms underlying cortical function, since many of the visual response properties in mouse V1 appear to be conserved across mammalian species (Balaram & Kaas, 2014; Niell, 2015). One such conserved property of mammalian V1 is the laminar organization of the cortical circuit (Van Hooser, 2007). V1 and other primary cortical sensory areas are organized into distinct layers, with neurons in each layer having unique functional and morphological characteristics (Hirsch & Martinez, 2006; Niell, 2015). Information flow in cortex stereotypically begins in layer 4, which receives input directly from thalamus (Hirsch & Martinez, 2006). Once received by layer 4, sensory information loops though cortex traveling first to layer 2/3, then to layer 5, and finally to layer 6, which projects back to thalamus (Hirsch & Martinez, 2006). Neurons in different layers of visual cortex receive, transfer, and process information differently, having distinct functional response properties that arise over development (Hoy & Niell, 2015; Niell & Stryker, 2008). The molecular mechanisms guiding the connectivity of neurons in different cortical layers are only beginning to be elucidated, and the mouse is an ideal system to dissect these mechanisms due to the large number of tools available to manipulate genetic programs (Nguyen & Xu, 2008). In this thesis, I use gene profiling to determine candidate genes and *in vivo* genetic manipulation

to test the role two cell adhesion molecules, nectin-1 and nectin-3, in layer-specific synapse formation in mouse visual cortex.

Stages of cortical neuron development

The laminar organization and distinct functional properties of visual cortical neurons develop in a series of stages, beginning with the migration of cortical neurons to their appropriate lamina. Excitatory cortical neurons are born at the surface of lateral ventricles in the germinal ventricular zone and migrate radially in an 'inside out' succession, with later born superficial neurons migrating past early born deep layer neurons to reach their final destination (Nadarajah, Alifragis, Wong, & Parnavelas, 2003). Deep and superficial layer neurons are thought to use distinct mechanisms for migration since the distances they need to travel are very different (Gil-Sanz et al., 2013; Hirota & Nakajima, 2017; Nadarajah et al., 2003). Superficial layer neurons depend on a glial scaffold to guide their migration through accumulated deep layer neurons, while deep layer neurons simply extend their leading process to the surface and migrate towards it in process called 'somal translocation' (Gil-Sanz et al., 2013; Hirota & Nakajima, 2017; Nadarajah et al., 2003). Disruption of either migratory pathway over development leads to distorted laminar patterning in V1 and aberrant cortical processing (Gil-Sanz et al., 2013; Hirota & Nakajima, 2017).

Most migration is complete by the time an animal is born with process extension occurring shortly thereafter (Yokota, Ring, Cheung, Pevny, & Anton, 2007). The extension of axons and dendrites is critical for finding the correct synaptic partners to form the laminar cortical circuit. At post-natal day 2 (P2), layer 2/3 neurons have already

developed axonal and dendritic projections (Yokota et al., 2007). Between P7 and P10, the number of branches off the main descending axon increases dramatically, and branches continue to increase in length and complexity between P10 and P21 (Larsen & Callaway, 2006). Axonal branching and termination largely determines where a given neuron sends information, and is distinct between neurons found in different cortical layers. Cytoskeletal regulation has been shown to be an important component of both migration and process extension during neuronal development, and a variety of molecular components, including many cell adhesion molecules, have been shown to contribute to these processes (Gärtner, Fornasiero, & Dotti, 2015; Gil-Sanz et al., 2013; Hirota & Nakajima, 2017; Kamiguchi, 2007; Kawauchi, 2011; Yokota et al., 2007).

Synaptogenesis is the next step in neuronal development, often occurring simultaneously with axon and dendrite extension (Niell, Meyer, & Smith, 2004). Synapses are the points of contact between pre-synaptic sites on axons (boutons), which are the points of neurotransmitter release, and post-synaptic sites on dendrites (often at dendritic 'spines'), which are the points of neurotransmitter receipt and current influx (Lin & Koleske, 2010; Tønnesen & Nägerl, 2016). The activation of post-synaptic signaling mechanisms at dendritic spines was found to stabilize dendritic arbors, which are constantly adding and removing branches during development (Lin & Koleske, 2010; Niell et al., 2004). Dendritic spines first develop as thin, motile filopodia that project from the dendritic shaft, containing scaffolding proteins and adhesion molecules necessary for spine maturation (Honda et al., 2006a; Mizoguchi et al., 2002; Niell et al., 2004; Ziv & Smith, 1996). Maturation is initiated by contact with axonal boutons and further facilitated through neuronal activity and signaling through the immature synapse

(Cruz-Martín, Crespo, & Portera-Cailliau, 2010; Harris, 1999; Lin & Koleske, 2010; Ziv & Smith, 1996; Zuo, Lin, Chang, & Gan, 2005). There is high turnover (formation and elimination) of spines early in development, and circuit maturation depends on the activity guided strengthening of some synapses and elimination of others (Chen, Lu, & Zuo, 2014; Cruz-Martín et al., 2010; Ziv & Smith, 1996). F-actin is highly enriched in dendritic spines, and the regulation of actin polymerization and depolymerization controls both the restructuring spines over development and the stabilization of mature spines (Chen et al., 2014; Cruz-Martín et al., 2010; Honkura, Matsuzaki, Noguchi, Ellis-Davies, & Kasai, 2008; Lin & Koleske, 2010). The ability of spines to remodel allows synapses to alter their strengths based on experience, i.e. synaptic plasticity, and is a critical component of the normal development of visual cortical circuits (Lin & Koleske, 2010). In this thesis, I identify genes expressed in V1 layer 2/3 neurons at eye opening, a time of intense synaptogenesis. I then examine the role of two nectin molecules, shown to interact with the actin cytoskeleton, in layer 2/3 neuronal synapse formation after eye opening.

Sensory input as an important regulator of synapse formation and maturation

As neurons develop, spine formation and elimination are regulated by mechanisms that are both dependent and independent of sensory experience (Hackett et al., 2015). It has previously been shown that early visual experience is necessary for the normal development of visual cortex, instructing the maturation and stabilization of spines (Lyckman et al., 2008; Mower, Berry, Burchfiel, & Duffy, 1981). In the week after eye opening, from P14 to P21, dendritic spine densities increase dramatically,

followed by 'pruning' or an overall reduction in spine densities from P21 to P35 (Vidal, Djurisic, Brown, Sapp, & Shatz, 2016). The period between P21 and P35 is often referred to as the critical period for ocular dominance plasticity (ODP), and is a period of dynamic experience dependent synaptic remodeling in V1 (Espinosa & Stryker, 2012a). There is an overall decrease in spine motility between P21 and P28, which is dependent on normal visual experience from the time of eye opening (Chen et al., 2014; Majewska & Sur, 2003). This decrease in motility correlates with increased spine pruning, which has also been shown to occur with synapse maturation over the critical period (Majewska & Sur, 2003; Vidal et al., 2016). This indicates that visual experience is required for the stabilization of some spines and elimination of others during the development of visual cortex, and this maturation can be stalled by decreased activity (Majewska & Sur, 2003).

A large body of research has uncovered several molecular mechanisms driving both the start and close of ODP, some of which appear dependent on normal visual experience from the time of eye opening (Benoit, Ayoub, & Rakic, 2015; Hooks & Chen, 2007; Majdan & Shatz, 2006). Gene pathways upregulated during the critical period for ODP were previously classified as having roles in actin cytoskeletal regulation, G-protein signaling, transcription, and myelination (Lyckman et al., 2008). Many genes highly expressed during the critical period were found to reduce their expression with monocular deprivation, which increases plasticity and synapse formation in non-deprived cortex (referred to as ocular dominance plasticity, ODP) (Lyckman et al., 2008). This suggests that the mechanisms driving synaptic stabilization during the critical period are reversed with ODP, facilitating enhanced synaptic motility, plasticity, and growth typical of the period just following eye opening (Lyckman et al., 2008). While a number of studies

suggest an interaction between experience and gene expression drives circuit maturation in V1 (Majdan & Shatz, 2006; Prasad et al., 2002; Tropea et al., 2006), there is still much to be learned about how genetic programs balance synaptogenesis, synaptic motility, and synaptic strength to develop distinct cell types with unique functional properties (Majdan & Shatz, 2006). In this thesis, I find that the cell adhesion molecule, nectin-3, regulates synapse formation after eye opening and may be important for the activity guided refinement of cortical circuits.

Cell adhesion molecules as important mediators of synapse formation

Cell adhesion molecules (CAMs) have been implicated as mediators of synapse formation and stabilization, since they interact with cytoskeletal components and are regulated by activity (Arikkath & Reichardt, 2008; Kitt & Nelson, 2011a; Tai, Mysore, Chiu, & Schuman, 2007). There are four major families of cell adhesion molecules: cadherins, immunoglobulin superfamily members, integrins, and the neurexins and neuroligins (Shapiro, Love, & Colman, 2007). Here, I briefly discuss cadherins and immunoglobulin superfamily members, which have been shown to interact during synaptic maturation and stabilization (Arikkath & Reichardt, 2008; Hertel & Redies, 2011; Mizutani & Takai, 2016; Rikitake, Mandai, & Takai, 2012; Shapiro et al., 2007; Takai & Nakanishi, 2003). There are many different cadherin domain proteins expressed in the brain, several of which are located at synapses and/or have distinct expression patterns in different cortical layers and cell types (Arikkath & Reichardt, 2008; Hertel & Redies, 2011; Tai et al., 2007). N-cadherin is a neuronal cadherin found at dendritic spines that interacts with actin though the binding of a beta-catenin (Tai et al., 2007).

Synaptic activity through NMDA receptors has been shown to drive b-catenin from the dendrite to localize and stabilize N-cadherin at dendritic spines (Tai et al., 2007). LTD was eliminated at spines where N-cadherin was stabilized for long periods, indicating cadherin binding may be an important regulator of synaptic plasticity (Tai et al., 2007).

Immunoglobulin superfamily (Ig-SF) CAMs are also linked to a variety of cytoskeletal components and have been found to both regulate and be regulated by cytoskeletal components (Leshchyns'ka & Sytnyk, 2016). The nectins are a family of Ig-SF CAMS that are also found at synapses and have been shown to interact with actin through the linker protein afadin (Rikitake et al., 2012; Satoh-Horikawa et al., 2000; Takai & Nakanishi, 2003). Nectins and cadherins interact to form puncta adherentia junctions, axon–dendrite junctions involved in synaptic stabilization that are distinct from synaptic junctions, which are the sites of synaptic neurotransmission (Mizoguchi et al., 2002; Satoh-Horikawa et al., 2000; Tachibana et al., 2000; Takai & Nakanishi, 2003). Nectin proteins bind *in trans* with other nectin family members and have been shown to facilitate long-term memory formation in hippocampus (Lachke et al., 2012; Rikitake et al., 2012; Takai & Nakanishi, 2003; Wang et al., 2013; Wang et al., 2017). Nectins have also been shown to regulate the signaling activity of small G-proteins, which facilitate synapse formation and stabilization through the activity dependent modulation of actin cytoskeletal components (Duman, Mulherkar, Tu, Cheng, & Tolias, 2015; Kawauchi, 2011; Kitt & Nelson, 2011a; Ogita & Takai, 2006; Tai et al., 2007). In Chapter V, I examine two nectin family members, nectin-1 and nectin-3, which have been shown to be important for hippocampal synapse formation and have enriched expression in layer 2/3 of visual cortex (Mizoguchi et al., 2002).

Layer 2/3 neurons: selective, plastic, and interconnected

Neurons found in layer 2/3 are thought to have important roles in cognitive function since they form connections with many different cortical regions (Petersen & Crochet, 2013). Layer 2/3 neurons form corticocortical connections with layer 2/3 and layer 5 neurons both in the same hemisphere and contralaterally, through the corpus callosum (Kwan, Sestan, & Anton, 2012; Narayanan, Udvary, & Oberlaender, 2017). The interconnectedness of layer 2/3 neurons combined with their unique functional properties, including sparse firing rates and high stimulus selectivity, have implicated these neurons as important for associative learning (Petersen & Crochet, 2013). Layer 2/3 neurons in motor cortex show a high degree of spine formation and elimination with task training and development (Ma et al., 2016). In addition, layer 2/3 and layer 5 corticocortical synapses in visual and somatosensory cortex display greater plasticity than thalamocortical (layer 4) synapses in slice, changing their response properties more rapidly after brief monocular deprivation (Bear & Rittenhouse, 1999; Feldman, Nicoll, & Malenka, 1999; Majewska & Sur, 2003; Trachtenberg, Trepel, & Stryker, 2000). While layer 2/3 neurons have been shown to have unique connectivity and functional properties, the molecular mechanisms guiding the development of these properties are just beginning to be understood.

Identifying molecular mechanisms important for the development of layer 2/3 cortical neurons

Understanding the unique patterns of gene expression governing the development of specific neuronal cell types can illuminate molecular mechanisms guiding the

formation of unique functional properties (Benoit et al., 2015; Wang, Gerstein, & Snyder, 2009). The quantity and identity of the RNA transcripts produced by a cell (gene expression) at a specific developmental stage or physiological condition is considered the cell's 'transcriptome' (Wang et al., 2009). Transcriptomic studies of different cell or tissue types has helped to illuminate many molecular components significant for development or disease (Wang et al., 2009). Recently, high-throughput RNA sequencing (RNA-seq) has been adopted as the primary technology for transcriptomic studies (Wang et al., 2009). While there have been many previous studies of gene expression during the development of visual cortex, few have isolated different cell types or cortical layers (Hackett et al., 2015; Liset, Sommeijer, Levelt, & Heimel, 2012; Lyckman et al., 2008; Prasad et al., 2002; Tropea et al., 2006).

Recent studies of gene expression in different cortical layers in mouse have used a dissection technique to isolate different layers for RNA-seq (Belgard et al., 2011; Benoit et al., 2015; Fertuzinhos et al., 2014). Single-cell RNA-seq, which requires the dissociation and isolation of cells from complex tissues, has also become a popular method for isolating cell-type specific transcriptomes (Poulin, Tasic, Hjerling-Leffler, Trimarchi, & Awatramani, 2016; Shapiro, Biezuner, & Linnarsson, 2013). While both of these methods are powerful for assessing cell-type and layer specific gene expression, cell dissociation can damage neuronal processes and dissection is unable to resolve gene expression between neuronal and non-neuronal types co-populating specific layers (Tallafuss, Washbourne, & Postlethwait, 2014). Recently, a number of techniques have been developed for isolating cell-type specific RNAs that involve tagging/labeling newly transcribed RNAs or ribosomes in specific cell types *in vivo*. This allows the isolation of

cell-type specific RNAs from whole tissue homogenates through antibody or biotin-streptavidin based purification. These techniques, including TRAP, Ribo-tag, TU-tagging, and more recently EC-tagging, ensure that RNAs from distinct genetically labeled cell types are isolated and preserve RNAs found in fine cellular processes (Doyle et al., 2008; Heiman et al., 2008; Hida et al., 2017; Sanz et al., 2009; Tallafuss et al., 2014; Tomorsky, DeBlander, Kentros, Doe, & Niell, 2017).

In Chapter II, I identify genes expressed in upper layer cortical neurons around eye opening using the TU-tagging technique. This work is published in the journal eNeuro and is co-authored with L. DeBlander, C. Kentros, C. Doe, and C. Niell. I was the first to use the TU-tagging technique with a transgenic mouse system to examine cell type-specific gene expression in neurons, and I explore the use of this technique to identify upper layer neuronal gene expression in both Chapters II and III. In Chapter IV, I identify genes with enriched expression in layer 2/3 neurons at P16, as well as genes with regulated expression levels between P12 and P16. In Chapter V, I examine the developmental function of a pair of cell adhesion molecules, nectin-1 and nectin-3, identified in Chapter II as being layer 2/3 enriched around eye opening. We find the dendritic spine densities of developing layer 2/3 neurons are affected by nectin expression level, and discuss the role of these molecules in balancing dendritic spine stability and motility after eye opening.

BRIDGE TO CHAPTER II

TU-tagging is an intersectional method for covalently labeling newly transcribed RNAs within specific cell types. Cell type specificity is generated through

targeted transgenic expression of the enzyme uracil phosphoribosyl transferase (UPRT); temporal specificity is generated through a pulse of the modified uracil analog 4-thiouracil (4TU). This technique has been applied in mouse using a Cre-dependent UPRT transgene, *CA>GFPstop>HA-UPRT,* to profile RNAs in endothelial cells, but it remained untested whether 4TU can cross the blood brain barrier (BBB) or whether this transgene can be used to purify neuronal RNAs. Here we crossed the *CA>GFPstop>HA-UPRT* transgenic mouse to a *Sepw1-cre* line to express UPRT in layer 2/3 of visual cortex or to an *Nr5a1-cre* line to express UPRT in layer 4 of visual cortex. We purified thiol-tagged mRNA from both genotypes at postnatal day 12, as well as from WT mice not expressing UPRT (background control). We found that a comparison of Sepw1-purified RNA to WT or Nr5a1-purified RNA allowed us to identify genes enriched in layer 2/3 of visual cortex. Here we show that Cre-dependent UPRT expression can be used to purify cell type specific mRNA from the intact mouse brain and provide the first evidence that 4TU can cross the blood brain barrier to label RNA in vivo.

CHAPTER II

TU-TAGGING: A METHOD FOR IDENTIFYING LAYER-ENRICHED NEURONAL GENES IN DEVELOPING MOUSE VISUAL CORTEX

JOURNAL STYLE INFORMATION

Johanna Tomorsky, Leah DeBlander, Clifford G. Kentros, Chris Q. Doe, and Cristopher M. Niell. Reproduced in part from *eNeuro*, 2017. Copyright 2017.

AUTHOR CONTRIBUTIONS

Chris Q. Doe, and Cristopher M. Niell provided mentorship for all aspects of the study and edited the manuscript. Clifford G. Kentros was a mentor for the development of the TetO-UPRT mouse. Leah DeBlander mentored and assisted with the development of the TetO-UPRT mouse. Johanna Tomorsky performed all experiments and wrote and prepared the manuscript.

INTRODUCTION

Quantifying patterns of gene expression during development or following exposure to different conditions, such as drug administration, can provide an understanding of genome function as it relates to underlying biological processes (Cahoy et al., 2008; Gay et al., 2013; Vandesompele et al., 2002; Wang et al., 2009). Unfortunately, many gene profiling techniques are limited by restricted access to specific cell types contained in complex tissues. The brain, which is the most complex mammalian organ containing cells with long-projecting delicate processes, presents a

unique challenge when attempting to isolate cell type specific transcripts. Though several techniques have been developed to characterize gene expression profiles in distinct cell types (Doyle et al., 2008; Poulin et al., 2016; Sanz et al., 2009; Shapiro et al., 2013; Tallafuss et al., 2014), most require either cell-dissociation or tissue sectioning, which can damage neuronal projections (Poulin et al., 2016; Shapiro et al., 2013; Tallafuss et al., 2014).

Translating Ribosome Affinity Purification (TRAP), RiboTag, and TU-tagging are transcriptional profiling techniques that do not require cell isolation. TRAP and RiboTag can be used to identify cell type specific translation of RNA by immunoprecipitating, from whole tissue homogenates, mRNAs attached to 80s ribosomes either HA-epitope tagged (RiboTag) or fluorescent reporter-tagged (TRAP) in distinct cell types (Doyle et al., 2008; Sanz et al., 2009). The TU-tagging technique, on the other hand, utilizes cell type specific expression of the enzyme UPRT to identify genes actively transcribed in those cell types (Gay, Karfilis, Miller, Doe, & Stankunas, 2014; Gay et al., 2013). UPRT works to convert injected 4-thiouracil (4TU) to 4-thiouridine, which is incorporated into newly transcribed RNA. Thiol-tagged RNA can later be purified from whole tissue homogenates and subjected to high-throughput Illumina sequencing (Gay et al., 2014, 2013). Unlike RiboTag and TRAP, TU-tagging can be used to identify RNAs that may not be actively translated or ribosome associated, and can therefore provide a broader picture of cell type specific gene expression. Here we applied the TU-tagging technique in mouse brain to identify genes expressed in upper layer neurons of the developing visual cortex.

Mouse visual cortex is organized in layers with distinct functional properties and unique timelines for the development of these properties (Hoy & Niell, 2015). Neurons in each layer of the cortical circuit need to find the correct synaptic partners during development for proper processing of visual information. Eye opening, which occurs between post-natal days 12 and 14 (P12-P14) represents a peak of synapse formation in the visual cortex, and is known to be a time of dynamic gene expression, which could be generating specific patterns of connectivity (Yoshii et al., 2011). Transcriptional profiling studies of layer specific gene expression in visual cortex often focus on adult or embryonic and newborn developmental time points, leaving the developmental stage around eye opening largely neglected (Belgard et al., 2011; Molyneaux et al., 2015; Poulin et al., 2016). Here, we used a modified TU-tagging protocol similar to that used in Chatzi et al., 2016 (Chatzi, Zhang, Shen, Westbrook, & Goodman, 2016) to profile neuronal RNA from visual cortex layer 2/3 at P12, a time point just before eye opening.

The TU-tagging technique was previously applied in mouse using a published UPRT transgene (Gay et al., 2013) to profile murine endothelial RNAs, and recently using viral injection to express UPRT in newly generated dentate granule neurons (Chatzi et al., 2016; Gay et al., 2013). Here we are the first to successfully apply TU-tagging in mouse neurons using a transgenic mouse, making the method more accessible to those wishing to isolate cell type specific mRNA from the mammalian brain. Through this study, we identified genes with expression enriched in visual cortex layer 2/3 at P12, while also providing evidence that 4TU can cross the blood brain barrier.

MATERIALS AND METHODS

All experimental protocols were approved by the University of Oregon Institutional Animal Care and Use Committees, in compliance with the National Institutes of Health guidelines for the care and use of experimental animals.

Layer-specific expression of UPRT and tissue dissection

Homozygous *CA>GFPstop>HA-UPRT* mice (Gay et al., 2013) were crossed with *Sepw1-cre* or *Nr5a1-cre* transgenic lines to achieve cortical layer-specific expression of the UPRT enzyme. Wild type (WT) mice were processed identically to Cre positive mice to produce the WT-pure sample type. The visual cortexes from four mice were required per sample to produce enough starting material for biotin-streptavidin purification of tagged RNA. Therefore, only litters with at least four Cre positive pups were used (each sample is a mix of genders). All samples were collected at postnatal day 12. 50 mg of 4-thiouracil (Sigma-Aldrich) was dissolved in 250 uL of DMSO for injection. Mice were injected with 4-thiouracil (430 mg/kg in DMSO) in the morning, and visual cortexes were collected 5-6 hours later. Dissection of visual cortex was performed in RNAlater (Thermo Fisher Scientific). Both left and right visual cortexes were stereotaxically marked with DiD fluorescent dye (2.5 mm from the midline and 1 mm from the back suture), and a ~1 mm^2 section of cortex was cut around the mark. Visual cortex samples were frozen in RNAlater (per manufacturer's instructions) at -80 ºC until RNA extraction and purification.

Immunohistochemistry

Immunohistochemistry was performed on double transgenic mice at P12 to confirm HA-UPRT expression in cortical layer-specific cell types (Figure 1). Mice were perfused and brains were extracted at P12 and fixed overnight at room temperature in 4% PFA (in 1 x PBS). Brains were then transferred to a 30% sucrose solution (in 1 x PBS) and either kept overnight at room-temperature or for 48 h at 4 ºC. Brains were then cryosectioned onto Superfrost Plus slides (Fisherbrand), and frozen at -80 ºC for long term storage. To stain, slides were removed from the freezer and treated for 5 min with 300 uL 0.05% trypsin (Thermo Fisher Scientific)[11]. Slides were then washed twice for 10 min with PBS and then once for 10 min with PBT (0.3% Triton X in PBS). A blocking solution of 5% goat and 5% donkey serum in PBT was then applied to the slides and allowed to incubate at room temperature for 1-3 h. Slides were then drained and a solution of 2 uL/mL of HA-mouse (Covance Research Products Inc. Cat# MMS-101P, RRID:AB_2314672) and 3uL/mL Anti-GFP chicken (Aves Labs Cat# GFP-1020 RRID:AB_10000240) primary antibodies in block was applied. Slides were stored with primary antibody at 4 ºC overnight. The next day, slides were washed 4 times for 10 min each in PBT. 4 uL/mL of secondary antibodies, mouse-555 (Thermo Fisher Scientific Cat# A-21424 RRID:AB_2535845) and chick-488 (Jackson ImmunoResearch Labs Cat# 703-545-155 RRID:AB_2340375), in PBT was then applied to the slides and either kept overnight at 4 ºC or for 3 h at room temperature. Slides were then subjected to four more 10 min washes, two in PBT and two in PBS. 2uL/mL of DAPI (4′, 6-diamidino-2-phenylindole) in PBS was then applied to slides for 5 min, after which slides were dried and mounted with VECTASHIELD mounting media (Vector Labs).

RNA processing and preparation for sequencing

To obtain thiol-tagged RNA from layer 2/3 neurons in visual cortex, we used a modified TU-tagging protocol similar to that published in Chatzi et al. 2016 (Chatzi et al., 2016). RNA was extracted by grinding tissue from mouse visual cortex into 1 mL of TRIzol (Thermo Fisher Scientific). Ground tissue in TRIzol stood at room temperature for 5 min before the addition of 200 uL of chloroform. The chloroform-TRIzol mix was vortexed for 15 s and allowed to separate for 2-3 min at room temperature before centrifuging at 4 ºC at 12,000 RPM for 15 min. The upper aqueous layer was kept, an equal volume of 70% ethanol was added, and the RNA was then purified on columns as per manufacturer's protocol (PureLink RNA Minikit, Ambion). The quality of all RNA samples was analyzed on an Agilent Bioanalyzer (2100), and only samples with RNA integrity numbers (RINs) greater than 8.0 were subsequently streptavidin purified. RNA was then biotinylated (10 uL 10X TE and 25 uL 1mg/mL EZ-link Biotin-HPDP in dimethylformamide) and streptavidin purified (uMACS Streptavidin Kit) as previously described (Gay et al., 2014).

RNA concentrations were determined via qubit fluorometric quantitation or using the Agilent Bioanalyzer (2100) before cDNA preparation. To preserve RNA quality and quantity, a previously described fragmentation step was removed from this modified workflow (Gay et al., 2014, 2013), and poly-A priming was used for cDNA synthesis (SMARTer Ultra Low Input RNA Kit for Sequencing–v3) instead of random priming after Ribo-Zero rRNA removal (Figure 1D) (Chatzi et al., 2016). 5-10 ng of RNA was used for cDNA preparation with the SMARTer kit. Library preparation was performed on

1 ng of cDNA using Illumina's Nextera XT Library Preparation kit. Samples were then pooled in groups of six and subjected to 100 bp single-end sequencing on an Illumina HiSeq instrument (Figure 1D).

Sequence Processing and Differential Expression Analysis

All sequences were first filtered to remove reads that did not pass Illumina's chastity filter. FastQC reports were then produced to identify overrepresented sequences and other quality concerns (Andrews, 2014). Overrepresented sequences (SMARTer adapter and Nextera primers) were then removed using the CutAdapt python package (Martin, 2011). The java program Trimmomatic was used to trim sequences based on quality (Bolger, Lohse, & Usadel, 2014). Quality-trimmed sequences were then aligned to the mouse genome assembly GRCm38 (downloaded off the Ensembl browser) using the Genomic Short-read Nucleotide Alignment Program (GSNAP) (Cunningham et al., 2014; Wu & Nacu, 2010). Finally, sequences that aligned to a particular gene were counted using the python program htseq-count in intersection-strict mode (Simon Anders, Pyl, & Huber, 2014). The final gene counts were further filtered to isolate protein coding genes (identified using Ensembl-BioMart) (Cunningham et al., 2014) for future analysis (raw gene counts are available in Supplementary Dataset 1). The DESeq package (version 1.24.0) (S Anders & Huber, 2012; Simon Anders et al., 2010) was used to analyze differential expression between sample types defined as streptavidin purified RNA from 1) a *Sepw1-cre; CA>GFPstop>HA-UPRT* cross (Sepw1-pure), 2) an *Nr5a1-cre; CA>GFPstop>HA-UPRT* cross (Nr5a1-pure), or 3) WT mice not expressing UPRT (WT-pure). Pairwise comparisons were performed between Sepw1-pure and Nr5a1-pure

sample types, and Sepw1-pure and WT-pure sample types, and a DESeq adjusted p-value (Benjamini-Hochberg adjusted for multiple testing) of 0.1 was used as a cutoff to determine enrichment (Simon Anders et al., 2010). Transcripts with few reads (3 or more samples containing fewer than 1 count per million) were removed before DESeq analysis.

The functional categories representing Sepw1-enriched genes was examined through gene ontology (GO) analysis using GO-TermFinder (Boyle et al., 2004) (go.princeton.edu) with a p-value cutoff of 0.01 and MGI (M. musculus) annotation. GO-enriched categories were then input to REVIGO (http://revigo.irb.hr/) (Supek, Bošnjak, Škunca, & Šmuc, 2011), an online tool used to summarize GO results by reducing redundant GO-terms and finding broader representative categories for collections of genes (Figure 4). The layer specificity of Sepw1-enriched genes was investigated by comparing DESeq gene enrichments to layer enriched genes (400 genes with the highest probability of enrichment in each cortical layer) from the online database described in Belgard et al. (2011), and examining Allen Brain Atlas developing mouse brain *in situ* data at P14 (Allen Developing Mouse Brain Atlas (2008)) (Sepw1-Nr5a1 comparison). Expression patterns observed in Allan Brain *in situ* data were classified manually as either 'enriched' (reasonable observer would identify expression as darkest in layer 2/3 visual cortex), 'present' (clear expression in layer 2/3 visual cortex, but not darkest here), or 'depleted' (expression is not seen or very light in 2/3, and is dark in other areas). *In situ* experiments that were unclear, were excluded from the analysis. In addition, in house *in situ* hybridizations were performed for seven Sepw1-enriched genes (Nr5a1-pure comparison) at P12.

In situ hybridization

Nonradioactive colorimetric RNA *in situ* to quantify gene expression patterns was performed as previously described (Lein et al., 2007; Wehr et al., 2009). Briefly, tissue was prepared and sectioned as described for immunohistochemistry, after which 30 µm sections were brought to room temperature, washed 3 times 30 min each in 1 x PBS, and then acetylated for 10 min in a 0.25% acetic anhydride solution in 0.1 M triethanolamine HCl (Lein et al., 2007). Slides were then covered with hybridization solution (50% formamide, 10% dextran sulfate, 1 x Denhardt's solution, 1 mg/mL yeast tRNA, 5 x SSC, 0.1% Tween-20, and 0.1 mg/mL heparin in DEPC-treated H_2O), fitted with a coverslip, and pre-hybridized for 2 h in a humidity chamber at 62 °C (WPRE probe) or 70 °C (all other probes). To visualize transgene expression in the newly developed *TetO-UPRT* mouse (see below), a digoxygenin-labeled riboprobe was used, targeting 302 bp of the wood chuck picornavirus response element (WPRE), diluted 1:500 in hybridization solution. This riboprobe was generated using T3 RNA polymerase in the presence of dig-labeled nucleotides using the pBSKS-WPRE construct linearized with Nco1 as template. The riboprobes to *Gad*, *Sez6l2*, *Speg*, *Frmpd4*, *Tspan6*, *Pvrl3*, *Rgs8*, and *Pvrl1,* were diluted to a final concentration of 1-2 ng/uL in hybridization solution and were generated using the SP6 RNA polymerase in the presence of dig-labeled nucleotides, using probe sequences and protocols described by the Allen Brain Institute (Allen Mouse Brain Atlas (2004); Allen Developing Mouse Brain Atlas (2008); Lein et al., 2007).

Slides were hybridized with each probe in hybridization solution overnight at the same temperature used for pre-hybridization. Sections were then washed 3 times for

30 min each at 62 °C (WPRE probe and GAD probe for FISH) or 70 °C (all other probes) in wash buffer (50% formamide, 0.5 x SSC, 0.1% Tween-20). Slides were then washed an additional 3 times for 30 min each at room temperature in MABT (1 x maleic acid, 20% Tween 20) and then incubated in blocking solution (MABT, 20% sheep serum, 2% blocking reagent Roche No. 11096176001) for 3 h. Anti-dig sheep Fab fragments conjugated to alkaline phosphatase (Roche No. 11093274910) diluted 1:2500 in blocking solution were then added, and the slices were incubated at 4 °C overnight. Slices were then washed at RT with MABT buffer 5 times for 5 min each and then AP staining buffer (0.1 M NaCl, 50 mM MgCl2, 10% polyvinyl alcohol 100,000–150,000 MW, 0.1 M Tris-HCl, pH 9.5), twice for 10 min each, after which 3.5 uL/mL NBT, 2.6 uL/mL BCIP, and 80 uL/mL levamisole were added. The colorimetric reaction was allowed to develop for 3–48 h at 37 °C, and stopped by washing twice with PBS (0.1% Tween-20) and twice with deionized H_2O. Slides were then either dehydrated in graded ethanols and mounted with Permount, or double labeled via immunohistochemistry as described above.

Microscopy

RNA *in situ* hybridizations to WPRE were viewed on an Olympus BX61 wide field epifluorescence microscope with Prior ProScanIII motorized stage and Lumen 200 mercury lamp. Images were acquired using an Olympus DP72 12.8 megapixel camera and a 10x objective (UPlanApo 0.4 numerical aperture). Whole-slice composites were generated automatically using MetaMorph premiere software.

All other *in situ* and immunohistochemistry experiments were viewed on a Zeiss Axio Imager.A2 wide field epifluorescence microscope with an X-Cite 120Q LED

excitation lamp. Images were acquired with a Zeiss AxioCam MRm 1.4 megapixel camera and EC Plan-NEOFLUAR 5x/0.16 or EC Plan-NEOFLUAR 40x/0.75 objectives. Images were viewed using ZEN lite imaging software (2012) and in silico background removal and color processing of images were performed using Adobe Photoshop CS6.

Statistical Analysis

A resampling approach was used to determine whether the amount of overlap seen between Sepw1-enriched genes and layer-enriched database genes was significantly greater than what might occur by chance (Supplementary Table 1). To accomplish this, a short program was written in R to randomly sample the same number of genes as was enriched in each experimental comparison (Sepw1-pure to WT-pure, 1907 Sepw1 enriched; Sepw1-pure to Nr5a1-pure, 634 Sepw1 enriched) from the filtered genes for that particular comparison, and then determine to what extent this random subset overlapped with database layer-enriched genes. This program was looped to repeat this random sampling and determination of overlap 1000 times to produce a resampling distribution with an estimate of the mean and 95% confidence intervals (CI). P-values were calculated using the equation: (sum(resampled values < (estimate – distance from experimental value)) + sum(resampled values > (estimate + distance from experimental value)))/1000). It was necessary to repeat this with each database list of layer-enriched genes, since a different number of database genes from each of these categories were present in the 'filtered counts' list of genes for each comparison (genes not in 'filtered counts' are excluded from DESeq differential expression determination).

Binomial logistic regression analysis was performed using the glm function in R, and plotted to show the predicted likelihood of finding layer 2/3 genes as a function of the rank of Sepw1-fold enrichment.

Development of the *TetO-UPRT* mouse

WPRE and SV40 intron sequence elements were amplified from a stock vector using primers containing EcoRV and XbaI restriction enzyme sites. The forward primer contained the EcoRV site: 5'TTTTTTGATATCTTGGTCCTGCTGGAGTTCGTGA, and the reverse primer contained the XbaI site: 5'AAAAAATCTAGAAACAGATGGCTGGCAACTAGAAG. After amplification, the WPRE-SV40 fragment and a pTRE-tight2 vector (containing the tetracycline responsive element and an SV40 poly A signal) were digested using aforementioned restriction enzymes and ligated together. The newly ligated vector was then used to transform E. coli and a single positive clone was selected for further amplification and purification using a PureYield plasmid Midiprep kit (Promega). The resulting pTRE-tight 2 vector containing WPRE-SV40 (subsequently referred to as pTT-WPRE) was sequenced using a primer to the SV40 intron to confirm sequence fidelity. To add UPRT to the pTT-WPRE vector, stock pBSSK(+)-UPRT (used for the original development of the *CA>GFPstop>HA-UPRT* transgene) was amplified and purified using the PureYield plasmid Midiprep kit (Promega). Purified pBSSK(+)-UPRT and pTT-WPRE were then digested overnight using restriction enzymes Not1 and Sal1 (the SV40 intron was removed with this step), ligated together, and used to transform *E. coli* overnight. Positive clones were selected by restriction enzyme screening and vector fidelity was

confirmed by sequencing. The final vector was purified (PureYield plasmid Midiprep kit) then digested overnight with Nsp1 to linearize and isolate the entire tetO-UPRT-WPRE-SV40 construct. The final construct was purified using a gel-extraction kit (Qiagen), and eluted in filtered microinjection buffer (low TE, pH 8.0) for pronuclear injection. Mice were genotyped to establish successful integration of the construct using primers to the WPRE element: 5'TCTCTTTATGAGGAGTTGTGGCCC, and 5'CGACAACACCACGGAATTGTCAGT. The resulting founder mice were crossed to a *CaMKII-tTA* line (Jackson labs) and screened for high levels of neuronal expression.

RESULTS

Generating UPRT expression and purifying RNA enriched in upper layer cortical neurons in the postnatal brain

To determine whether the *CA>GFPstop>HA-UPRT* mouse line (Figure 1A) (Gay et al., 2014, 2013) could be used to express UPRT in postnatal mouse neurons, we first crossed this mouse to *Sepw1(NP39)-cre*, a Cre driver line produced by the GENSAT project (Gerfen, Paletzki, & Heintz, 2013) with expression previously described, and confirmed here, to be enriched in layer 2/3 cortical pyramidal neurons (Figure 1C, E, G). In this experiment, all Cre-negative cells should be GFP-positive and UPRT:HA-negative whereas all Cre-positive cells should be UPRT:HA-positive and GFP-negative (Figure 1B). We found that in P12 visual cortex, *Sepw1-cre* generated UPRT expression that was enriched in layer 2/3 (Figure 1C, E, G). We concluded that the *Sepw1-cre* line could be used to express UPRT in layer 2/3 of P12 mouse visual cortex.

After confirmation of UPRT expression, *Sepw1-cre; CA>GFPstop>HA-UPRT* double transgenic mice were used to thiol-tag and purify RNA from layer 2/3 cortical neurons, subsequently called "Sepw1-pure" RNA (Figure 1H). Briefly, we injected 4TU subcutaneously into mice double positive for the *Sepw1-cre* and *CA>GFPstop>HA-UPRT* transgenes at P12, and 5-6 hours later, dissected out the left and right visual cortexes. Each sample contained a pool of visual cortexes from 4 mice of mixed genders to provide enough material for subsequent purification. RNA was extracted, biotinylated, and streptavidin purified to produce samples enriched with thiol-tagged transcripts. All samples were then prepared for Illumina sequencing (Figure 1I and Methods).

We prepared two different sample types as comparisons to find genes enriched in the Sepw1-pure samples. WT mice lacking the UPRT transgene were processed and streptavidin purified identically to the mice expressing UPRT in upper layer cortical neurons to approximate "background" from unlabeled and mislabeled RNAs (subsequently referred to as WT-pure). In addition, we used identically processed, thiol-tagged RNA from *CA>GFPstop>HA-UPRT* mice crossed to an *Nr5a1-cre* line, which we and others have demonstrated labels neurons in layer 4 of visual cortex (Harris et al., 2014; Oh et al., 2014) (subsequently referred to as Nr5a1-pure; Figure 1D, F, H). We found it was important to only compare sample types that experienced a similar processing pipeline, i.e. subjected to the same purification procedure. For this reason, we avoided comparing purified RNA to 'total' unpurified RNA samples, as was done in the first published TU-tagging protocols (Gay et al., 2014, 2013).

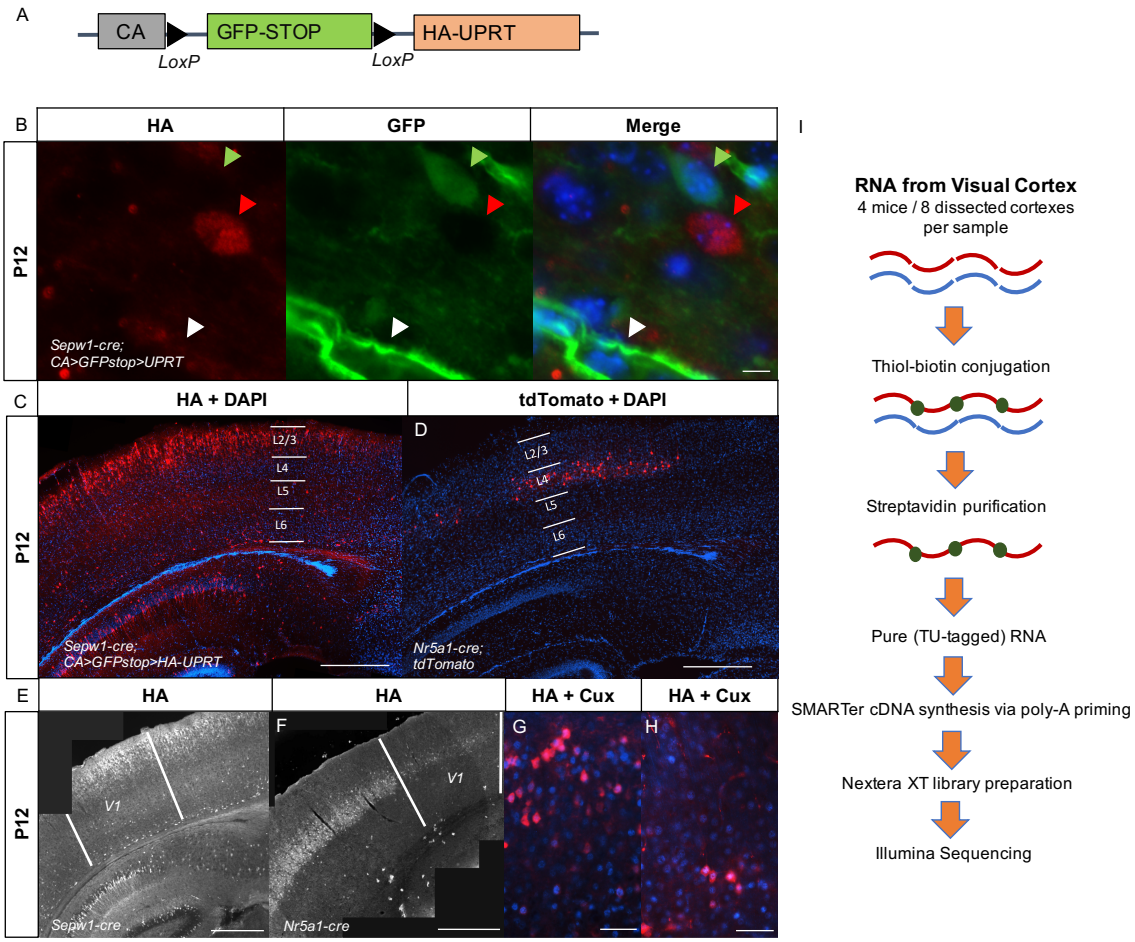

Figure 1. Upper cortical layer-enriched neuronal expression of HA-UPRT.
(A) Diagram of the *CA>GFPstop>HA-UPRT* transgene(Gay et al., 2014).
(B) Expression of the *CA>GFPstop>HA-UPRT* transgene(Gay et al., 2014) crossed to a *Sepw1-cre* line in neurons and endothelial cells (40x objective, scale bar: 10 µm). Green arrow: GFP positive, Cre-negative neuron; White arrow: GFP positive, Cre-negative endothelial cell; Red arrow: UPRT:HA positive, Cre positive neuron.
(C) *Sepw1-cre* drives UPRT expression in layer 2/3 and to a lesser extent layer 4. Immunostaining for HA at P12 in a *Sepw1-cre; CA>GFPstop>HA-UPRT* cross demonstrating layer 2/3 enriched expression at P12 (10x objective, scale bar: 500 µm). DAPI is included to show cortical structure.
(D) *Nr5a1-cre* drives expression in a sparse subset of layer 4 neurons. *Nr5a1-cre* crossed to a tdTomato marker at P12 is specific to layer 4. DAPI is included to show cortical structure (10x objective, scale bar: 500 µm).
(E-F) UPRT (immunostained for HA) expression in visual cortex of *Sepw1-cre* (E) or *Nr5a1-cre* (F) mouse lines crossed to the *CA>GFPstop>HA-UPRT* line (5x objective, scale bar: 500 µm).
(G-H) *Sepw1-cre* and *Nr5a1-cre* drive expression in neurons found predominantly in layer 2/3 or layer 4 of visual cortex, respectively. 40x image of neurons immunostained for the HA epitope on UPRT (red) in *Sepw1-cre; CA>GFPstop>HA-UPRT* or *Nr5a1-*

cre; CA>GFPstop>HA-UPRT crosses, and co-stained for the upper layer neuronal marker Cux1 (blue) (scale bar: 50 μm).
(I) TU-tagging workflow using poly-A priming for cDNA synthesis and Nextera XT for library preparation.

DESeq differential expression analysis reveals transcripts enriched in layer 2/3

To determine novel genes enriched in layer 2/3 of developing visual cortex, Sepw1-pure, WT-pure, and Nr5a1-pure RNA sample types were sequenced to a depth ranging from 21 to 38 million reads (SRA accession number: *SRP097635*). FastQC reports demonstrated high sequence quality (average per base sequence quality > 30 at all positions) and low duplication rates (> 70% remaining after deduplicaton) for all samples after trimming and filtering sequences. Over 90% of reads for all samples uniquely mapped to the mouse genome (Cunningham et al., 2014) using the splice-aware Genomic Short-read Nucleotide Alignment Program (GSNAP) (Wu & Nacu, 2010). Mapped sequences that aligned to particular genes were then counted using the python program htseq-count, filtered to remove genes with low reads (Robinson, McCarthy, & Smyth, 2010), and normalized to counts per million (cpm) using the DESeq package (version 1.24.0) in R (Anders & Huber, 2012; Simon Anders et al., 2010). Removing low-count transcripts reduced the total number of genes analyzed by DESeq from 22,078 (entire mouse transcriptome) to 13,849 for the Sepw1–Nr5a1 comparison or 13,891 for the Sepw1–WT comparison.

To approximate expression differences between samples, we generated a multiple dimensional scaling plot using the limma package in R (Law, Alhamdoosh, Su, Smyth, & Ritchie, 2016; Ritchie et al., 2015), which revealed the three sample types formed distinct clusters (Figure 2A). We then performed pairwise comparisons between Sepw1-pure and

WT-pure or Sepw1-pure and Nr5a1-pure sample types in DESeq (Anders & Huber, 2012) to determine genes with differential expression. The dispersion values for the filtered count data and fitted curve calculated for the negative binomial statistical model used in DESeq (Anders & Huber, 2012), are shown in Figure 2B (Sepw1 vs. Nr5a1) and 2C (Sepw1 vs. WT). Genes with DESeq calculated adjusted p-values > 0.1 were considered differentially expressed between sample types (Figure 2D, E).

We next analyzed the success of the Sepw1–WT and Sepw1–Nr5a1 comparisons by identifying whether the Sepw1-gene enrichments obtained via DESeq differential expression analysis met experimental expectations. We expected to see an enrichment of genes found in upper cortical layers when Sepw1-pure sample types were compared to WT-pure or Nr5a1-pure sample types. Upper cortical layer enriched genes can be thought of as our 'signal' for this experiment, and genes expressed in lower cortical layers can be thought of as 'noise'. For an unbiased description of layer enriched genes, we used an online transcriptomic atlas of mouse neocortical layers published in Belgard et al., 2011. Though this database was created using adult rather than P12 mice, layer-defining gene expression appears to be relatively consistent after the first postnatal week when neurons have largely finished migrating (Ignacio, Kimm, Kageyama, Yu, & Robertson, 1995). With a few exceptions (e.g. Pou3f1), we found similar expression patterns for Sepw1-enriched genes at both P14 and in adult mice after examining Allen Brain Atlas *in situ* data at both time points (Figure 5A: blue, P14 expression; orange, adult expression).

Comparing Sepw1-pure samples to WT-pure samples yielded a significant enrichment of genes expressed highly in upper cortical layers (significant differences from resampled estimates, Supplementary Table 1, Table 1, Figure 3). However, many

non-specific gene enrichments were also produced using this comparison. Of the 1907 Sepw1-enriched genes identified (Tomorsky et al., 2017), only a small fraction show layer 2/3 specific expression, presumably a consequence of the large differences in gene expression found between a heterogeneous populations of cortical cells and the subset of upper layer excitatory neurons we labeled (Chatzi et al., 2016). Transcripts found in all neuronal cells, or with high rates of transcription and/or low transcript half-lives might also be enriched using the WT-pure comparison (see discussion). We conclude that the Sepw1-pure to WT-pure comparison has limited utility in identifying cell-type enriched gene expression.

To obtain a greater enrichment of transcripts specific to layer 2/3, we compared Sepw1-pure samples to purified RNA from the *Nr5a1-cre* line, which sparsely labels cells in layer 4, but little if any in layer 2/3 at P12 (Figure 1D, F). We hypothesized that the comparison of *Sepw1-cre* labeled RNAs found in layers 2/3 and 4 and *Nr5a1-cre* labeled RNA's found only in layer 4, would yield an enrichment of layer 2/3 specific transcripts. As expected, comparing highly similar neuronal cell types (layer 2/3 versus layer 4) produced fewer differentially expressed genes (634 Sepw1-enriched transcripts) (Figure 2B) than comparing less similar Sepw1-pure and WT-pure sample types (1907 Sepw1-enriched transcripts) (Figure 2C). In addition, a much greater proportion of the Sepw1-enriched transcripts from the Sepw1-Nr5a1 comparison (as compared to the Sepw1-WT comparison) overlapped with genes expressed in layer 2/3 neurons (Table 1, Figure 3C).

We examined the probability of finding layer 2/3 enriched transcripts using either Sepw1–Nr5a1 or Sepw1–WT comparisons by logistic regression analysis (Figure 3A).

Both comparisons demonstrated an increased probability of finding a layer 2/3 enriched gene with increased Sepw1-fold enrichment, and this relationship is more pronounced when using Nr5a1-pure as a comparison (Figure 3A). The Venn diagram in Figure 3B shows that the highest percentage (23.1%) of layer 2/3 genes are found among the overlapping 260 genes enriched using both comparisons, with 11.4% and 3.4% classified as layer 2/3 enriched among the genes found exclusively using the Nr5a1-pure or WT-pure comparison, respectively. Because the list of Sepw1-enriched genes identified using the Nr5a1-pure comparison contained the greatest percentage of layer 2/3 transcripts (Figure 3C), we conclude that this dataset would be the most useful for finding genes important for the development of visual cortex layer 2/3 (Tomorsky et al., 2017). It should be noted, however, that there are many possible explanations for why different Sepw1-gene enrichments are observed when using either Nr5a1-pure or WT-pure as a comparison (see discussion).

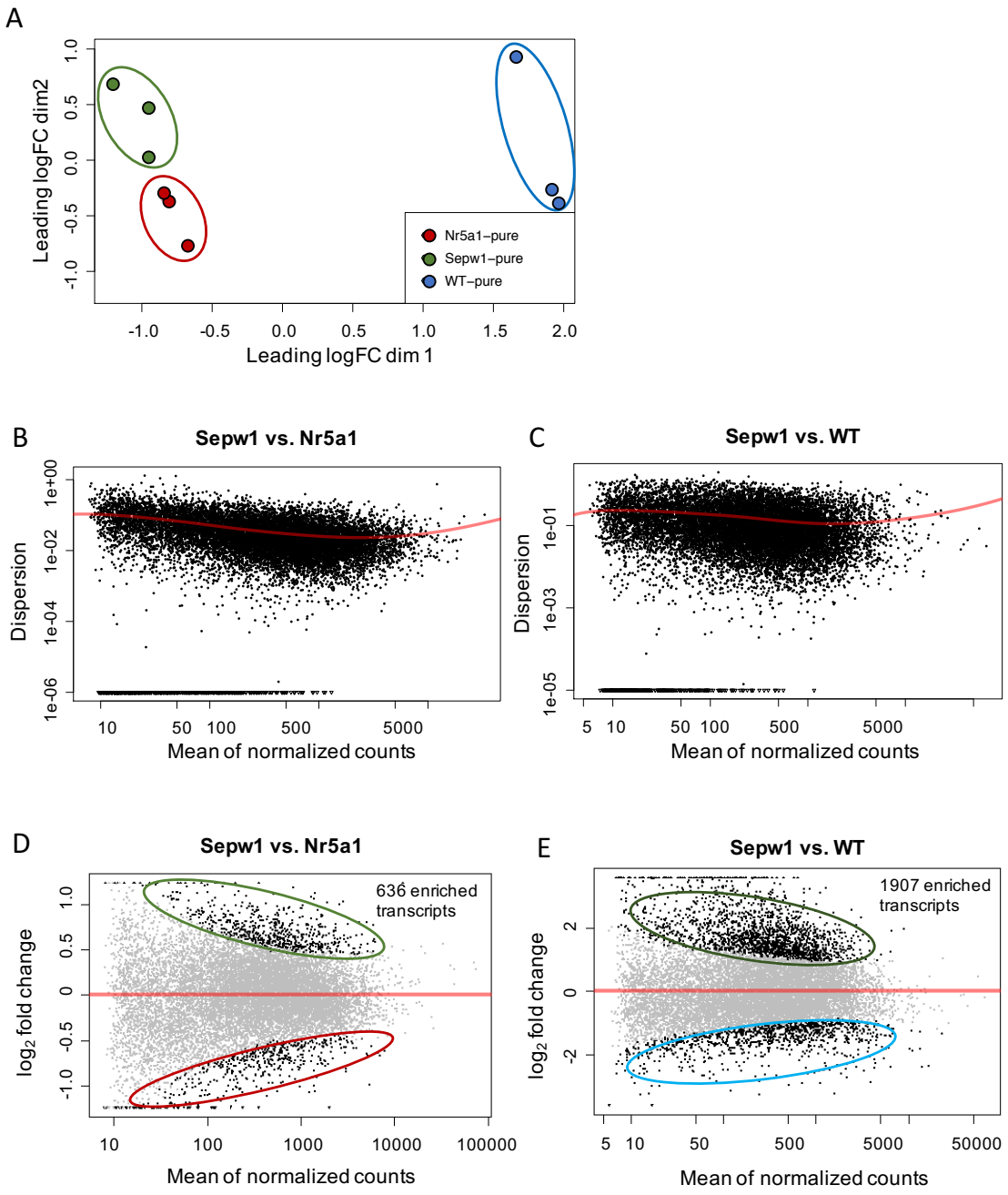

Figure 2. NMDS clustering of sample types and differential expression analysis.
(A) Multiple dimensional scaling plot showing clustering of samples with the first dimension representing leading fold change distances (root mean square of the 500 largest fold changes between pairs of samples) (Chen, Lun, & Smyth, 2014; Huber et al., 2015; Law et al., 2016) between Sepw1-pure, Nr5a1-pure, and WT-pure RNA sample types (filtered and normalized gene counts).
(B and C) DESeq generated graphs showing the estimated dispersion values and fitted curves produced using filtered count data (Anders & Huber, 2012) for the Sepw1-pure to Nr5a1-pure (B) or Sepw1-pure to WT-pure (C) comparisons.

(D and E) Differentially expressed genes after DESeq analysis was performed on filtered and normalized gene counts from comparisons of Sepw1-pure samples to either Nr5a1-pure (D) or WT-pure sample types (E).

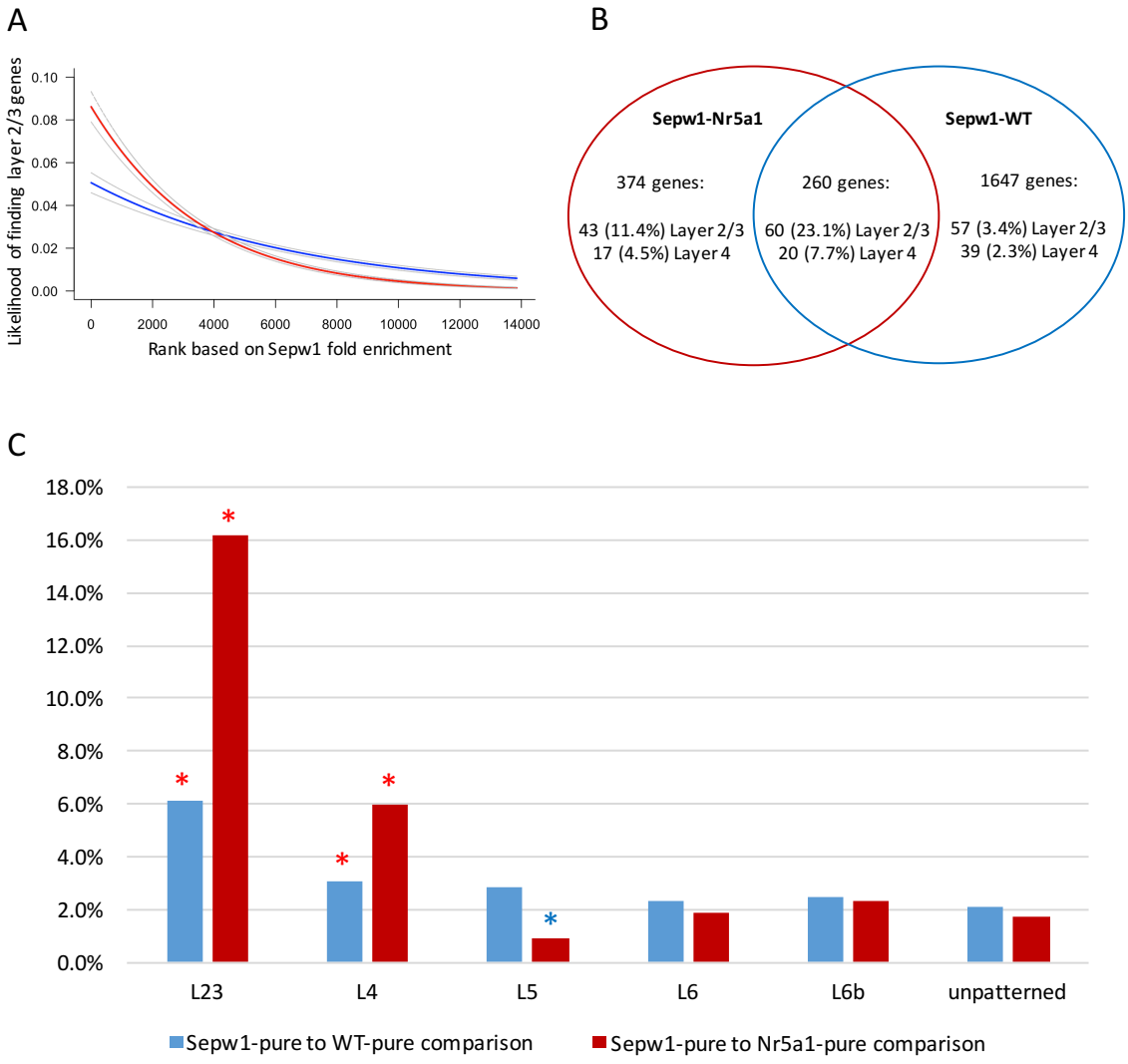

Figure 3. Differences in composition of Sepw1-pure enriched genes identified using Sepw1–Nr5a1 or Sepw1–WT comparisons.
(A) The likelihood of a gene having enriched expression in layer 2/3 is higher with increased Sepw1-fold enrichment. Logistic regression analysis shows the likelihood of finding layer 2/3 enriched genes from Belgard et al., 2011 as a function of the fold change in transcript expression associated with Sepw1-enrichment. Fold changes were used to rank genes based on the level of Sepw1 enrichment, with the highest Sepw1-fold enrichment given a rank of 1 and decreasing fold enrichments given progressively higher ranks. Using both Nr5a1 (red) and WT (blue) comparisons, the likelihood of finding layer 2/3 genes is significantly greater with higher Sepw1-fold enrichment (Logistic regression, $P < 2e\text{-}16$ for both WT and Nr5a1 comparisons).

(B) Venn diagram showing the number and proportion of genes that are upper layer enriched when Sepw1-pure samples are compared to WT-pure or Nr5a1-pure samples. (C) Genes found in layer 2/3 are highly represented among Sepw1-enriched genes. The percentage of Sepw1-enriched genes from different comparisons that overlap with database genes found to be layer enriched, is shown. Numbers of overlapping genes falling outside the upper (red) or lower (blue) 95% confidence limits of the mean (derived from resampled distributions indicated in Supplementary Table 1) are marked with an asterisk.

Comparison	Sepw1-WT	Sepw1-Nr5a1
Number enriched (padj = 0.1)	1907	634
Layer 2/3	117*	103*
Layer 4	59*	37*
Layer 5	55	6*
Layer 6	45	12
Layer 6b	47	15
Unpatterned	40	11

Table 1. Number and classification of transcripts enriched in Sepw1-pure compared to WT-pure or Nr5a1-Pure RNA sample types
Genes significantly enriched in various cortical layers (400 top enriched genes per layer from an online database published in Belgard et al., 2011 were compared to the genes most significantly enriched (after DESeq differential expression analysis) in Sepw1-pure samples when compared to WT-pure, or Nr5a1-pure sample types. Experimentally derived numbers of overlapping genes falling outside the upper (layer 2/3 and layer 4) or lower (layer 5) 95% confidence limits of the mean (derived from resampled distributions indicated in Supplementary Table 1) are marked with an asterisk.

Gene ontology analysis of layer 2/3 gene expression reveals genes associated with neuron projection development

To determine the potential functions of genes identified as enriched using both Sepw1–WT and Sepw1–Nr5a1 comparisons, we used GOTermFinder

(http://go.princeton.edu/cgi-bin/GOTermFinder) to obtain gene ontology (GO) terms that were significantly overrepresented among Sepw1-enriched transcripts. GO terms were summarized using REVIGO (http://revigo.irb.hr/), a tool designed to remove redundant terms and visualize broad categories of gene function (Boyle et al., 2004; Supek et al., 2011). The REVIGO tree-maps in Figure 4A and 4B show that Sepw1-pure genes are over-represented for "neuron projection development", and differences are observed in overall gene-classification when either Nr5a1-pure (Figure 4A) or WT-pure (Figure 4B) is used as a comparison (see discussion).

A Sepw1-enriched (Nr5a1-pure comparison)

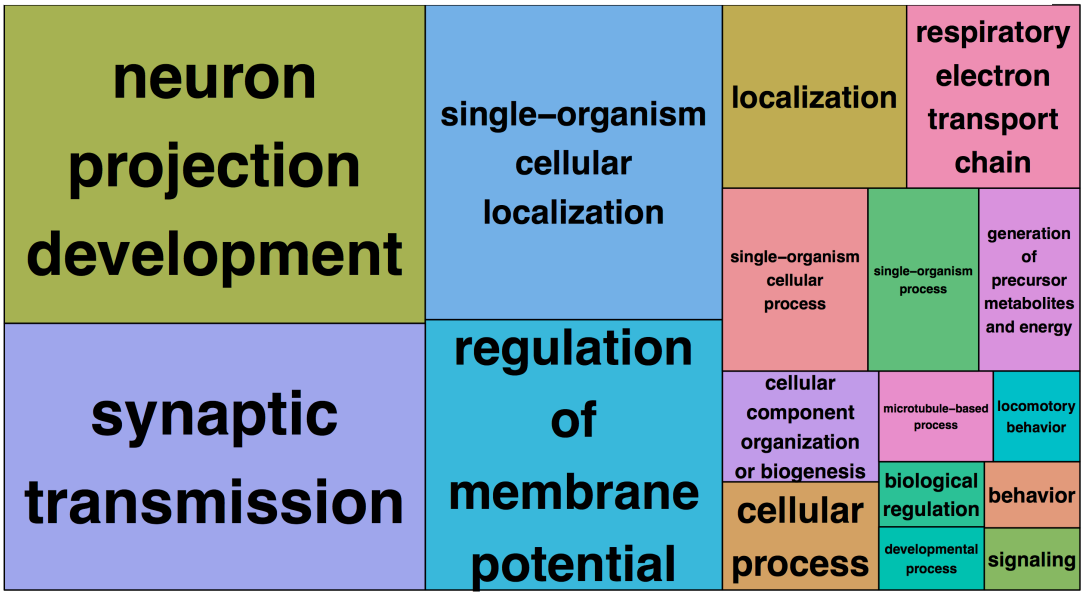

B Sepw1-enriched (WT-pure comparison)

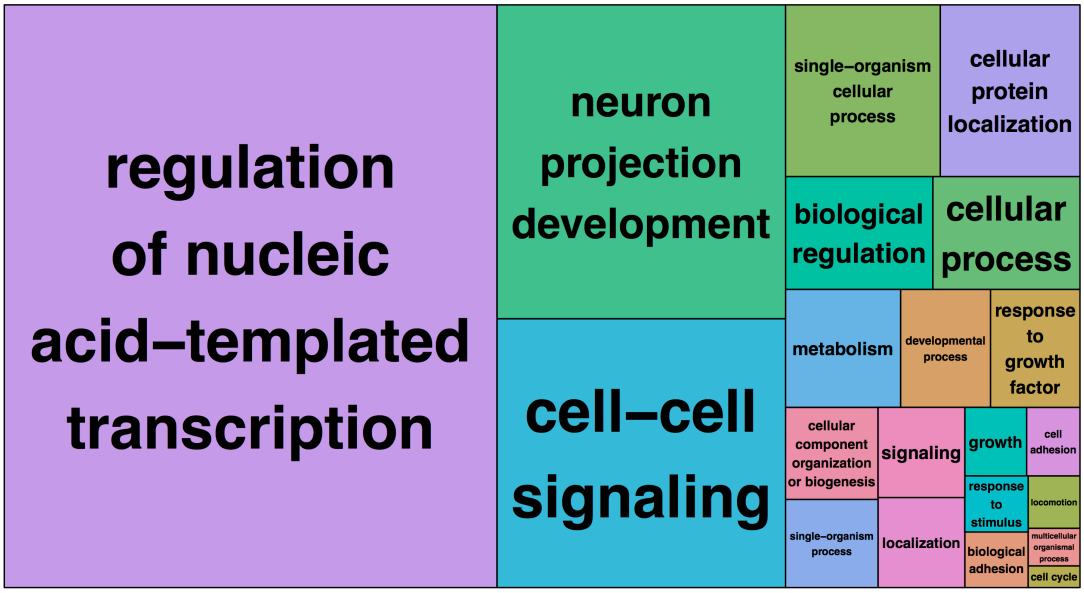

Figure 4. REVIGO Gene Ontology tree-maps showing differences in Sepw1-enriched gene classifications using WT-pure or Nr5a1-pure comparisons.
(A) REVIGO tree-map showing gene ontology clusters identified using Sepw1-enriched transcripts when Nr5a1-pure is used as a comparison.
(B) REVIGO tree-map showing gene ontology clusters identified using Sepw1-enriched transcripts when WT-pure is used as a comparison.

Validation of layer 2/3 enrichment of Sepw1-pure RNAs by *in situ* hybridization

We performed *in situ* hybridization experiments to determine the laminar expression of Sepw1-pure RNAs found enriched using the Nr5a1-pure comparison. We determined the expression patterns of seven genes of interest directly by performing *in situ* hybridizations at P12. Genes of interest were chosen based on presence in the gene ontology (GO) categories, biological adhesion (*Tspan6, Pvrl3, Pvrl1, Speg*), biological regulation (*Rgs8*), or synapse formation (*Sez6l2, Frmpd4*) (Boyle et al., 2004; Mi, Muruganujan, Casagrande, & Thomas, 2013; Mi, Poudel, Muruganujan, Casagrande, & Thomas, 2016). We found that four of these seven genes displayed enriched expression in layer 2/3 at P12 (*Pvrl3*, *Rgs8*, *Pvrl1*, and *Tspan6,* Figure 5A). The remaining three genes were expressed in all cortical layers (*Frmpd4*, *Sez6l2*, *Speg,* Supplementary Figure 1).

We additionally used *in situ* data available at the Allen Brain Atlas website (Allen Mouse Brain Atlas (2004); Allen Developing Mouse Brain Atlas (2008)) to determine the expression patterns of Sepw1-pure genes. Though Allen Brain Atlas (Allen Mouse Brain Atlas (2004); Allen Developing Mouse Brain Atlas (2008)) did not have expression data at P12, the stage our experiments were done, *in situ* data at P14 was available for 44 of the top 300 Sepw1-enriched genes (compared to Nr5a1-pure). To determine the expected expression patterns of Sepw1-pure genes, we carefully considered our Sepw1–Nr5a1 comparison, which should yield an enrichment of genes expressed highly in layer 2/3 as compared to layer 4. This leaves a variety of expected layer 2/3 'enriched' expression patterns, including genes with expression darkest in layer 2/3 and 5 (*Tspan6*), and genes expressed throughout cortex but darkest in layer 2/3 (*Bhlhe22*). For this reason, genes with layer 2/3 'enriched' expression that were not necessarily layer 2/3

'specific' were considered experimental successes and counted as enriched in our analysis. Manual classification of the expression patterns of Sepw1-pure genes revealed that the majority (~ 70%) were enriched in cortical layer 2/3, and that the expression patterns of these genes did not dramatically change between P14 and adulthood (Figure 5B).

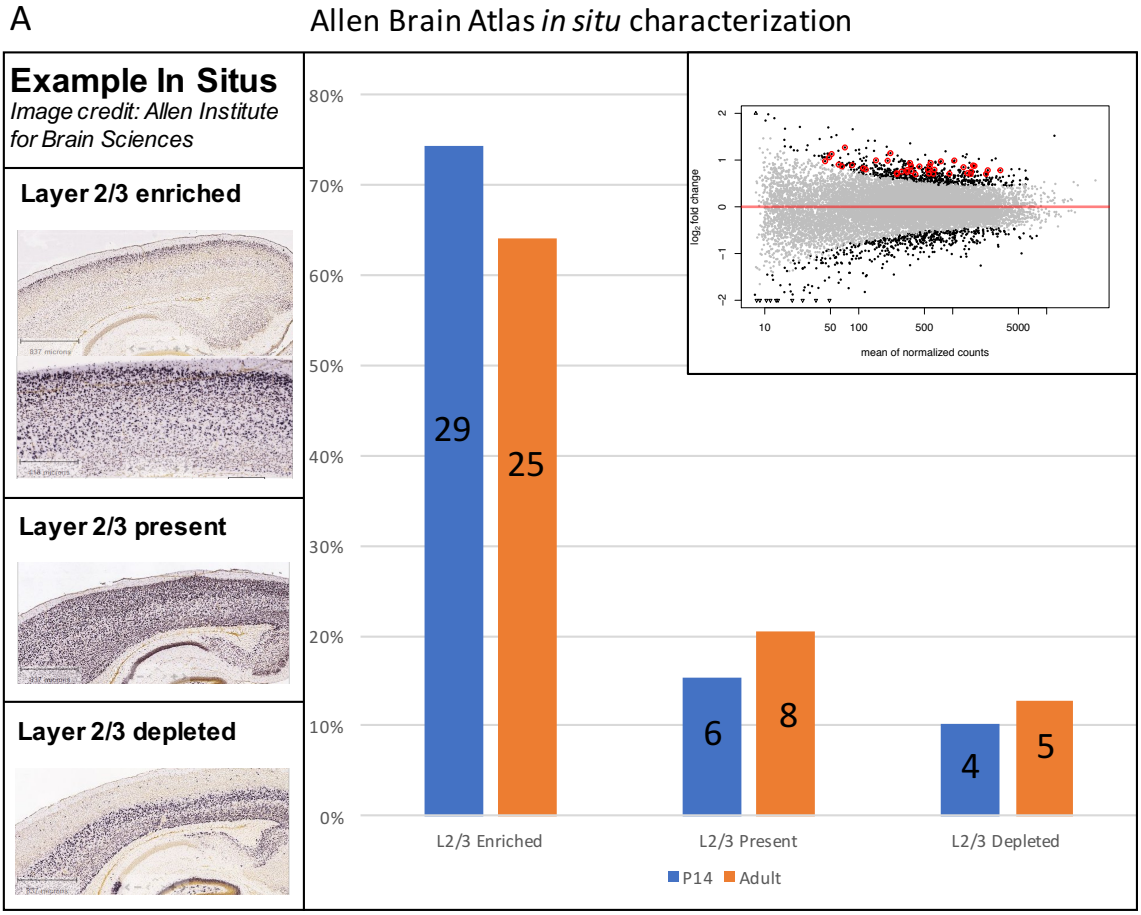

Figure 5. *In situ* confirmations of Sepw1-enriched genes.
(A) In house *in situ* hybridizations to four genes of interest *Pvrl3*, *Rgs8*, *Pvrl1,* and *Tspan6*, demonstrated upper layer specific or enriched expression at P12 (Scale bar: 200 μm). *In situ* hybridizations to three additional genes showed expression throughout cortex (Supplementary Figure 1).
(B) Approximately 70% of select Sepw1-enriched genes show layer 2/3 enrichment, confirmed using *in situ* data. The percentage of Sepw1-enriched genes (Sepw1-pure to Nr5a1-pure comparison) found in various expression categories, based on Allen Brain Atlas *in situ* data is shown. Of the top 300 genes found to be Sepw1 enriched, 44 had existing *in situ* data at P14 found at allenbrain.org (Allen Developing Mouse Brain Atlas (2008)). These *in situ* experiments were classified manually as: layer 2/3 enriched, layer 2/3 present (no enrichment), or layer 2/3 depleted. Unclear database *in situ* hybridizations were excluded from this analysis. Most genes were found to be either enriched or present in cortical layer 2/3 neurons. While the expression patterns of a few of these genes changed from P14 (blue) to adult (orange), most showed similar expression patterns over development. Genes included in the analysis are circled in the DESeq differential expression plot in red (upper right).

Demonstrating 4TU crosses the blood-brain barrier using a newly developed *TetO-UPRT* transgenic mouse

While it is clear from the data presented here that 4TU injected subcutaneously can pass the blood brain barrier (BBB) at P12, it is unknown if this is the case in adult animals. We found it was not possible to test whether 4TU was passing the BBB in adults using the *CA>GFPstop>HA-UPRT* mouse, since this mouse experiences transgene silencing in adult neurons (Figure 6A).

To determine whether 4TU injected subcutaneously can reach adult neurons, we developed a new *TetO-UPRT* mouse. When this line is crossed to a cell type-specific tTA or rtTA line, UPRT expression is induced depending on the absence (tTA) or presence (rtTA) of tetracycline or doxycycline (DOX). The transgene itself incorporates a tetracycline operator (tetO) sequence driving the expression of a hemagglutinin (HA) epitope-tagged UPRT gene followed by a Woodchuck Hepatitis Virus Posttranscriptional Regulatory Element (WPRE), intended to increase levels of

gene expression (subsequently called *TetO-UPRT*) (Supplementary Figure 2). When crossed to the *CaMKII-tTA* neuronal line, we observed high transgene expression in adult neurons (Figure 6C), and treatment of this mouse with DOX reduced transgene expression (Supplementary Figure 2). However, we detected 'leaky' neuronal expression that persisted after DOX administration (Supplementary Figure 2) and was also present in animals carrying only the TetO-UPRT transgene (Supplementary Figure 3). For this reason, we conclude that this mouse should only be used cautiously for future TU-tagging experiments. However, since even the leaky expression was neuronal, we were able to use the line to determine whether 4TU crossed the BBB.

For this experiment, 4TU was injected subcutaneously into two WT and two *TetO-UPRT; CaMKII-tTA* adult mice, hippocampi were dissected, and RNA was extracted, biotinylated and streptavidin purified. After purification, the levels of tagged RNA from the transgenic cross far exceeded that of the WT mice (Table 2). In addition, this experiment was performed using a *TetO-UPRT* mouse not crossed to anything to determine the amount of RNA tagged by 'leaky' neuronal UPRT expression. Consistent with UPRT expression levels (Figure 6, Supplementary Figure 3), the amount of RNA purified from single positive *TetO-UPRT* hippocampal tissue fell between the quantities obtained using WT or double positive *CaMKII-tTA; TetO-UPRT* hippocampal tissue (Table 2). The increased levels of purified RNA obtained from hippocampi with neuronal UPRT expression (compared to UPRT negative tissue) indicate that 4TU injected subcutaneously in adult mice is passing the BBB and

reaching neurons.

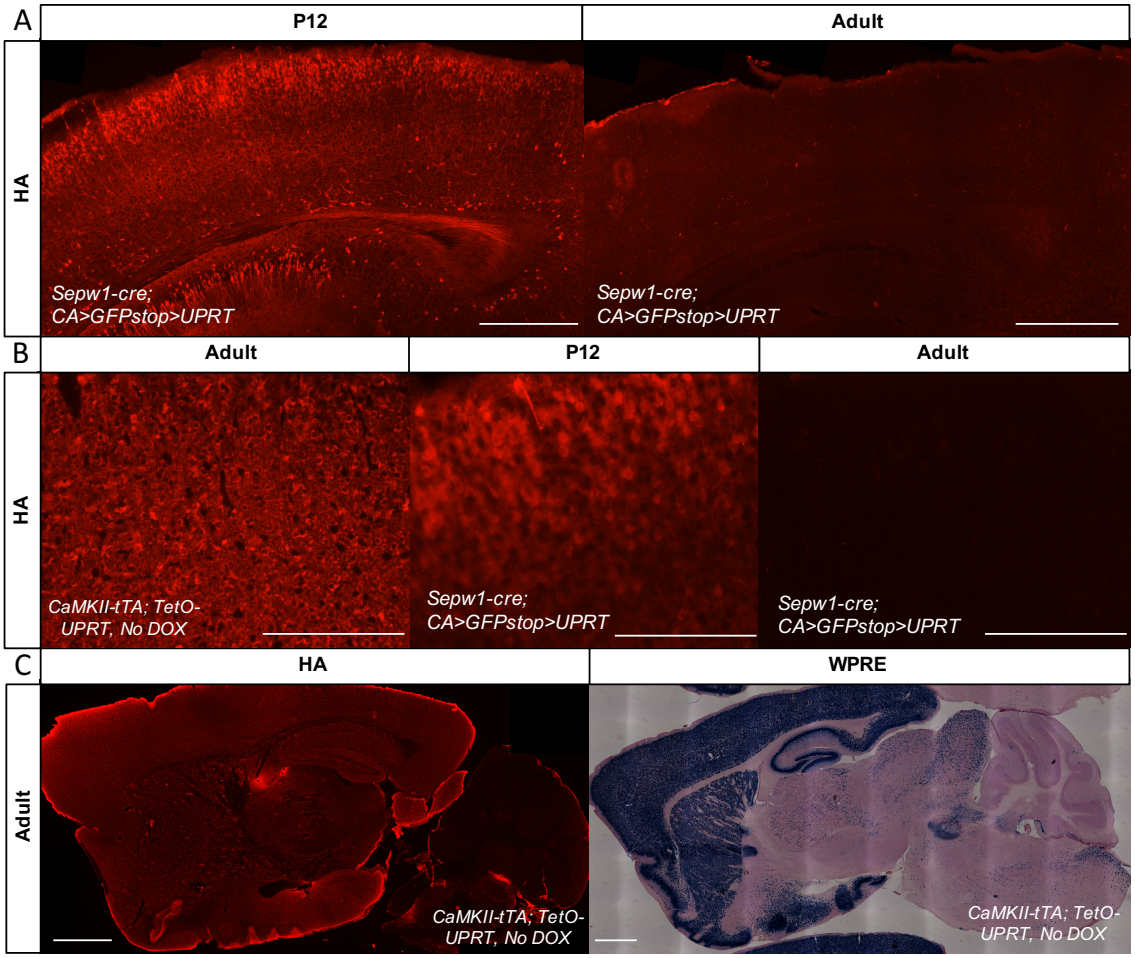

Figure 6. Adult neuronal expression of UPRT using a newly developed *TetO-UPRT* mouse.

(A) Immunohistochemistry for UPRT using an HA antibody in P12 and adult *Sepw1-cre; CA>GFPstop>HA-UPRT* animals (scale bar = 500 μm) demonstrates silencing of the *CA>GFPstop>HA-UPRT* transgene in adult neurons. Images of visual cortex shown were processed identically (10x objective, 250 ms exposure, Photoshop adjusted brightness = -30, contrast = 100).

(B) A transgenic cross between the newly developed *TetO-UPRT* transgene (off DOX) (Supplementary Figure 2) and a *CaMKII-tTA* mouse, drove high UPRT expression in adult neurons (immunohistochemistry for UPRT using an HA antibody). Adult neuronal expression of UPRT in the *CaMKII-tTA; TetO-UPRT* cross was similar to that seen in a *Sepw1-cre; CA>GFPstop>HA-UPRT* cross at P12. Images shown were processed identically (20x objective, scale bar = 200 μm, 14 ms exposure, Photoshop adjusted contrast = 70).

(C) Immunohistochemistry using an HA-antibody demonstrates expression of UPRT in CaMKII positive adult neurons in a *CaMKII-tTA; TetO-UPRT* cross (scale bar = 1000

μm, 5x objective, exposure = 150 ms, Photoshop adjusted brightness = 30, contrast = 100). *In situ* hybridization to WPRE RNA in a *CaMKII-tTA; TetO-UPRT* mouse demonstrates strong neuronal expression of the transgene (scale bar = 1000 μm, 10x objective). Both immunostaining for HA-UPRT and *in situ* hybridization to WPRE also demonstrated 'leaky' expression of UPRT in animals carrying only the *TetO-UPRT* transgene not crossed to a tTA line (Supplementary Figure 3).

Sample Type	Age	Tissue	Percent yield
TetO-UPRT; CaMKII-tTA	P50	hippocampus	3.90%
TetO-UPRT; CaMKII-tTA	P90	hippocampus	3.20%
TetO-UPRT	P120	hippocampus	2.00%
TetO-UPRT	P120	hippocampus	2.00%
WT	P50	hippocampus	0.07%
WT	P90	hippocampus	0.10%

Table 2. Percent yield of thiol-labeled RNA from hippocampal neurons after subcutaneous administration of 4TU.
CaMKII-tTA; TetO-UPRT double positive mice, *TetO-UPRT* single positive mice, or WT control mice were injected subcutaneously with 4TU and hippocampus was removed 5 hours later. After RNA extraction and streptavidin purification, the amount of tagged RNA obtained was much higher from hippocampal samples expressing UPRT in neurons (*CaMKII-tTA* driven neuronal expression and 'leaky' neuronal expression in single positive *TetO-UPRT* mice) (Supplementary Figure 3).

DISCUSSION

The TU-tagging method described here can be used to isolate cell-type specific RNA in vivo through the targeted expression of the enzyme UPRT. This technique may be particularly useful for identifying nascent RNAs in neuronal cell types, since the long axonal/dendritic processes that define these cell types can be damaged or removed during physical isolation processes such as laser capture microdissection or cell-sorting. There are multiple ways to target UPRT expression to a specific cell type.

A recent paper used virus to express UPRT in two different neuronal types (Chatzi et al., 2016). Though virus is an effective way to control the number and type of UPRT expressing cells, working with virus requires special safety considerations and manipulations, and is capable of inducing an immune response in vivo (Lowenstein, Mandel, Xiong, Kroeger, & Castro, 2007). Virus injection also requires invasive surgery, which is not always practical depending on age. Using transgenic mice to target UPRT expression to specific cell types requires no such manipulations, and can be an excellent alternative to viral methods depending on the experimental question. Here we demonstrate the first successful application of TU-tagging in mouse neurons using transgenic mice, and are also the first to demonstrate 4TU injected subcutaneously can pass the blood brain barrier (BBB).

In this experiment, we used TU-tagging to identify genes enriched in layer 2/3 of murine visual cortex around eye opening. To thiol-label nascent RNAs in cell types enriched in layer 2/3 of developing visual cortex, we crossed *CA>GFPstop>HA-UPRT* and *Sepw1-cre* transgenic mice. To identify genes enriched in layer 2/3, we compared RNA purified from *Sepw1-cre* labeled neurons (Sepw1-pure), to RNA purified from: 1) a sparse subset of layer 4 neurons labeled using an *Nr5a1-cre; CA>GFPstop>HA-UPRT* transgenic cross (Nr5a1-pure), or 2) WT cortical tissue not expressing UPRT (WT-pure). To maximize our yields of tagged RNA, we used a modified TU-tagging protocol, which included a 5–6 hour wait time between 4TU injection and visual cortex dissection (we have found that the amount of purified RNA from a ubiquitously expressing UPRT mouse P6 brain peaks between 4 and 6 hours after 4TU injection; L. Gay and C.Q.D., unpublished), and poly-A selection of

unfragmented RNA after streptavidin purification (Chatzi et al., 2016). This TU-tagging workflow allowed the preparation of small amounts of RNA for sequencing, and made possible the comparison of purified RNA from a neuronal cell type to extremely low yields of WT purified RNA. In our hands, the amount of RNA purified from both neuronal UPRT+ and WT tissue was insufficient to process for sequencing using the previously published TU-tagging protocol (Gay et al., 2014) (data not shown).

By directly comparing samples containing *Sepw1-cre* labeled RNAs to Nr5a1-pure and WT-pure sample types, we successfully isolated genes enriched in layer 2/3 of visual cortex at P12. Though the highest percent enrichment of layer 2/3 genes was found using the Sepw1–Nr5a1 comparison (Figure 3, Table 1), the Sepw1–WT comparison may provide more expansive information about the differences between layer 2/3 neurons and the rest of cortex. Due to the higher variability between Sepw1-pure and WT-pure sample types, genes with low fold enrichments had overall higher DESeq adjusted p-values using this comparison than with the Sepw1–Nr5a1 comparison (lowest fold changes of enriched genes with an adjusted p-value < 0.1; Sepw1–WT = 1.9; Sepw1–Nr5a1 = 1.36). Therefore, it appears the Nr5a1 comparison allowed the detection of genes with subtler Sepw1 enrichment, which may not be represented using the WT comparison (Figure 3B, 374 exclusive Sepw1-gene enrichments found using the Nr5a1 comparison). A gene ontology analysis of Sepw1-enriched transcripts revealed that many were involved in neuron projection development, suggesting that our selection of the P12 time point allowed the identification of genes involved in synapse formation (Figure 4). We conclude that the

comparison of two streptavidin purified sample types can help to isolate 'signal' in a TU-tagging experiment, and comparing two highly similar sample types, such as Sepw1-pure and Nr5a1-pure, may help narrow results to those specifically enriched in a particular cell type.

While our method was successful in isolating cell type-enriched genes, the direct comparison of purified RNAs isolated using different Cre lines may yield biases related to litter and strain differences. This is a potential confound for all RiboTag, TRAP, and TU-tagging studies where cell type-enriched RNAs were isolated using multiple mouse strains. An unbiased correction for strain differences would require access to the same specific cell types across strains, and is beyond the scope of this paper. Since the *CA>GFPstop>HA-UPRT* strain would have provided 50% of the genetic make-up for crosses containing the *Sepw1-cre* and *Nr5a1-cre* lines, genetic differences between these crosses should have been minimal. The WT samples were also composed of mice sharing at least 50% genetic similarity to the *Sepw1-cre* mice. Future experiments comparing two different Cre lines may further reduce strain differences by crossing transgenic lines to an inbred strain over multiple generations. Though it is possible that strain differences resulted in false positives in our enrichment data, it is unlikely that we would have seen the pattern of layer 2/3 enrichment observed if we were not isolating true differences between cell types.

When designing a TU-tagging experiment it is important to consider many variables that may affect whether final gene enrichments reflect true differences in expression between cell types. While the original TU-tagging method (Gay et al., 2014, 2013) called for the direct comparison of streptavidin purified RNA to unpurified 'total'

RNA, the comparison of two RNA samples that experienced different types of processing could yield non-specific gene enrichments. Since RNA transcripts can vary in their susceptibility to degradation, whole sample changes in transcript composition can occur with heavy processing of RNA during purification. Bias can be introduced at various stages in sample preparation: early, due to transcript to transcript variability in the efficiency of thiol-labeling and conjugation to HDPD biotin, and later, during cDNA synthesis of poly-A selected RNAs and Nextera library preparation (Cui et al., 2010; Duffy et al., 2015; Head et al., 2014; Lahens et al., 2014). Since sample preparation alone can produce differential gene expression unrelated to underlying biological processes, we avoided comparisons between streptavidin-purified RNA samples and unpurified RNA in this study.

It is also possible for RNA thiol-labeled outside the UPRT expressing cell type to contaminate a streptavidin purified sample. There are a few biochemical pathways in mammals that can, at a much lower rate, carry out the same 4TU to 4-thiouridine conversion performed by UPRT, which may lead to a small amount of non-specific thiol-labeling of RNAs (Tallafuss et al., 2014). The use of transgenic mice may also contribute to noise if low levels of non-specific UPRT transcription occurs outside of cell types expressing Cre or tTA (leaky UPRT expression) (Supplementary Figure 3). The 4-thiouridine made by UPRT+ cells may also diffuse into neighboring UPRT-negative cells, leading to thiol-labeled RNA in these cells. This has been observed in co-culture experiments (G. Zhang and R. Goodman, Vollum Institute, personal communication), and may be amplified by developmental processes such as apoptosis or synaptic pruning in vivo. Here we attempted to reduce noise effects caused by non-

specific labeling and 4-thiouridine diffusion by comparing similarly processed sample types and limiting our wait time between 4TU injection and tissue harvest to 5–6 hours.

Varying wait times between 4TU injection and tissue harvest can also influence noise that arises from transcript to transcript differences in transcription rate and half-life. In our experiments, WT-pure samples are likely largely composed of contaminating unlabeled RNAs derived from 'total' RNA, containing many fewer newly transcribed RNAs than the Sepw1-pure sample types. When there is a large discrepancy in the levels of newly transcribed RNA between compared sample types, as is the case with the Sepw1–WT comparison, many gene enrichments or depletions may simply reflect transcriptional dynamics. Comparing streptavidin purified RNA samples to total RNA samples is analogous to a ratio of newly transcribed RNA / total RNA, a ratio which has also been used to infer transcript half-lives (Dölken et al., 2008). Consequently, transcriptional dynamics alone can produce large enrichments for genes with high transcription rates (large numerator) and high rates of decay (small denominator), depending on the time allowed for transcription. Interestingly, 'regulation of nucleotide templated transcription' was the most highly represented cluster from the REVIGO analysis of Sepw1-enriched genes from the Sepw1–WT comparison using a 5 hour wait time (genes involved in 'regulation of transcription' have some of the shortest half-lives (Sharova et al., 2009)) (Figure 4). Using longer wait periods may instead select for transcripts with long half-lives, such as extracellular matrix, cytoskeletal, metabolism, and protein synthesis related genes (Sharova et al., 2009). In this study, the Sepw1–Nr5a1 comparison appeared to largely eliminate this type of noise (Figure 4).

One of the most important considerations when designing a TU-tagging experiment, is the selection of sample type comparisons. It is important to note that the specificity of expression obtained (cell type 'enriched' vs. cell type 'specific') is contingent on the comparison used. When using Cre lines that drive sparse expression in specific cell types, a significant portion of the streptavidin-purified samples derived from these lines may contain 'noise' from unlabeled or mislabeled RNAs. For this reason, the Cre line for which expression data is desired should have equal or greater UPRT expression (and therefore labeled RNAs) than the Cre line used as a comparison. For example, we would not recommend using a pan-neuronal Cre line as a comparison for a sparse neuronal Cre line, since background from mislabeled or unlabeled RNAs may be enriched in the sample derived from the sparse Cre line. Contaminating RNAs not specific to the UPRT expressing cell type should be less influential when using Cre lines with dense expression (increased signal to noise), and may eventually be eliminated with improvements to RNA labeling and purification protocols (Duffy et al., 2015; Hida et al., 2017).

With the appropriate selection of a sample type comparison, the TU-tagging method described here can identify newly transcribed genes in sparse cell types in vivo. While some protocol alterations made here may eliminate a few possible benefits of the method (poly-A selection prevents the isolation of microRNAs or long non-coding RNAs, and removal of the fragmentation step may decrease overall levels of gene enrichment), by selecting a streptavidin purified comparison, the technique becomes significantly more sensitive to changes in gene expression. Current improvements to the chemistry of biotinylation (Duffy et al., 2015), the development

of new labeling and purification protocols (Hida et al., 2017), new transgenic lines for targeted UPRT expression, and a better understanding of the types of noise to expect, should together help make the TU-tagging technique more accessible for future transcriptional profiling experiments.

BRIDGE TO CHAPTER III

In Chapter II, I discussed the identification of genes enriched in developing layer 2/3 visual cortical neurons using the TU-tagging technique. We used a modified TU-tagging protocol to prepare thiol-tagged neuronal RNA for sequencing and two different sample-type comparisons to identify genes enriched in layer 2/3 neurons (Sepw1-pure compared to Nr5a1-pure and WT-pure sample types). We found that the Nr5a1-pure sample type comparison worked best to identify genes enriched in layer 2/3 neurons, but only briefly discussed the reasons for this.

In Chapter III, I examine the composition of Nr5a1-pure samples by describing the genes enriched in this sample type when compared to WT-pure samples. I discuss the gene enrichments identified in the context of what we know about the expression of the *Nr5a1-cre* line, both in mature mice and during development. I also compare these gene enrichments to the Sepw1-enriched genes identified in Chapter II using the Sepw1–WT comparison. I found that the genes enriched in *Sepw1-cre* and *Nr5a1-cre* samples, as compared to WT samples, largely overlapped, indicating that upper layer excitatory neurons in visual cortex may have similar gene expression profiles at P12. The way these profiles differ can be most directly assessed through the Sepw1–Nr5a1 comparison described in Chapter II. This comparison worked well to identify *Sepw1-cre* enriched

genes (layer 2/3, neuronal) but not *Nr5a1-cre* enriched genes. Nr5a1 enrichment from this comparison was largely 'background' overlapping with genes enriched in deep cortical layers and endothelial cells. Here, I discuss reasons for this result, including that the *Nr5a1-cre* line exhibits very sparse neuronal labeling at P12 and that the cells labeled by the *Nr5a1-cre* line are likely a subset of the cells labeled by the *Sepw1-cre* line.

CHAPTER III

EXPLORING TU-TAGGING GENE ENRICHMENTS FROM SPARSE AND DENSE EXPRESSING NEURONAL TRANSGENIC MOUSE LINES

INTRODUCTION

The identification and characterization of specific neuronal cell types has become an important approach to the study brain function (Cembrowski & Menon, 2018; Fishell & Heintz, 2013; Luo, Callaway, & Svoboda, 2008). In mice, various transgenic lines have been developed to drive the expression of genetic elements in specific populations of neurons to describe their development, function, and morphology (Fishell & Heintz, 2013; García-Otín & Guillou, 2006; Gerfen et al., 2013; Luo et al., 2008). Recently, transcriptomics has become an important way to identify different cell types, with inferred functional and morphological similarities correlating to similar gene-expression profiles (Fishell & Heintz, 2013; Luo et al., 2008; Poulin et al., 2016). Several different techniques, often utilizing the transgenic tools available in mice, have been developed for cell-type specific transcriptomics including Ribo-tag/TRAP (Doyle et al., 2008; Heiman et al., 2008; Sanz et al., 2009), single-cell RNA-seq (Poulin et al., 2016), and TU-tagging (Chatzi et al., 2016; Gay et al., 2014, 2013; Miller, Robinson, Cleary, & Doe, 2009; Tallafuss et al., 2014; Tomorsky et al., 2017). The TU-tagging technique allows the spatial and temporal isolation of gene expression by cell-type specific expression of the enzyme UPRT using transgenic animals or viral infection (Chatzi et al., 2016; Gay et al., 2014, 2013; Miller et al., 2009; Tallafuss et al., 2014; Tomorsky et al., 2017). The UPRT enzyme converts an injected 4-thiouracil to 4-thiouradine, which is then incorporated in place of uridine in RNA transcribed in the UPRT expressing cell (Chatzi et al., 2016; Gay

et al., 2014, 2013; Miller et al., 2009; Tallafuss et al., 2014; Tomorsky et al., 2017). These tagged RNAs can then be biotinylated and streptavidin purified from whole brain lysates and prepared for RNA-seq (Chatzi et al., 2016; Gay et al., 2014, 2013; Miller et al., 2009; Tallafuss et al., 2014; Tomorsky et al., 2017).

Previously, we described using the Cre-lox system of transgenics to perform TU-tagging on populations of upper layer neurons in developing mouse visual cortex (Tomorsky et al., 2017). This study successfully isolated genes enriched in layer 2/3 (L2/3) visual cortical neurons at post-natal day 12 (P12), a time of intense synaptogenesis in these neurons (Tomorsky et al., 2017). In Chapter II, we used two Cre lines, *Sepw1-cre* and *Nr5a1-cre*, to isolate subpopulations of upper layer excitatory neurons in mouse visual cortex (Tomorsky et al., 2017). The *Nr5a1-cre* line, which is enriched in layer 4 (L4) cortical neurons, was used as a comparison for the *Sepw1-cre* line (enriched in L2/3) to isolate genes expressed in developing L2/3 neurons (Tomorsky et al., 2017). This study described the genes enriched in *Sepw1-cre* neurons relative to both *Nr5a1-cre* neurons and a WT purified sample type (WT-pure, purified background unlabeled RNAs) (Tomorsky et al., 2017). While Sepw1-enriched transcripts were described fully, we did not describe genes enriched in the *Nr5a1-cre* neurons (Tomorsky et al., 2017).

Here, I describe genes found enriched in the *Nr5a1-cre* line at P12 using the WT-pure comparison. I then compare these gene enrichments to genes found in Chapter II to be enriched in the *Sepw1-cre* line using the same comparison. I find that *Nr5a1-cre* enriched genes (WT-pure comparison) significantly overlap with genes previously associated with L2/3 neurons (Belgard et al., 2011), but not L4 neurons. This comparison also produced overall fewer upper layer neuronal gene enrichments than were found

using the *Sepw1-cre* line. I discuss this result in the context of our current understanding of the identity of *Nr5a1-cre* labeled neurons. Finally, I consider how differences in the proportion of 'background' unlabeled RNA in the Nr5a1-pure and Sepw1-pure sample types might arise given the sparse and dense neuronal expression patterns of these Cre lines, respectively.

MATERIALS AND METHODS

Layer-specific expression of UPRT and tissue dissection

Mouse strains and tissue preparation were as previously described (Tomorsky et al., 2017). Briefly, homozygous *CA>GFPstop>HA-UPRT* mice (Gay et al., 2013) crossed to *Nr5a1-cre* or *Sepw1-cre* transgenic lines and wild type (WT) mice were processed identically to produce Nr5a1-pure, Sepw1-pure, and WT-pure sample types. The visual cortexes from four mice were collected at P12 for each sample, and three to four samples per condition were prepared. 5–6 hours after 4-thiouracil was injected (430 mg/kg in DMSO), mouse visual cortexes were collected for processing. ~1 mm^2 sections of left and right visual cortexes were dissected in RNAlater and frozen at -80 ºC until RNA extraction and purification.

Immunohistochemistry

Tissue preparation for immunohistochemistry (IHC) was performed as previously described (Tomorsky et al., 2017). Briefly, perfused brains were fixed overnight in 4% PFA (in 1 x PBS), after which brains were immersed in a 30% sucrose solution (in 1 x PBS) for 24–48 hours. Brains were then cryosectioned onto Superfrost Plus slides (Fisherbrand), stored at -80 ºC, and stained as previously described (Tomorsky et al.,

2017). Briefly, slides were treated for 5 min with 300 µL 0.05% trypsin (Thermo Fisher Scientific) (Hoy et al., 2013), washed in PBS and PBST, and blocked for 1–3 h with a solution of 5% donkey and 5% goat serum in PBT. A primary antibody solution of 2 µL/mL of Anti-HA mouse (Covance Research Products Inc. Cat# MMS-101P, RRID:AB_2314672) or 3 µL/mL Anti-Cux1 rabbit (Santa Cruz Biotechnology Cat# sc-13024, RRID:AB_2261231) in block was then applied overnight at 4 ºC. Slides were then washed, and 4 µL/mL of secondary antibodies, mouse-555 (Thermo Fisher Scientific Cat# A-21424 RRID:AB_2535845), mouse-488 (Jackson ImmunoResearch Labs Cat# 715-545-151, RRID:AB_2341099), or rabbit-488 (Jackson ImmunoResearch Labs Cat# 711-545-152, RRID:AB_2313584), in PBT was applied. Slides were incubated with secondary antibodies either overnight at 4 ºC or for 3 h at room temperature, then washed, treated with DAPI (4′, 6-diamidino-2-phenylindole), and mounted using VECTASHIELD mounting media (Vector Labs).

RNA processing and preparation for sequencing

RNA was processed for sequencing as previously described (Tomorsky et al., 2017). Briefly, RNA was extracted from mouse cortical tissue using a TRIzol-chloroform extraction method (Thermo Fisher Scientific). Chloroform extracted RNA was purified on columns as per manufacturer's protocol (PureLink RNA Minikit, Ambion). An Agilent Bioanalyzer (2100) was used to analyze RNA quantity and quality, and an RNA integrity number (RIN) higher than 8.0 was required for subsequent streptavidin purification. A uMACS Streptavidin Kit was used to streptavidin purify biotinylated RNA (10 µL 10X TE and 25 µL 1mg/mL EZ-link Biotin-HPDP in dimethylformamide),

as previously described (Gay et al., 2014). The SMARTer Ultra Low Input RNA Kit for Sequencing – v3 was then used for cDNA synthesis on 5–10 ng of RNA. 1 ng of cDNA was then used to prepare libraries with Illumina's Nextera XT Library Preparation kit, after which 100 bp single-end sequencing was performed on an Illumina HiSeq instrument (Figure 1C).

Sequence Processing and Differential Expression Analysis

Sequence processing and differential expression analysis were performed as previously described (Tomorsky et al., 2017). Briefly, poor quality (Illumina's chastity filter) and overrepresented sequences (CutAdapt python package (Martin, 2011)) were removed, after which sequences were trimmed based on quality using the java program Trimmomatic (Bolger et al., 2014). The mouse genome assembly GRCm38 (downloaded off the Ensembl browser) was used for sequence alignment with the Genomic Short-read Nucleotide Alignment Program (GSNAP) (Cunningham et al., 2014; Wu & Nacu, 2010), and gene alignments were counted using htseq-count in intersection-strict mode (Simon Anders et al., 2014). We next isolated protein coding genes using Ensembl-BioMart (Cunningham et al., 2014) (raw gene counts are available in Supplementary Dataset 1). Differential expression between processed samples from an *Nr5a1-cre; CA>GFPstop>HA-UPRT* cross (Nr5a1-pure) and WT mice not expressing UPRT (WT-pure) was identified using the DESeq package (version 1.24.0) (Anders & Huber, 2012; Simon Anders et al., 2010), as previously described (Tomorsky et al., 2017) (Nr5a1-enriched genes available in Supplementary Dataset 2). Multidimensional scaling analysis was performed using the EdgeR package (Chen et al., 2014; Robinson et al., 2010), and

DESeq identified Nr5a1-enriched genes were examined for layer specificity via comparison to layer enriched genes (400 genes with the highest probability of enrichment in each cortical layer) from an online database (Belgard et al., 2011).

Fluorescent *in situ* hybridization

Fluorescent *in situ* hybridization (FISH) to *Gad1* was performed as previously described to determine whether inhibitory neurons were labeled by *Sepw1-cre* (Lein et al., 2007; Wehr et al., 2009). Briefly, tissue was prepared and sectioned as described for immunohistochemistry, after which 30 µm sections were brought to room temperature, washed 3 x 30 min each in 1 x PBS, and acetylated for 10 min in a 0.25% acetic anhydride solution in 0.1 M triethanolamine HCl (Lein et al., 2007). Slides were then covered with hybridization solution (50% formamide, 10% dextran sulfate, 1 x Denhardt's solution, 1 mg/mL yeast tRNA, 5 x SSC, 0.1% Tween-20, and 0.1 mg/mL heparin in DEPC-treated H_2O), fitted with a coverslip, and pre-hybridized for 2 h in a humidity chamber at 62 °C. The riboprobe to *Gad1* was diluted to a final concentration of 1–2 ng/µL in hybridization solution and was generated using SP6 RNA polymerase in the presence of DIG-labeled nucleotides, using the probe sequence and protocol described by the Allen Brain Institute (Allen Mouse Brain Atlas (2004); Allen Developng Mouse Brain Atlas (2008); Lein et al., 2007).

Slides were hybridized with the *Gad1* probe in hybridization solution overnight at 62 °C. Sections were washed 3 x 30 min each at 62 °C in wash buffer (50% formamide, 0.5 x SSC, 0.1% Tween-20). Slides were washed an additional 4 x 5 min each in TBST, and treated for 20 min with a 2% H_2O_2 solution in TBST. 4 x 5 min

washes in TBST were repeated, and slides were incubated in the blocking solution included in the Tyramide Signal Amplification (TSA) kit (TSA Plus Cyanine 3 System, Perkin Elmer: NEL744001KT) for 4 h. Slides were then coated with an Anti-DIG POD antibody (Roche No. 11207733910, diluted 1:1000 in blocking solution) and allowed to sit at 4 °C overnight. The next day slides were washed 3 x 10 min each with TBST and then washed with the amplification buffer included in the TSA kit for 10 min. Slides were then treated with Cy3 diluted 1:50 in amplification buffer for 45 min, and washed 3 x 10 min with TBST. Slides were then washed in PBS and double labeled via immunohistochemistry, as described above.

Microscopy

In situ hybridizations and immunohistochemistry was imaged using a Zeiss Axio Imager.A2 wide field epifluorescence microscope also having an X-Cite 120Q LED excitation lamp. A Zeiss AxioCam MRm 1.4 megapixel camera and EC Plan-NEOFLUAR 5x/0.16, EC Plan-APOCHROMAT 10x/0.45, or EC Plan-APOCHROMAT 20x/0.8 objectives were used to take images. ZEN lite imaging software (2012) was used to view images, and color processing or in silico background removal were performed using Adobe Photoshop CS6.

Statistical Analysis

To determine whether Nr5a1-enriched genes and database layer-enriched genes significantly overlapped, we used a previously described resampling approach (Tomorsky et al., 2017) (Supplementary Table 1). Briefly, we randomly sampled 1673 genes

(differentially expressed in Nr5a1 samples compared to WT) from the DESeq filtered genes for the Nr5a1–WT comparison and then determined to what degree this random sample overlapped with 400 database genes enriched in each cortical layer (Belgard et al., 2011). This random sampling and determination of overlap was repeated 1000 times to produce a resampling distribution with an estimate of the mean and 95% confidence intervals (CI) for overlapping genes. P-values were calculated as previously described (Tomorsky et al., 2017).

RESULTS

Purification of RNA enriched in layer 4 excitatory neurons in postnatal visual cortex

As in Chapter II, we crossed the *CA>GFPstop>HA-UPRT* mouse line (Figure 1A) (Gay et al., 2014, 2013) to an *Nr5a1-cre* line, which we and others characterized to have enriched expression in excitatory neurons found in L4 of postnatal visual cortex (Figure 2A and 2C) (Gerfen et al. 2013; Harris et al., 2014; Oh et al., 2014; Poulin et al., 2016; Tomorsky et al., 2017; Allen Mouse Brain Connectivity Atlas, 2011). We found that in P12 visual cortex, the *Nr5a1-cre* line generated sparse UPRT expression that appeared enriched in layer 4 (Figure 1B, left) (Tomorsky et al., 2017). To obtain thiol-tagged RNA from neurons labeled by the *Nr5a1-cre* line, we injected 4TU subcutaneously into *Nr5a1-cre; CA>GFPstop>HA-UPRT* double transgenic mice at P12, and 5–6 hours later, dissected out visual cortex. RNA was then extracted from pooled cortical tissue (left and right visual cortexes from 4 animals per sample) and streptavidin purified to isolate labeled RNAs, as described in Methods (subsequently referred to as Nr5a1-pure, Figure 1C). As in Chapter II, WT control samples were produced from mice not expressing

UPRT. After streptavidin purification, the RNA extracted from WT cortexes approximates 'background' mislabeled or unlabeled RNAs (subsequently referred to as WT-pure). Following cDNA synthesis, the Nextera XT kit was used for library preparation after which samples were sent for Illumina sequencing (Figure 1C). This TU-tagging protocol allowed for the preparation of extremely small amounts of RNA for sequencing, which was necessary to produce the low yield WT-pure samples (Tomorsky et al., 2017). Here we characterize the genes enriched in the Nr5a1-pure sample type (WT-pure comparison) and compare these gene enrichments to those found using the same technique with a *Sepw1-cre; CA>GFPstop>HA-UPRT* transgenic cross. *Sepw1-cre* also labels excitatory neurons enriched in upper cortical layers, described in Chapter II (L2/3 enriched) (Figure 1B, right, Figure 2) (Tomorsky et al., 2017).

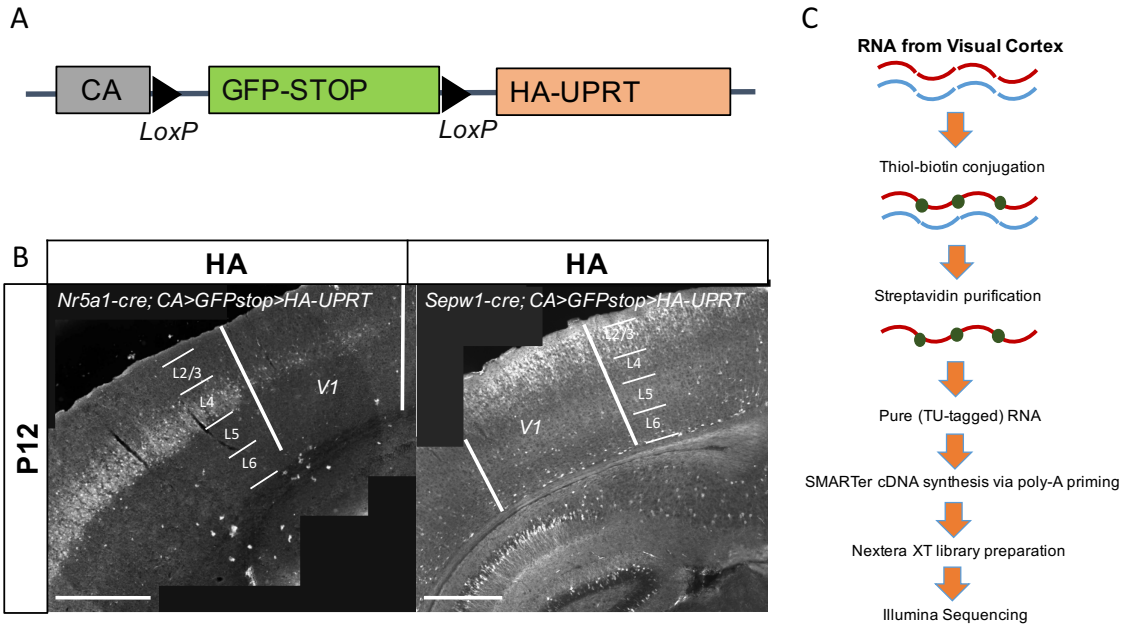

Figure 1. Isolating visual cortex layer enriched transcripts using the TU-tagging technique.
(A) Diagram of the *CA>GFP-stop>HA-UPRT* transgenic construct, from Tomorsky et al., 2017 (Gay et al., 2014, 2013; Tomorsky et al., 2017).

(B) Immunohistochemistry for the HA-tag on the UPRT protein in *Nr5a1-cre; CA>GFPstop>HA-UPRT* (left) and *Sepw1-cre; CA>GFPstop>HA-UPRT* (right) transgenic crosses, modified from Tomorsky et al., 2017 (scale bar = 500 µm).
(C) RNA processing pipeline for all samples, from Tomorsky et al., 2017.

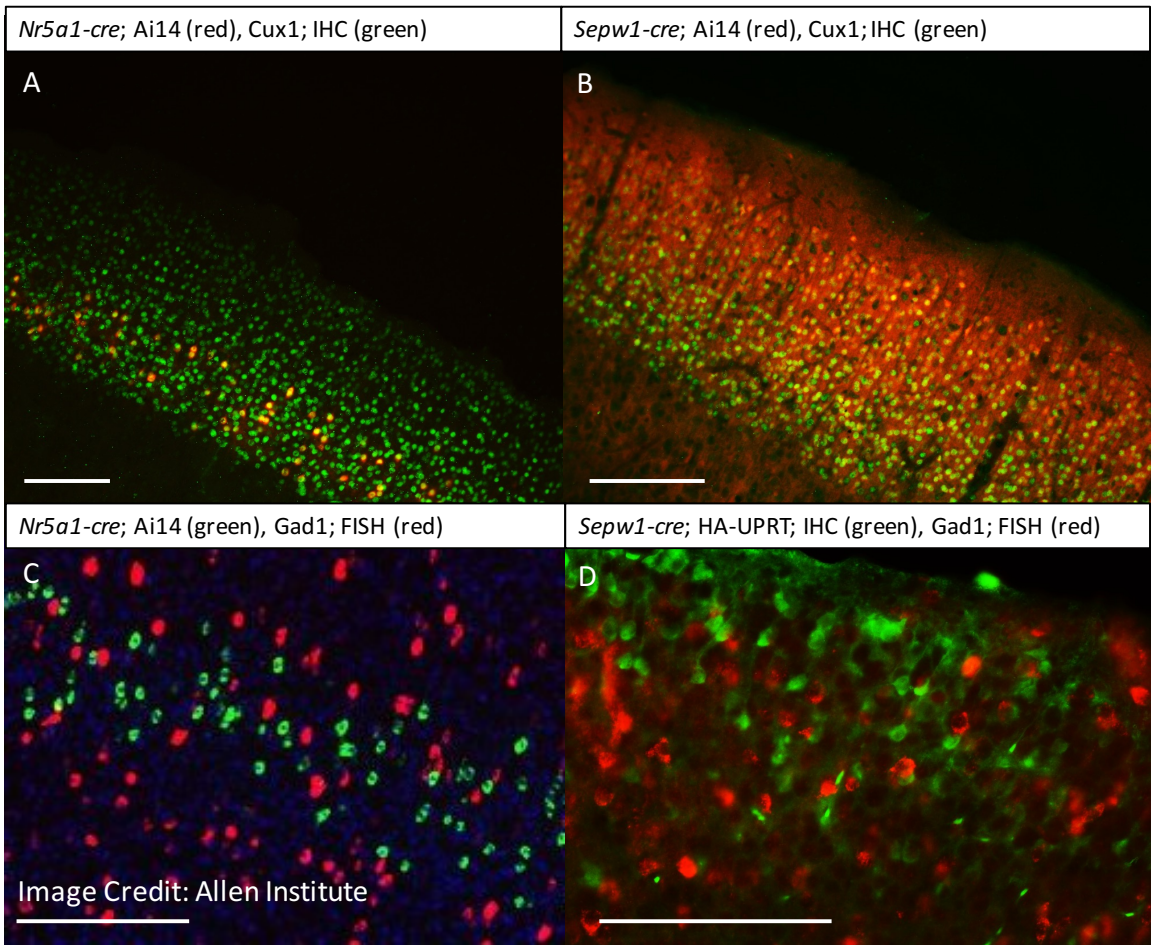

Figure 2. *Nr5a1-cre* and *Sepw1-cre* label populations of upper layer excitatory neurons.
(A) Immunohistochemistry (IHC) for Cux1 overlaps with *Nr5a1-cre; Ai14* positive neurons demonstrating L4 enriched neuronal expression (scale bar = 200 µm).
(B) Immunohistochemistry for Cux1 overlaps with *Sepw1-cre; Ai14* positive neurons demonstrating upper layer neuronal expression enriched in L2/3 (scale bar = 200 µm).
(C) Allen Brain Atlas (Allen Mouse Brain Connectivity Atlas (2011)) characterization showing non-overlapping inhibitory neurons (labeled by fluorescent *in situ* hybridization to *Gad1*, red) and *Nr5a1-cre; Ai14* positive neurons (green) (scale bar = 200 µm).
(D) Characterization showing non-overlapping inhibitory neurons (labeled by fluorescent *in situ* hybridization to *Gad1*, red) and *Sepw1-cre; CA>GFPstop>HA-UPRT* positive neurons (labeled by immunohistochemistry for HA, green), demonstrating *Sepw1-cre* labels excitatory cell types (scale bar = 200 µm).

DESeq differential expression analysis reveals 1673 Nr5a1-enriched transcripts

To find genes with enriched expression in *Nr5a1-cre* labeled neurons in P12 visual cortex, Illumina sequenced transcripts from Nr5a1-pure and WT-pure sample types were aligned to the mouse genome (Cunningham et al., 2014) using the Genomic Short-read Nucleotide Alignment Program (GSNAP) (Wu & Nacu, 2010). Sequences that aligned to a particular gene were counted using the python program htseq-count (Simon Anders et al., 2014). The EdgeR package was used to visualize normalized and filtered read counts by multidimensional scaling analysis, considering the top 500 genes with the largest log fold change differences for each sample type (Chen et al., 2014; Law et al., 2016; Robinson et al., 2010). The Nr5a1-pure and WT-pure sample types formed distinct clusters when visualized by this method (Figure 3A). Next DESeq was used to assess overall differential expression between Nr5a1-pure and WT-pure sample types using a negative binomial distribution to model the data (Figure 3B). This analysis found 1673 genes that were enriched in the *Nr5a1-cre* labeled neurons relative to the WT-pure sample type (Figure 3C, Supplementary Dataset 2).

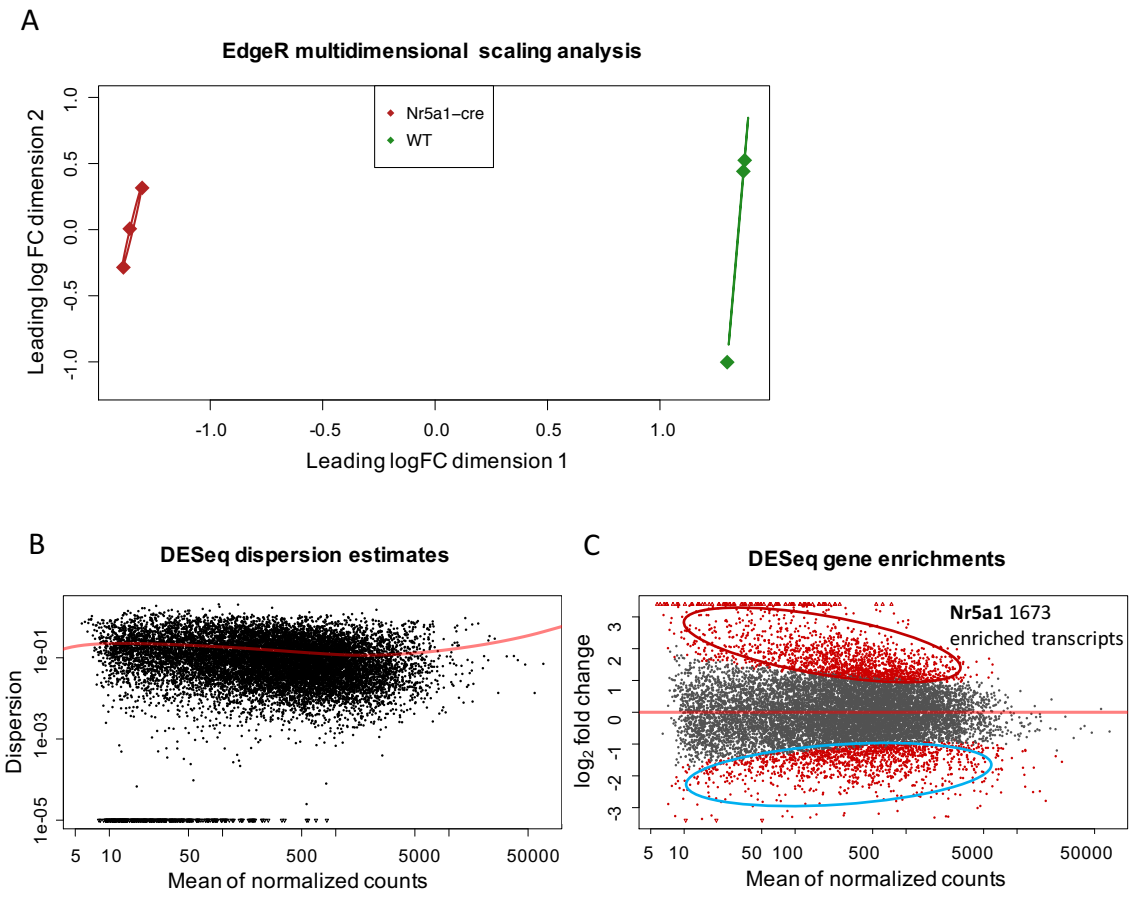

Figure 3. MDS clustering of sample types and differential expression analysis.
(A) MDS analysis was performed using EdgeR on Nr5a1-pure and WT-pure samples after RNA-seq and bioinformatic processing of count data. The two groups formed distinct clusters.
(B) DESeq dispersion estimates of count data for the Nr5a1-pure to WT-pure sample type comparison modeled using a negative binomial distribution.
(C) 1673 genes were found enriched in the Nr5a1-pure samples as compared to WT-pure samples after DESeq differential expression analysis using filtered and normalized gene counts.

Genes enriched in Nr5a1-pure samples resemble those enriched in Sepw1-pure samples at P12

We next examined the cell types and cortical layers in which Nr5a1-enriched genes (WT-pure comparison) were previously found to be expressed. Since *Nr5a1-cre* labels upper layer excitatory neurons (Figure 1 and Figure 2), we expected to find genes

expressed in neurons and upper layers of cortex ('signal') among the Nr5a1-enriched transcripts. Genes expressed in endothelial cells or lower cortical layers were not expected to be enriched in this experiment and can be thought of as contaminating background or 'noise'. To estimate the degree of neuronal representation, genes enriched in Nr5a1-pure samples were compared to the top 500 neuronal or endothelial enriched genes found using an online database (Zhang et al., 2014) (Cell type enrichment generator, genes enriched in neurons relative to endothelial cells and vice versa). For an unbiased description of layer-enriched genes, we used an online transcriptomic atlas of mouse neocortical layers (Belgard et al., 2011). Though this database was created using adult mice, we hypothesized that many layer-specific genes would have consistent expression patterns from P12 through to adulthood (Table 1, Figure 4).

The Nr5a1–WT comparison yielded a significant number of Nr5a1-enriched genes expressed highly in both neurons and upper cortical layers (differences from resampled estimates, Supplementary Table 1, Table 1, Figure 4C). A significant number of L6 genes were also found to overlap with Nr5a1-enriched genes. The number of Nr5a1-enriched genes overlapping with L4 genes (37 transcripts) was barely insignificant (estimated p-value = 0.053, Supplementary Table 1). There was a high degree of similarity between Sepw1- (Tomorsky et al., 2017) and Nr5a1-gene enrichments using the WT-pure comparison (1388 overlapping genes), indicating the upper cortical-layer excitatory neurons labeled by the *Sepw1-cre* and *Nr5a1-cre* lines have comparable gene expression at P12 (Figure 4A). Of the genes that did not overlap, 67 of the 519 Sepw1-enriched and only 4 of the 285 Nr5a1-enriched corresponded with database upper-layer genes (Figure 4A).

Because each streptavidin-purified sample can be considered a combination of tagged-RNA 'signal' and 'noise' (see discussion) (Tallafuss et al., 2014), we conclude that the Sepw1-pure sample type contained proportionally higher levels of 'signal' than the Nr5a1-pure sample type, consistent with relative levels of UPRT gene expression in visual cortex (Figure 1, Figure 2, and Figure 4B). Given this, it is not surprising that a direct comparison of the Sepw1-pure and Nr5a1-pure sample types yielded a significant number of upper-layer and neuronal genes among the Sepw1-enriched transcripts, while the Nr5a1-enriched (Sepw1-depleted) transcripts demonstrated a depletion of this 'signal' and an enrichment of 'noise' (Table 1).

	Pure to WT-pure comparison		**Sepw1-pure to Nr5a1-pure comparison**	
Neuron type	Sepw1	Nr5a1	Sepw1	Nr5a1 (Sepw1-depleted)
Number enriched (padj = 0.1)	1907	1673	636	485
Neuronal	129	93	78	8
Endothelial	27	30	3	39
L23	117	76	103	4
L4	59	37	38	4
L5	55	53	6	14
L6	45	52	12	22
L6b	47	49	15	17
Unpatterned	40	43	11	9

Table 1. Number and type of transcripts enriched in upper layer neuronal cell types using different comparisons.
Genes significantly enriched in neurons or endothelial cells (500 top enriched genes from an online database (Zhang et al., 2014)), or various cortical layers (400 top enriched genes from an online database (Belgard et al., 2011)) were compared to the genes most

significantly enriched in Sepw1-pure and Nr5a1-pure samples when compared to WT-pure sample types, or when compared directly to one another. Blue text demonstrates significant depletion and red text indicates significant enrichment based on differences from the resampled distributions listed in Supplementary Table 1 with a p-value ≥ 0.05.

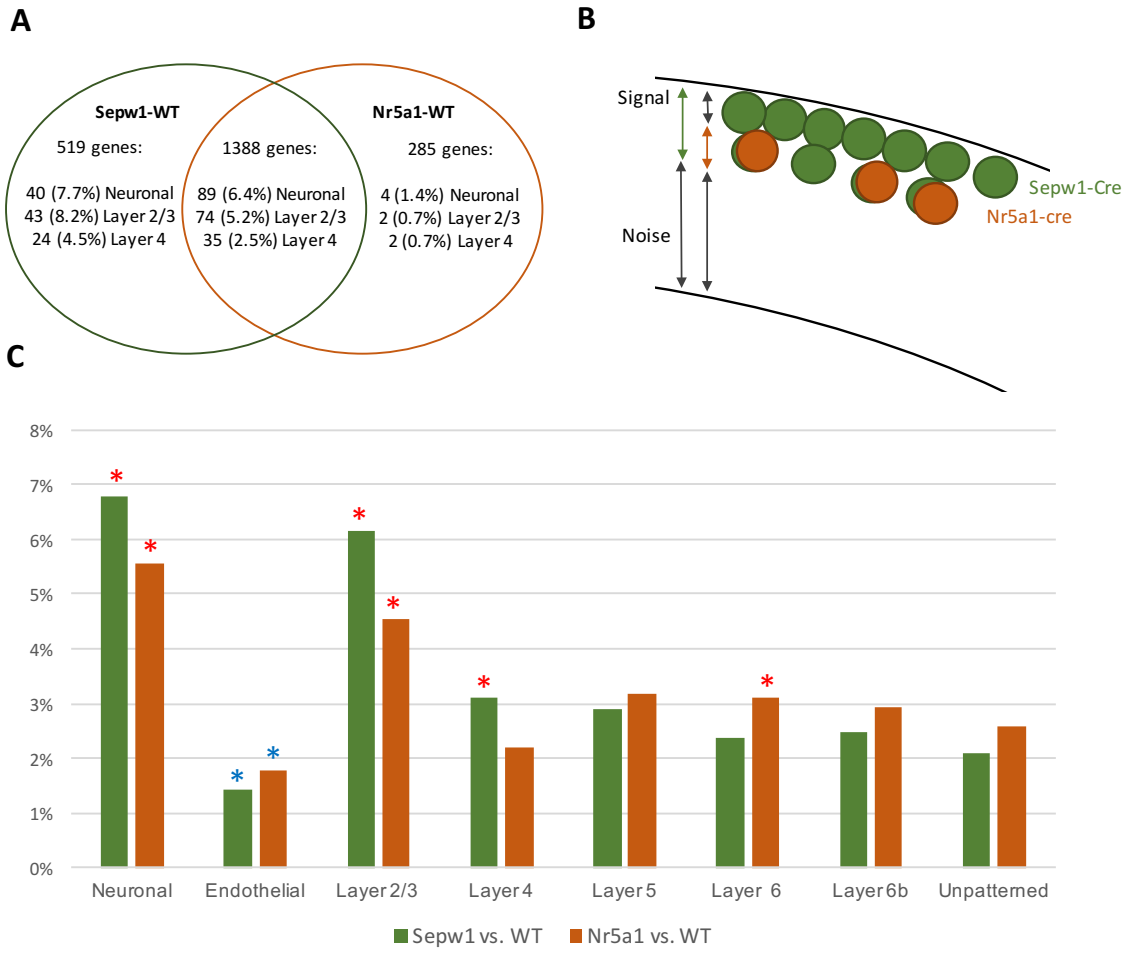

Figure 4. Comparison of genes enriched in Sepw1-pure vs. Nr5a1-pure samples when compared to a WT-pure control.
(A) Venn diagram showing the number and proportion of genes that are upper-layer enriched when Sepw1-pure and Nr5a1-pure samples are compared to WT-pure samples. Many of the same genes (1388) are enriched in both Sepw1-pure and Nr5a1-pure sample types when compared to WT-pure samples.
(B) Diagram explaining the relative representation of signal and noise in Sepw1-pure and Nr5a1-pure samples. When directly compared, the 'signal' from the *Nr5a1-cre* line would be washed out by the proportionally higher upper-layer neuronal 'signal' from the *Sepw1-cre* line. In addition, the proportionally higher 'noise' in Nr5a1-pure samples would appear Nr5a1-enriched (Sepw1-depleted) after DESeq differential expression analysis.

(C) DESeq differential expression analysis yielded 1673 or 1907 genes found to be Nr5a1-enriched or Sepw1-enriched, respectively, when WT-pure was used as a template. These enriched gene sets were compared to 500 database enriched neuronal or endothelial genes or 400 database genes found to be enriched in various cortical layers (Belgard et al., 2011; Zhang et al., 2014). The percentage of Nr5a1- or Sepw1-enriched genes from different comparisons that overlap with database genes found to be neuronal, endothelial, or layer enriched, is shown. Significance was determined using a resampling approach to estimate the means and associated confidence intervals expected by chance when neuronal, endothelial, or layer enriched genes were identified in a randomly selected group of 1647 (or 1907) genes (Supplementary Table, S1). Asterisks label percent overlaps found to be significantly (p-value ≥ 0.05) above (red) or below (blue) those expected to occur by chance.

DISCUSSION

In this chapter, we identify and compare genes found to be enriched in *Nr5a1-cre* vs *Sepw1-cre* labeled neurons, isolated using the TU-tagging technique. We selected Cre lines based on their relative expression in different cortical layers, but layer enriched Cre lines are not necessarily layer specific and may still label, to a lesser degree, cell types found in other layers. Even layer specificity must be distinguished from cell-type specificity, with each layer being composed of several different cell types (Poulin et al., 2016). A recent characterization of the cell types labeled by different Cre lines in mouse visual cortex found that *Nr5a1-cre* labels five different excitatory cell types, three of which are in found in L4, with the remaining two falling in L2/3 and 5a (Poulin et al., 2016). This study also characterized the cell types labeled by *Cux2-cre*, a driver line traditionally associated with being specific to L2/3 and L4 (Cubelos et al., 2010, 2008; Nieto et al., 2004; Poulin et al., 2016). Even this line was found to label cells identified as layer 5a excitatory neurons, in addition to six additional cell types spanning L2/3 and L4. Similarly, a close examination of the *Sepw1-cre* line reveals L2/3 enrichment, with some sparse labeling of cells in deeper cortical layers. Though expression level appears

reduced in the subset of cells that are labeled outside L2/3, there appears to be some degree of overlap with the deeper layers labeled by Cux1 (overlapping expression with Cux2), indicating *Sepw1-cre* may also label cell types spanning layers 2/3-5a (Figure 2B) (Cubelos et al., 2010, 2008; Nieto et al., 2004).

Besides being sparser, *Nr5a1-cre* labeled cell types are also likely a subset of those labeled by *Sepw1-cre* (Figure 4B). Supporting this idea, the genes enriched in Sepw1-pure and Nr5a1-pure sample types using the WT-pure comparison are largely the same (1388 overlapping gene enrichments, Figure 4A), with differences between the two attributed to either higher levels of upper layer-enriched genes (Sepw1-pure) or cell-type non-specific noise (Nr5a1-pure) (Figure 1, Table 1, Figure 4). One L2 excitatory cell type labeled by *Cux2-cre* and not *Nr5a1-cre* was defined by the gene marker *Ngb*, which is Sepw1-enriched when compared to Nr5a1-pure sample types (Poulin et al., 2016). The Sepw1-pure to WT-pure comparison, on the other hand, should identify genes found in a greater number of cell types, diluting the L2/3 specific fraction of gene enrichments. In this way, the Sepw1-pure to Nr5a1-pure comparison described in Chapter II, may help limit the number of cell types to which Sepw1-enriched genes can be ascribed. Since there are very few transgenic lines that label one cell type exclusively, this type of comparative exclusion may prove useful for narrowing in on gene enrichments specific to particular cell types.

Keeping in mind the overall cell-type composition of the Cre lines used in this study may help to explain the gene enrichments produced using the Sepw1–WT (Chapter II) and Nr5a1–WT comparisons (Table 1). The presence of L4 gene enrichments using the Sepw1–WT comparison can be explained by the composition of cell types labeled by

the *Sepw1-cre* line, which is enriched in but not specific to layer 2/3. Considering the composition of the *Nr5a1-cre* line, we expected to see both L2/3 and L4 gene enrichments using a WT-pure comparison. While we saw a significant overlap with genes categorized as L2/3 enriched with this comparison, the overlap of Nr5a1-enriched genes with L4 transcripts was barely insignificant (p-value = 0.052, Supplementary Table 1). In addition, there was a significant overlap between Nr5a1 genes and transcripts enriched in L6 (p-value = 0.007, Supplementary Table 1). There are many possible technical and biological reasons why L2/3 but not L4 genes appeared significantly enriched in the Nr5a1-pure sample type. One technical consideration is that the database used here to estimate our success in identifying upper layer-enriched genes was constructed using data from a microarray study of adult cortex where different layers were isolated by dissection. Unfortunately, dissection techniques can be prone to error, and indeed, a great amount of overlap between L2/3 and L4 gene enrichments is observed in this database (125 of 400 L2/ 3 and L4 enriched genes overlap). Since Nr5a1-labeled cells send many of their projections toward upper layers, many genes enriched in these neuronal cell types may show up in a dissected L2/3 sample. While this database (Belgard et al., 2011) worked well to approximate the success of our experiment in identifying layer enriched genes, it should not be taken as an absolute description of genes enriched in developing layer-specific cell types.

In this study, imperfect purification techniques require that we not only consider the cell types being compared, but also the level of unlabeled or mislabeled RNA in our purified samples. UPRT expression was sparser in the *Nr5a1-cre* line than in the *Sepw1-cre* line (Figure 1B). This appears reflected in the smaller proportion of neuronal genes

found to overlap with Nr5a1- vs Sepw1-enriched genes (WT-pure comparison) (Table 1, Figure 4C). Proportional to neuronal 'signal' RNA, there seemed to be relatively higher non-neuronal 'noise' in the Nr5a1-pure samples as compared to the Sepw1-pure samples. Based on average percent yields for Nr5a1-pure, Sepw1-pure and WT-pure samples, the percent 'noise' from unlabeled or mislabeled RNAs could be estimated to be ~2.9% for the Nr5a1 samples and ~2.4% for the Sepw1 samples (data not shown). The proportionally higher levels of background RNA in the Nr5a1-pure samples likely contributed to increased non-neuronal and deep cortical layer Nr5a1-gene enrichments (WT-pure comparison) (Table 1, Figure 2, Figure 3). When directly compared, the Sepw1-pure sample type demonstrated an enrichment of L2/3 neuronal 'signal' and the Nr5a1-pure sample type demonstrated an enrichment of non-neuronal background (Table 1). This is an expected outcome based on the sample types compared. In this way, the Sepw1–Nr5a1 comparison worked well to eliminate background RNA from the Sepw1-pure gene enrichments, but was unable to isolate L4 neuronal genes from Nr5a1-enriched transcripts.

There are several possible biological explanations for the high degree of overlap found between L2/3 genes and Nr5a1-enriched transcripts (WT-pure comparison). This L2/3 enrichment may indicate that at P12, *Nr5a-cre* is either labeling L2/3 cells most strongly, or is labeling immature L4 cells with transcriptional profiles resembling L2/3 neurons. In either case, it is likely that the transcriptional profile Nr5a1-labeled cells changes between P12 and maturity. The idea of cells existing as strictly defined cell types is beginning to change, with cell identity being thought of more as a continuum of different morphologies and functions (Cembrowski & Menon, 2018; Fishell & Heintz,

2013; Luo et al., 2008). A functional characterization of cells labeled by *Nr5a1-cre* has not been performed this early in development. However, in older mice, functionally defined L3 and L4 cells have been found after recording the electrophysiological properties of *Nr5a1-cre* neurons (personal communication, J. Hoy and A. Weible). The presence of *Nr5a1-cre* labeled L3 cells could explain the strong enrichment of genes associated with adult L2/3 neurons among *Nr5a1-cre* transcripts. On the other hand, the significant overlap between Nr5a1-enriched genes and genes enriched in L6 might also be biologically relevant, since there are many functional similarities between L4 and L6 neurons. This could support the idea that *Nr5a1-cre* cells are immature L4 neurons that are transcriptionally similar to L3 and L6 neurons at P12. It has been suggested that neuronal cell types may have similar expression patterns when immature, only to take on more specific characteristics after developing distinct functional properties during critical periods of development (Fishell & Heintz, 2013). This is the first time the transcriptional profile of *Nr5a1-cre* neurons has been shown at P12, and suggests that young *Nr5a1-cre* neurons may be transcriptionally distinct from mature neurons labeled by the same Cre line.

BRIDGE TO CHAPTER IV

In the visual system, eye opening stands out as a major development turning point for cortical development. With the influx of visually evoked neuronal activity, the system must adapt and respond to input from the periphery through changes in gene expression and activity. While several studies have examined gene expression in visual cortex over development, in Chapter IV, I provide the first transcriptomic study of genes regulated in the period immediately surrounding eye opening. Here, I examine genes with regulated

expression levels over eye opening both in all of cortex and in layer 2/3 neurons (isolated using the TU-tagging technique). Examining all of cortex, I found evidence that the cell type composition of visual cortex changes from just before (P12) to after (P16) eye opening, with an increase in non-neuronal, and specifically oligodendrocyte and astrocytic, gene expression. I also categorized genes enriched in layer 2/3 cortical neurons with changing expression levels during this developmental period by gene ontology analysis. I found that genes enriched at P12 were largely involved in neuron projection development and genes enriched at P16 were largely involved in developmental regulation and synaptic transmission. This is the first study to examine broad changes in gene expression focusing on a narrow developmental window surrounding eye opening (P12–P16), and provides a rare glimpse into the processes regulating the development of all visual cortex as well as a subset of upper layer cortical neurons at this time.

CHAPTER IV

TRANSCRIPTOMIC ANALYSIS OF GENE REGULATION OVER EYE OPENING IN ALL VISUAL CORTEX AND IN LAYER 2/3

INTRODUCTION

Developmental neuroscience has increasingly relied on gene-expression studies over developmental to assess which genes are up or down regulated as the brain goes through distinct developmental stages. Many early transcriptional studies examining the development of visual cortex (V1) have focused on identifying genes associated with or modulated during the critical period for ocular dominance plasticity (ODP) (Benoit et al., 2015; Lyckman et al., 2008; Majdan & Shatz, 2006; Prasad et al., 2002; Tropea et al., 2006; Yang, Pan, Zhou, Lin, & Wu, 2009). This is a developmental period of enhanced synaptic plasticity in visual cortex occurring between P21 and P35, where manipulations to visual activity can cause large changes in synapse number and function (Majdan & Shatz, 2006). Several genes have been identified with up or downregulated expression during the critical period for ODP (Lyckman et al., 2008; Prasad et al., 2002; Yang et al., 2009). Interestingly many of these genes have been found to reverse their transcriptional regulation when visual input is manipulated through monocular deprivation, indicating that genes important for ODP may be tightly regulated by activity (Lyckman et al., 2008). One study found several genes whose expression is correlated with visual activity exclusively at certain developmental time points either before (P18), during (P28) or after (P60) the critical period for ODP, again indicating tight regulation of activity dependent genes expression during this period of postnatal development (Lyckman et al., 2008;

Majdan & Shatz, 2006). However, it is unknown how and whether these genes are regulated during the developmental onset of vision to prepare the brain for this period of enhanced plasticity.

Recently, it has become possible to refine developmental transcriptomic studies to isolate genes expressed during the development of distinct brain regions or cell types (Fertuzinhos et al., 2014; Tallafuss et al., 2014). A recent study examined the development of V1 with both spatial and temporal specificity by dissecting out distinct cortical layers, and comparing V1 to prefrontal cortex at P5, P26, and P180 (Benoit et al., 2015). This study mapped gene expression patterns across cells found in different cortical layers over development, and identified several genes with layer or area specific expression (Benoit et al., 2015). Specifically, they found genes enriched in layer 2/3 (L2/3) were largely involved in cytoskeletal assembly, calcium signaling, *Mapk* signaling and long term potentiation, suggesting these neurons are capable of high levels of synaptic plasticity (Benoit et al., 2015). This study, while large in scope, focused on three developmental time points separated by several weeks or months of development. Many developmental processes may be missed when comparing transcriptomes at such different ages, leaving the question of how and when L2/3 neurons develop their uniquely plastic expression type unanswered.

While gene regulation involved in ODP has largely been the focus of developmental transcriptomic studies in V1, similar studies in other sensory cortical regions have narrowed in on developmental gene regulation modulated by the onset of sensory activity (Fertuzinhos et al., 2014; Hackett et al., 2015). One study examined gene expression profiles by RNA-seq in auditory cortex before and after the onset of hearing

(P12) by isolating tissue at P7, P14, and P21 (Hackett et al., 2015). This study found the greatest number of differentially expressed genes between P7 and P14, indicating that the onset of sensory experience was a major regulator of gene expression (Hackett et al., 2015). Another study, which examined gene expression differences between dissected supragranular (L2/3), granular (L4) and infragranular (L5 and L6) layers in postnatal somatosensory cortex over development, also found significant changes in gene expression with the onset of whisking activity around P11 (Fertuzinhos et al., 2014). This study observed that SgL neurons appeared particularly sensitive to the onset of whisking, with an increase in the expression genes associated with activity (immediate early genes, IEG) in these layers occurring between P10 and P14. Interestingly, deeper layers experienced upregulated IEG expression at earlier developmental time points (Fertuzinhos et al., 2014). While these previous studies examined gene regulation with the onset of sensory input in auditory and somatosensory cortical regions, changes in gene expression with the developmental onset of visual experience in V1 have yet to be described.

In this chapter, we examine gene expression in visual cortex before and after the onset of visually driven activity at eye opening (~P14). There is approximately one week of development before the onset of the critical period for ODP, where visually-driven activity in V1 may guide the maturation of cortical circuits (Majdan & Shatz, 2006). Few studies have focused on this period, and a comprehensive analysis of genes specifically regulated with eye opening, before the onset of the critical period, has yet to be explored (Majdan & Shatz, 2006; Yang et al., 2009). This is known to be a time of intense synaptogenesis in V1, corresponding with the developmental shift from vision

independent to visually guided synaptic establishment (Desai et al., 2002; Hooks & Chen, 2007; Lu & Constantine-Paton, 2004; Shen & Colonnese, 2016). Here, we identify genes with regulated expression levels over a four-day period surrounding eye opening, extracting V1 cortical tissue at P12 and P16 and examining the differential expression of genes between these time points. In this way, we isolated genes developmentally regulated by visual input but not specifically associated with the unique plasticity observed during the critical period for ODP (Majdan & Shatz, 2006).

As in Chapter II, here we also examine gene expression in L2/3 excitatory neurons at eye opening using the TU-tagging technique to isolate L2/3 enriched transcripts (Chatzi et al., 2016; Gay et al., 2014, 2013; Miller et al., 2009; Tomorsky et al., 2017). The TU-tagging technique allows for the spatial and temporal isolation of newly transcribed RNAs for RNA-seq (Gay et al., 2014, 2013; Miller et al., 2009; Tomorsky et al., 2017). This technique does not require cell isolation or dissection, as was used for previous studies of layer-specific gene expression over cortical development (Benoit et al., 2015; Fertuzinhos et al., 2014). This allowed us to identify RNAs expressed in a specific excitatory neuronal cell type enriched in L2/3, while preserving RNAs transcribed in axonal and dendritic processes. A previously published study (Tomorsky et al., 2017) (Chapter II) examined gene expression in L2/3 neurons at P12 using the TU-tagging technique. Here, we add to this study by using the same method to identify genes expressed in the same L2/3 neurons at P16. We discovered a set of genes enriched in these neurons at P16 that were not enriched at P12, most of which had gene ontology-predicted roles in metabolism or transcriptional regulation. Finally, we isolated genes enriched in L2/3 neurons that are also developmentally regulated with eye opening

(overlapping with gene differentially expressed in all of cortex between P12 and P16). This is the first study to examine genes enriched in visual cortex during a narrow developmental window surrounding eye opening (P12–P16) and describes genes regulated in a population upper-layer cortical neurons during this time.

MATERIALS AND METHODS

Layer-specific expression of UPRT and tissue dissection

Mouse strains and tissue preparation were as previously described (Tomorsky et al., 2017). Briefly, *Sepw1-cre* or *Nr5a1-cre* transgenic lines were crossed to homozygous *CA>GFPstop>HA-UPRT* mice (Gay et al., 2013) and processed identically to produce Sepw1-pure or Nr5a1-pure sample types at P16 (Figure 1). Both left and right mouse visual cortexes were stereotaxically marked (2.5 mm from the midline and 1 mm from the back suture) and dissected (~1 mm square sections) in RNAlater, 5–6 hours after subcutaneous injection with 4-thiouracil (430 mg/kg in DMSO). Visual cortexes were stored in RNAlater per manufacturer's instructions at -80 ºC until use. Before purification, 'total' RNA from all V1 was saved at P12 (Tomorsky et al., 2017) and P16 for differential expression analysis between these two time points. Four mice were used per sample, and three (*Sepw1-cre*, P16) to four (*Nr5a1-cre*, P16) samples per condition were streptavidin purified. Seven 'total' RNA samples from both Sepw1 and Nr5a1 crosses at P12 and P16 were used for differential expression analysis to identify gene expression changes in all V1 between these time points.

Immunohistochemistry

Tissue preparation for immunohistochemistry (IHC) was performed as previously described (Tomorsky et al., 2017). Briefly, brains were prepared for IHC by first fixing perfused brains overnight in 4% PFA (in 1 x PBS), after which brains were immersed in 30% sucrose (in 1 x PBS) for 24–48 hours. Brains were cryosectioned to 30 µm, placed on Superfrost Plus slides (Fisherbrand) for storage at -80 ºC, and then stained as previously described (Tomorsky et al., 2017). Briefly, slides were immersed in 0.05% trypsin for 5 min (Thermo Fisher Scientific) (Hoy et al., 2013), washed in PBS and PBST, and blocked for 1–3 h in 5% goat and 5% donkey serum in PBT. A primary antibody solution of 2 µL/mL of Anti-HA mouse (Covance Research Products Inc. Cat# MMS-101P, RRID:AB_2314672) in block was then applied overnight at 4 ºC. After washing, 4 µL/mL of mouse-555 secondary antibody (Thermo Fisher Scientific Cat# A-21424 RRID:AB_2535845) in PBT was applied, and slides were incubated either for 3 h at room temperature or overnight at 4 ºC. Slides were then washed, treated with DAPI (4′, 6-diamidino-2-phenylindole), and mounted (VECTASHIELD mounting media, Vector Labs).

RNA processing and preparation for sequencing

RNA was processed for sequencing as previously described (Tomorsky et al., 2017). Briefly, RNA was extracted from mouse cortical tissue using TRIzol (Thermo Fisher Scientific) and chloroform. Chloroform extracted RNA was purified using a PureLink RNA Minikit (Ambion) as per manufacturer's instructions. Total RNA from all V1 was saved from tissue extracted from both *Sepw1-cre, CA>GFP-stop>HA-UPRT* and

Nr5a1-cre, CA>GFP-stop>HA-UPRT crosses at P12 and P16 for differential gene expression analysis between these time points. An Agilent Bioanalyzer (2100) was used to determine RNA quality, and we required each sample have an RNA integrity number (RIN) higher than 8.0. To produce 'purified' sample types, RNA was biotinylated (10 µL 10X TE and 25 µL 1 mg/mL EZ-link Biotin-HPDP in dimethylformamide) and purified using a uMACS Streptavidin Kit, as previously described (Gay et al., 2014). cDNA was prepared using a SMARTer kit with 5–10 ng of RNA (SMARTer Ultra Low Input RNA Kit for Sequencing – v3). 1 ng of cDNA was used to prepare all libraries using the Nextera XT Library Preparation kit (Illumina). Pools of 6 samples each were then sequenced on an Illumina HiSeq instrument (100 bp single-end sequencing) (Figure 2).

Sequence Processing and Differential Expression Analysis

Sequence processing and differential expression analysis were performed as previously described (Tomorsky et al., 2017). Briefly, sequences that were overrepresented (CutAdapt python package (Martin, 2011)) or of poor quality (Illumina's chastity filter) were removed, after which Trimmomatic (Java) was used for the quality trimming of sequences (Bolger et al., 2014). The mouse genome assembly GRCm38 (downloaded off the Ensembl browser) was used for sequence alignment with the Genomic Short-read Nucleotide Alignment Program (GSNAP) (Cunningham et al., 2014; Wu & Nacu, 2010), and gene alignments were counted using htseq-count (Python) in intersection-strict mode (Simon Anders et al., 2014). We then identified and isolated the protein coding genes from our gene counts using Ensembl-BioMart (Cunningham et al., 2014) (raw gene counts are available in Supplementary Dataset 1). DESeq (version

1.24.0) (Anders & Huber, 2012; Simon Anders et al., 2010) was used to assess differential gene expression between *Sepw1-cre; CA>GFPstop>HA-UPRT* (Sepw1-pure) and *Nr5a1-cre; CA>GFPstop>HA-UPRT* (Nr5a1-pure) transgenic crosses at P16 (Supplementary Dataset 3), as well as between RNA samples collected from all V1 at P12 and P16 (Supplementary Dataset 4). A multidimensional scaling analysis was performed using the EdgeR package (Chen et al., 2014; Robinson et al., 2010). Sepw1-enriched genes were then compared to layer enriched genes from an online database (Belgard et al., 2011) to assess layer specificity.

Microscopy

Immunohistochemistry was imaged using a Zeiss AxioCam MRm 1.4 megapixel camera and an EC Plan-NEOFLUAR 5x/0.16 objective on a Zeiss Axio Imager.A2 wide field epifluorescence microscope having an X-Cite 120Q LED excitation lamp. ZEN lite imaging software (2012) was used for in silico background removal. Adobe Photoshop CS6 was used for the color processing of images.

Functional analysis, Gene Ontology, and DAVID analysis

To determine potential functional categories of genes enriched at P12 or P16 in *Sepw1-cre* labeled neuronal cell types, we performed gene ontology (GO) analysis using GO-TermFinder (Boyle et al., 2004) (go.princeton.edu) with a p-value cutoff of 0.01 and the MGI annotation. For genes that were both L2/3 enriched and developmentally regulated, GO-enriched categories were visualized using tree maps produced with REVIGO (http://revigo.irb.hr/) (Supek et al., 2011) (Figure 9). To determine the

functional categories of genes enriched in Sepw1-pure sample types exclusively at P12 or P16, we used both GO-TermFinder and the DAVID 6.8 functional annotation tool found at https://david.ncifcrf.gov (Huang, Sherman, & Lempicki, 2009). Terms shown in Figure 4 that represent functional annotation clusters found using DAVID are identified in the figure legend. DAVID functional annotation clustering was also used to identify the functions of genes up and down regulated with eye opening in all visual cortex. Figure 6 shows the top 20 clusters identified using DAVID, plus a select 6–7 clusters with lower enrichment scores and functions important for synapse formation, adhesion, or development. DAVID enrichment scores are plotted on the x-axis. Finally, we examined genes identified in a previous publication as having functional roles in synapse formation, experience dependent activity, inhibitory neurotransmission, excitatory neurotransmission, axonogenesis, or dendritogenesis (Fertuzinhos et al., 2014). The DESeq calculated log fold changes from P12 to P16 for each of these genes was plotted to identify trends in expression patterns over this time. Genes with a DESeq adjusted p-value < 0.1 are marked with an asterisk.

Statistical Analysis

To determine whether Sepw1-, P12-, or P16-enriched genes overlapped with layer- or cell type-enriched database genes to a degree that was significantly greater than expected by chance, we used a previously described resampling approach (Tomorsky et al., 2017) (Supplementary Table 1). Briefly, we randomly sampled 367 (enriched in Sepw1 samples compared to Nr5a1 samples at P16), 1421 (enriched in all cortex at P12), or 1674 (enriched in all cortex at P16) genes from the DESeq filtered gene counts for the

Sepw1–Nr5a1 (P16) or P12–P16 (all V1) comparisons. It was then determined whether the randomly sampled subsets overlapped with database genes found enriched in each cortical layer (Belgard et al., 2011), or cell type (Cahoy et al., 2008). This random sampling and overlap determination was repeated 1000 times for each layer or cell type per condition. In this way, we produced estimates of the mean, 95% confidence intervals (CI), and a P-value for each condition, as previously described (Tomorsky et al., 2017).

RESULTS

Purification of RNA enriched in upper layer excitatory neurons in postnatal visual cortex at P16

Nr5a1-cre and *Sepw1-cre* lines were used to isolate cell-type specific RNA from different populations of upper layer cortical neurons. These same Cre lines were used in Chapter II to isolate cell-type specific RNA at P12, and this comparison is discussed at length in Chapters II and III (Tomorsky et al., 2017). As in Chapters II and III, we crossed the *CA>GFPstop>HA-UPRT* mouse line (Gay et al., 2014, 2013) to *Sepw1-cre* and *Nr5a1-cre* lines, which we and others characterized to have enriched expression in excitatory neurons found in L2/3 and L4 of postnatal visual cortex, respectively (Figure 1) (Gerfen et al., 2013; Harris et al., 2014; Oh et al., 2014; Poulin et al., 2016; Tomorsky et al., 2017; Allen Mouse Brain Connectivity Atlas (2011)). We found that in P16 visual cortex, the *Nr5a1-cre* line produced UPRT expression that appeared enriched in L4, while the *Sepw1-cre* line produced UPRT expression that appeared enriched in L2/3 (Figure 1) (Tomorsky et al., 2017). The *Nr5a1-cre* line exhibits sparse UPRT expression as compared to the *Sepw1-cre* line. In addition, the

Nr5a1-cre line likely labels a subset of the neurons labeled by *Sepw1-cre*, which has enriched expression in L2/3 but is also expressed to a lesser degree in L4. In this study, as in Chapter II, a comparison of RNA extracted from *Sepw1-cre* and *Nr5a1-cre* neurons is used specifically to identify Sepw1-enriched genes. This comparison should help to isolate L2/3 specific genes, since L4 specific genes should have similar expression levels between the two sample types.

To obtain thiol-tagged RNA from *Sepw1-cre* or *Nr5a1-cre* labeled neurons, we injected 4TU subcutaneously into transgenic mice double positive for the *CA>GFPstop>HA-UPRT* transgene and either *Sepw1-cre* or *Nr5a1-cre* at P16, and dissected out visual cortex 5–6 hours later (see Methods). RNA was extracted and biotin/streptavidin purified to produce samples enriched with transcripts that were thiol-labeled in both neuronal cell types (subsequently referred to as Sepw1-pure and Nr5a1-pure sample types, Figure 2). Following cDNA synthesis, the Nextera XT kit was used for library preparation, after which samples were sent for Illumina sequencing (Figure 2). We characterized genes enriched in the Sepw1-pure sample type as compared to the Nr5a1-pure sample type at P16 and compared these gene enrichments to those found in Chapter II using the same technique with the same transgenic crosses at P12 (Tomorsky et al., 2017).

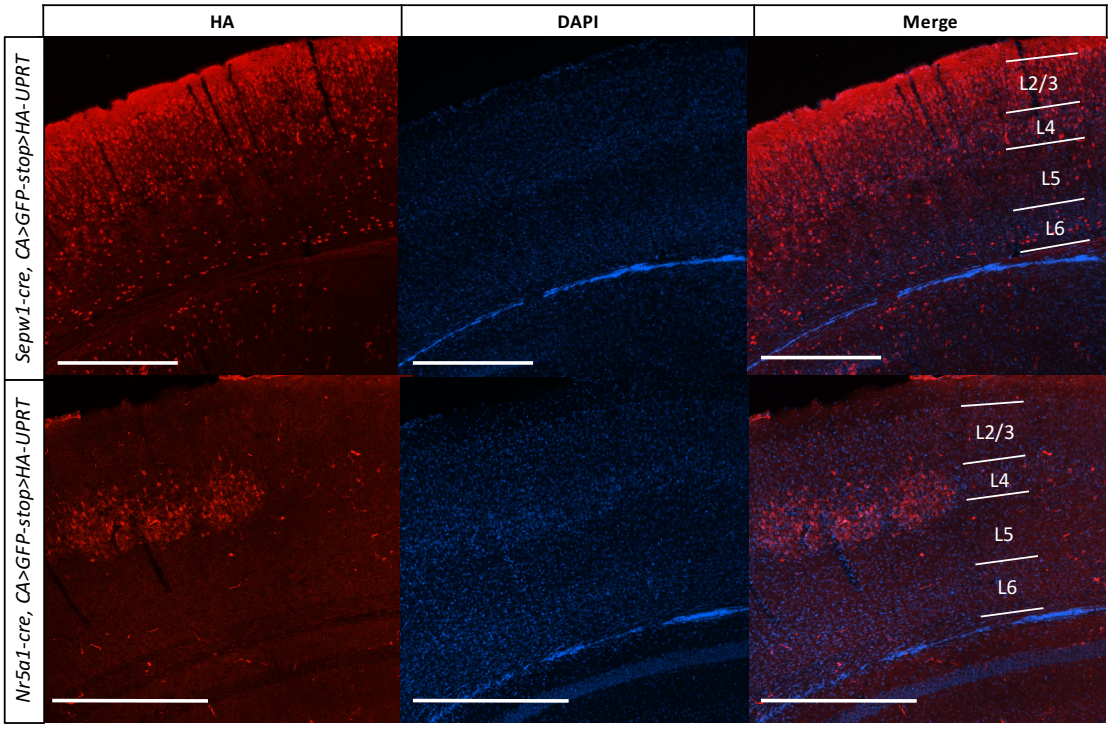

Figure 1. *Sepw1-cre* and *Nr5a1-cre* label populations of upper layer cortical neurons. Immunohistochemistry for the HA-tag on the UPRT protein in *Sepw1-cre; CA>GFPstop>HA-UPRT* (top) and *Nr5a1-cre; CA>GFPstop>HA-UPRT* (bottom) transgenic crosses at P16 (scale bars = 500 μm).

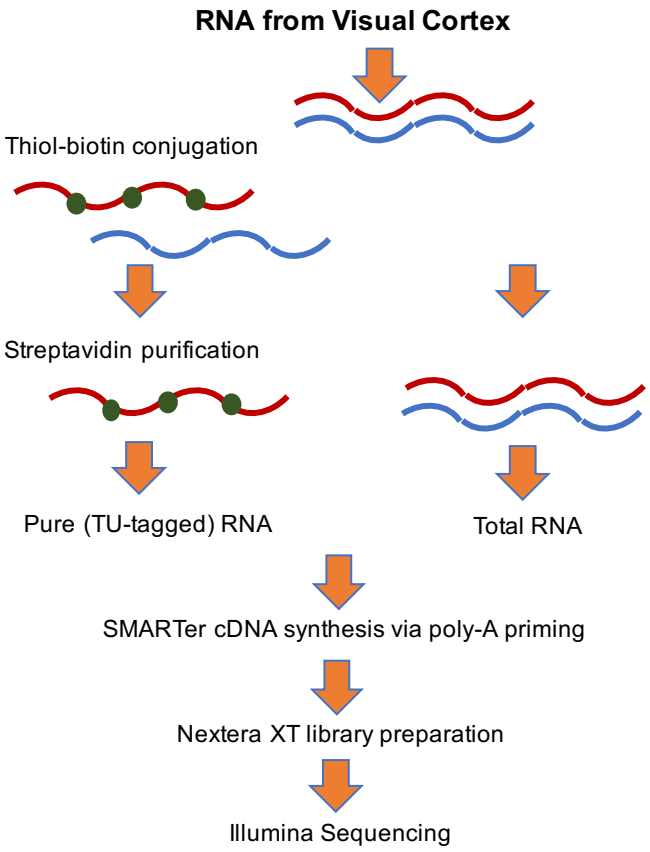

Figure 2. RNA processing pipeline for all samples.
Samples for analysis of differential expression between P12 and P16 in all V1 were prepared from 'total' RNA set aside before streptavidin purification. Samples of purified 'tagged' RNA from *Sepw1-cre, CA>GFP-stop>HA-UPRT* and *Nr5a1-cre, CA>GFP-stop>HA-UPRT* were biotinylated and streptavidin purified as shown.

DESeq differential expression analysis reveals 367 Sepw1-enriched transcripts at P16

To identify genes enriched at P16 in L2/3 of developing visual cortex, Illumina sequenced transcripts from Sepw1-pure and Nr5a1-pure sample types were aligned to the mouse genome (Cunningham et al., 2014) using the Genomic Short-read Nucleotide Alignment Program (GSNAP) (Wu & Nacu, 2010), and sequences that aligned to a particular gene were counted using htseq-count (Python). The EdgeR package was used to visualize normalized and filtered read counts by multidimensional scaling analysis,

considering the top 500 genes with the largest log fold change differences for each sample type. The Sepw1-pure (N = 3 samples) and Nr5a1-pure (N = 4 samples) sample types formed clear clusters using this method (Figure 3A). Next DESeq was used to assess overall differential expression between Sepw1-pure and Nr5a1-pure sample types at P16 using a negative binomial distribution to model the data (Figure 3B). This analysis found 367 genes that were enriched in the Sepw1-pure samples relative to the Nr5a1-pure samples (Figure 3C, Supplementary Dataset 3).

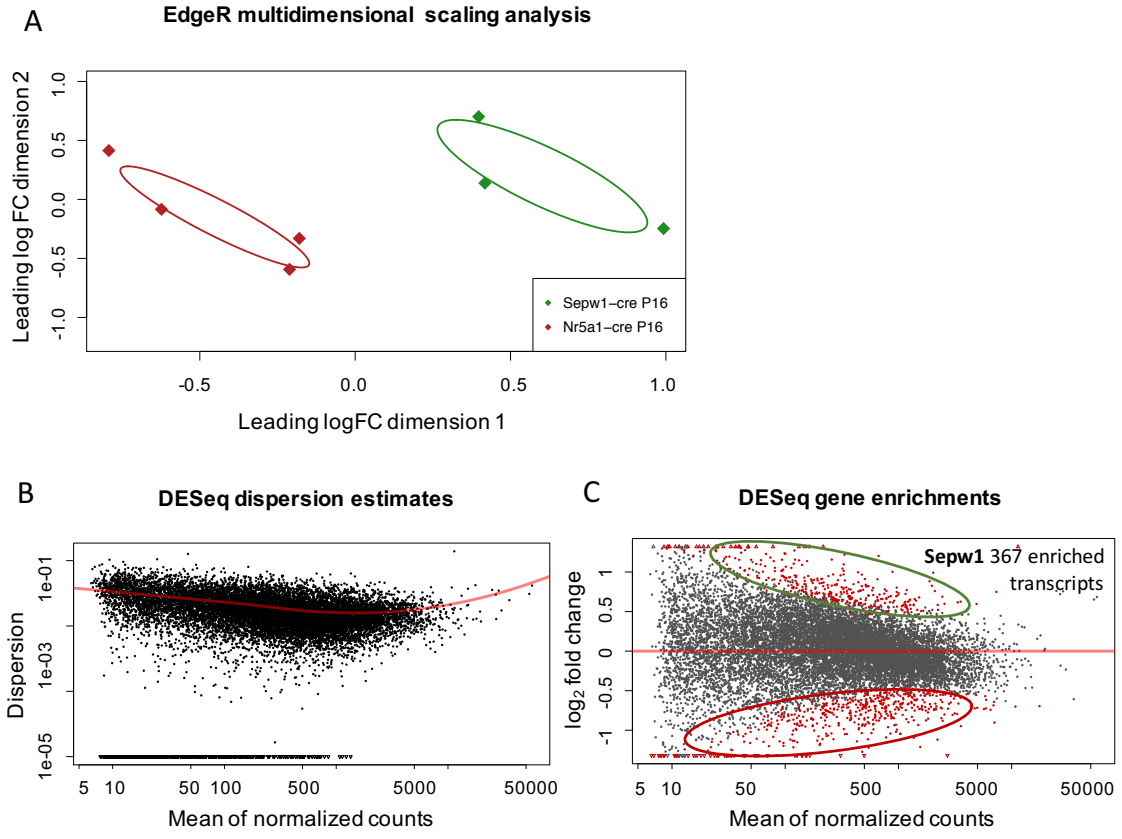

Figure 3. MDS clustering of Sepw1-pure and Nr5a1-pure sample types at P16 and differential expression analysis.
(A) MDS analysis was performed using EdgeR on Sepw1-pure and Nr5a1-pure samples after RNAseq and bioinformatic processing of count data. The two groups formed distinct clusters.
(B) DESeq dispersion estimates of count data for the Sepw1–Nr5a1 sample-type comparison modeled using a negative binomial distribution.

(C) 367 genes were found enriched in the Sepw1-pure samples as compared to Nr5a1-pure samples after DESeq differential expression analysis using filtered and normalized gene counts (genes where 3 or more samples had read numbers < 1 count per million were removed from analysis).

Sepw1-enriched genes compared to Nr5a1-samples show significant overlap with genes found in upper cortical layers

After DESeq differential expression analysis, we compared Sepw1-enriched genes at P16 (Nr5a1-pure comparison) to adult layer enriched genes found in an online database (400 genes most highly enriched in each cortical layer) (Belgard et al., 2011). Sepw1-enriched genes were also compared to the top 500 neuronal or endothelial genes found in an online database (Cahoy et al., 2008). We used a statistical resampling approach to determine whether DESeq Sepw1-enriched genes overlapped with layer- or cell type-enriched genes (Belgard et al., 2011), as was previously described for Sepw1-enriched genes at P12 (Tomorsky et al., 2017) (Supplementary Table 1, Figure 4C). We found a significant number of L2/3 and L4 database genes (Belgard et al., 2011) overlapped with Sepw1-enriched genes at P16 (Figure 4C). When compared to genes previously shown to be Sepw1-enriched using the same comparison at P12 (Tomorsky et al., 2017) (Chapter II), we found 175 overlapping genes between the two time points (Figure 4A). Genes found to be exclusively enriched at P16 in *Sepw1-cre* neurons had functional roles in metabolism and transcriptional regulation, while genes found to be exclusively enriched at P12 had functional roles in synaptic signaling and neuron projection development (Figure 4B).

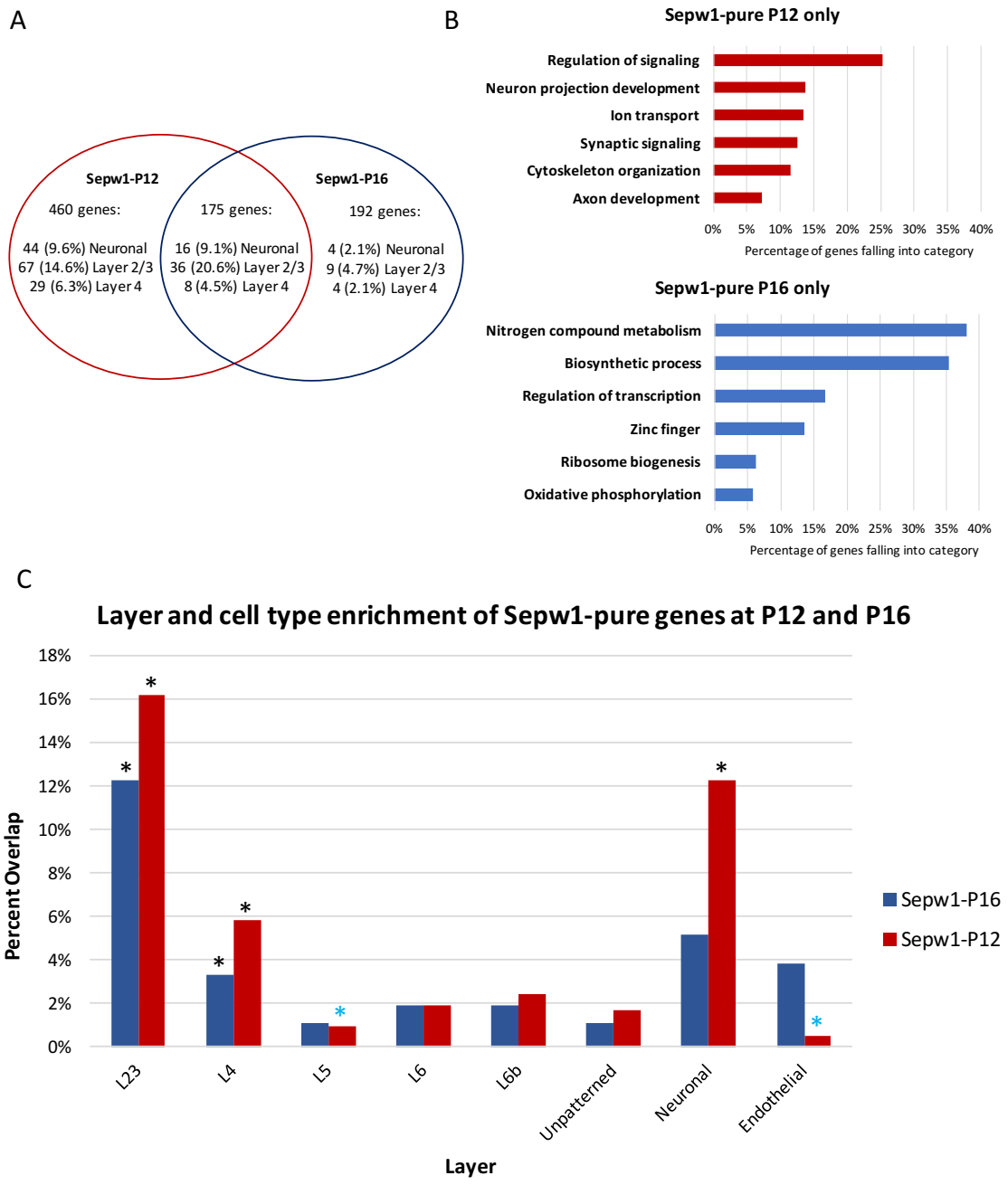

Figure 4. Sepw1-enriched genes at P16 are expressed in upper cortical layers and have roles in energy metabolism.
(A) 175 overlapping genes were found between Sepw1-enriched transcripts at P12 and P16 (Nr5a1-pure comparison). 192 and 460 genes were identified as Sepw1-enriched exclusively at P16 or P12, respectively. The percentage of Sepw1 genes in each category overlapping with upper-layer or neuronal genes is shown (identified using online databases) (Belgard et al., 2011; Cahoy et al., 2008).

(B) Gene-ontology analysis revealed a large percentage of genes found to be exclusively Sepw1-enriched at P16 were involved in metabolism and transcriptional regulation. In addition, many genes with functions in neuron projection development, synaptic signaling and cytoskeletal organization were enriched at P12 but not at P16. Functional categories were identified using GO-TermFinder (Boyle et al., 2004) (go.princeton.edu) and DAVID functional annotation clustering (https://david.ncifcrf.gov). Most categories were identified using GO-TermFinder (Boyle et al., 2004) with the exception of zinc finger (UP_KEYWORDS), oxidative phosphorylation (KEGG_PATHWAY), and regulation of transcription (DNA-templated, GO_TERM_BP_DIRECT), which were found using DAVID (Huang et al., 2009). P-values for enrichment were significant for all pathways, and the percentage of Sepw1-enriched genes falling into each category is represented on the x-axis.
(C) The percentage of Sepw1-enriched genes at P16 (347 genes) or P12 (635 genes) that overlap with database genes (Belgard et al., 2011; Cahoy et al., 2008) found to be neuronal, endothelial, or layer enriched, is shown. Significance was determined using a resampling approach to estimate means and associated confidence intervals expected to occur by chance when of neuronal, endothelial or layer enriched genes were identified in a randomly selected group of 347 (or 635) genes (Supplementary Table 1). Asterisks indicate that the percentage of overlapping genes was found to be significantly (p-value $\geq$ 0.05) above (black) or below (blue) that which could be expected to occur by chance.

DESeq analysis reveals several developmentally regulated genes around eye opening

To determine novel genes developmentally regulated with the onset of visual activity, Illumina sequenced transcripts from dissected V1 cortical tissue at P12 (before eye opening) and P16 (after eye opening) were aligned to the mouse genome and counted as described for Sepw1-pure and Nr5a1-pure sample types (Cunningham et al., 2014; Wu & Nacu, 2010). The EdgeR package was used to visualize normalized and filtered read counts by multidimensional scaling analysis, and P12 and P16 samples formed distinct well-separated clusters using this method (Figure 5A). Next DESeq was used to assess differentially expressed genes between P12 and P16 sample types using a negative binomial distribution to model the data (Figure 5B). This analysis found 1674 genes that were developmentally downregulated (enriched at P12; Supplementary Dataset 4,

bottom) and 1421 genes that were developmentally upregulated (enriched at P16; Supplementary Dataset 4, top) with eye opening (Figure 5C).

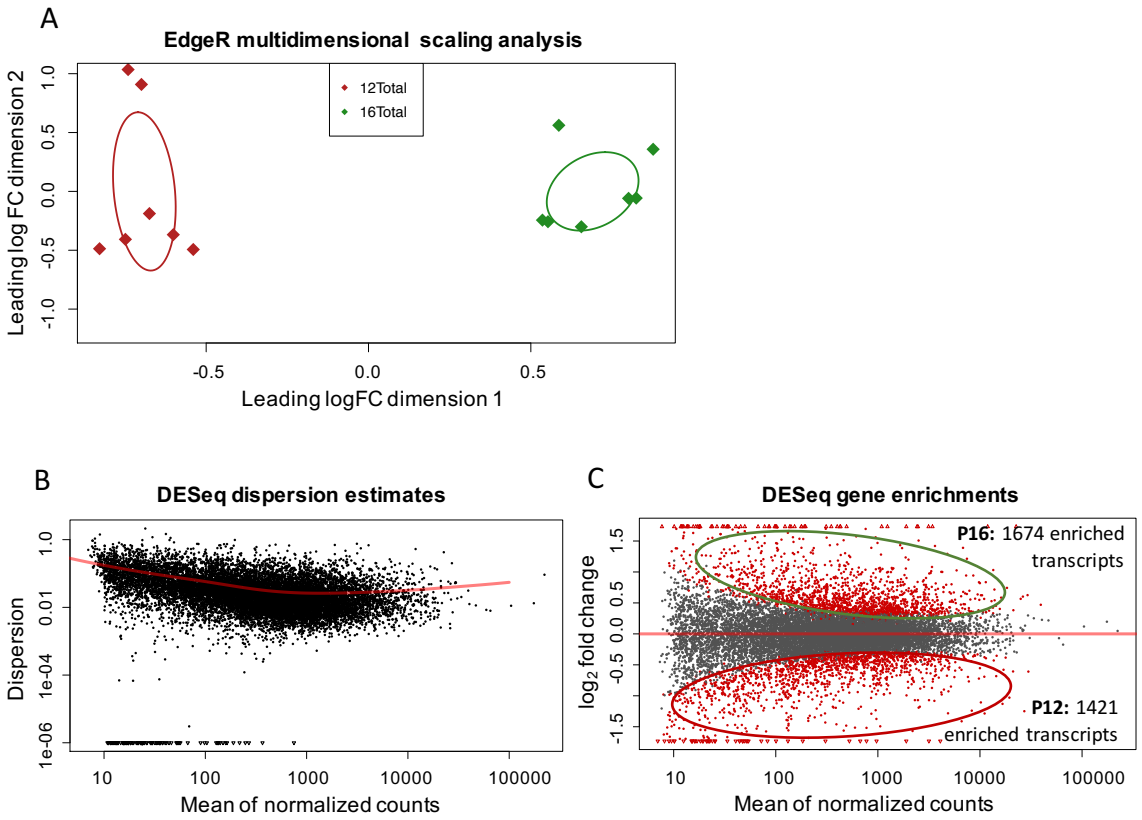

Figure 5. MDS clustering and differential expression analysis of P12 and P16 samples prepared from dissected V1 cortical tissue.
(A) MDS analysis was performed using EdgeR on P12 and P16 samples after RNAseq and bioinformatic processing of count data. The two groups formed distinct well-separated clusters.
(B) DESeq dispersion estimates of count data for the comparison of P12 and P16 samples modeled using a negative binomial distribution.
(C) 1421 genes were found to be enriched at P12 and 1674 genes were found to be enriched at P16 after DESeq differential expression analysis using filtered and normalized gene counts (genes where 3 or more samples had read numbers < 1 count per million were removed from analysis).

Down and up-regulated genes with eye opening fall into distinct categories

Genes found to be enriched at P12 or P16 were examined using the online tool DAVID (Huang et al., 2009) for the functional classification of gene lists (Figure 6).

Using this tool, we found genes that decreased their expression levels with eye opening were largely cell-cycle and cytoskeletal proteins with DAVID enrichment scores of 22.43 and 18.88, respectively. At P12 structural proteins falling into the DAVID categories tubulin, collagen, extracellular matrix, microtubule and actin-binding, are among the most enriched, indicating cortex is actively building and stabilizing its neuronal network before the eyes open. At P16, the category with the highest DAVID enrichment score (21.34) is 'cell junction/synapse', indicating a large degree of synapse formation/reorganization is occurring after eye opening. Supporting this, the second most enriched category at P16 comprises the 'pleckstrin homology domain' proteins, with an enrichment score of 12.25. This is a lipid binding family of proteins, which is synapse associated and important for synaptic vesicle transport (Klopfenstein & Vale, 2004). Proteins found at the cell membrane and associated with ion transport and signaling are the next most enriched categories, indicating increased neuronal activity, synaptic signaling, and synaptogenesis after eye opening.

Next we examined the P12–P16 changing expression levels of genes described in a previous publication (Fertuzinhos et al., 2014) to be associated with the following processes: synaptogenesis, experience-dependent activity, dendritogenesis, axonogenesis, excitatory neurotransmission, and inhibitory neurontransmission (Figure 7). With a few exceptions, genes associated with synaptogenesis, experience-dependent activity, excitatory neurotransmission, and inhibitory neurotransmission were overwhelmingly upregulated after eye opening. On the other hand, genes associated with dendritogenesis did not show any specific pattern of regulation, with certain genes being upregulated and others being downregulated. Genes associated with axonogenesis were mostly

downregulated over this period. Interestingly, the only 'experience-dependent activity' gene downregulated from P12–P16, *Jun*, is also associated with neurite outgrowth and axon regeneration and was previously shown to decrease expression after P15 (Moore & Goldberg, 2011; Ruff et al., 2012).

Finally, we examined how eye opening affected the expression of genes found to be developmentally regulated in previous transcriptomic studies of visual cortex (Table 1). Genes found to be continuously increased or decreased over development were found to have expected patterns of regulation from P12 to P16 (Yang et al., 2009). Interestingly many genes previously associated with the critical period for ODP, having expression levels that peaked at P28 as compared to P14, were also highly upregulated from P12 to P16. In particular, *Mal*, *Tcnn1,* and *Plp1,* identified as having strong enrichment from P14 to P28, were also very highly upregulated from P12 to P16, indicating that the regulation of these genes may happen earlier than previously thought and may not be specific to the critical period for ODP. We also examined a select set of genes from Majdan and Shatz (2006) found to have regulated expression with monocular deprivation (MD) before, during, and after the critical period for ODP that was either dependent or independent of normal visual experience with eye opening. Many of these genes also had significantly increased or decreased expression levels with eye opening. In addition, the direction of genetic regulation with eye opening could not be predicted by the direction of regulation later in development, further illuminating a complex system of activity dependent and independent processes controlling visual cortical development.

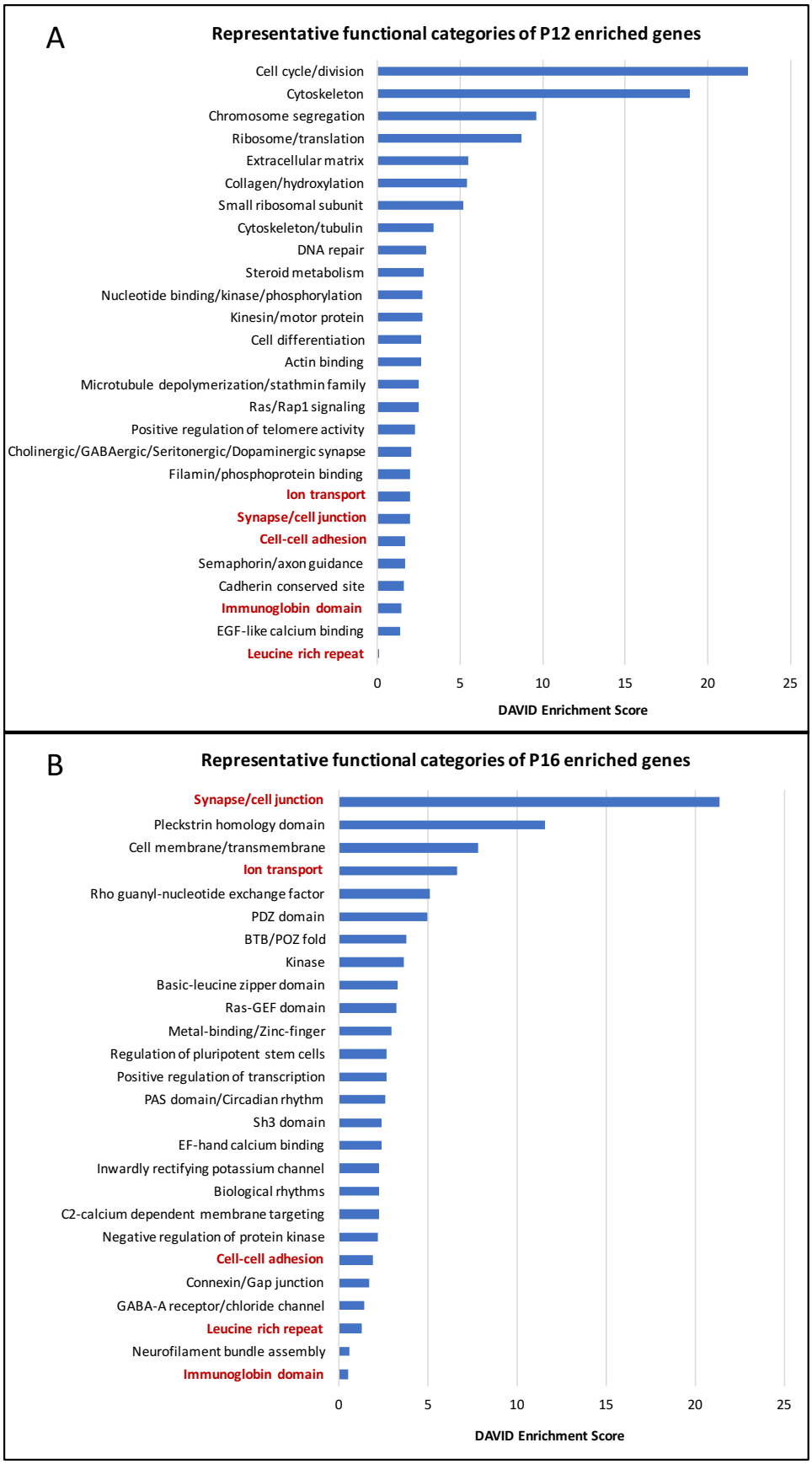
A
Representative functional categories of P12 enriched genes
Cell cycle/division
Cytoskeleton
Chromosome segregation
Ribosome/translation
Extracellular matrix
Collagen/hydroxylation
Small ribosomal subunit
Cytoskeleton/tubulin
DNA repair
Steroid metabolism
Nucleotide binding/kinase/phosphorylation
Kinesin/motor protein
Cell differentiation
Actin binding
Microtubule depolymerization/stathmin family
Ras/Rap1 signaling
Positive regulation of telomere activity
Cholinergic/GABAergic/Seritonergic/Dopaminergic synapse
Filamin/phosphoprotein binding
Ion transport
Synapse/cell junction
Cell-cell adhesion
Semaphorin/axon guidance
Cadherin conserved site
Immunoglobin domain
EGF-like calcium binding
Leucine rich repeat
0
5
10
15
20
25
DAVID Enrichment Score
B
Representative functional categories of P16 enriched genes
Synapse/cell junction
Pleckstrin homology domain
Cell membrane/transmembrane
Ion transport
Rho guanyl-nucleotide exchange factor
PDZ domain
BTB/POZ fold
Kinase
Basic-leucine zipper domain
Ras-GEF domain
Metal-binding/Zinc-finger
Regulation of pluripotent stem cells
Positive regulation of transcription
PAS domain/Circadian rhythm
Sh3 domain
EF-hand calcium binding
Inwardly rectifying potassium channel
Biological rhythms
C2-calcium dependent membrane targeting
Negative regulation of protein kinase
Cell-cell adhesion
Connexin/Gap junction
GABA-A receptor/chloride channel
Leucine rich repeat
Neurofilament bundle assembly
Immunoglobin domain
0
5
10
15
20
25
DAVID Enrichment Score

Figure 6. Select DAVID functional clusters for genes enriched at P12 or P16
DAVID functional annotation clustering analysis was performed on genes enriched in visual cortex at P12 (A) and P16 (B) using the online tool at http://david.ncifcrc.gov (Huang et al., 2009b). Clusters with the 20 highest enrichment scores were chosen for visualization as well as an additional 6–7 select clusters with lower enrichment scores having functions related to adhesion or signaling. Names were chosen to best represent all functional categories grouped in a given cluster.

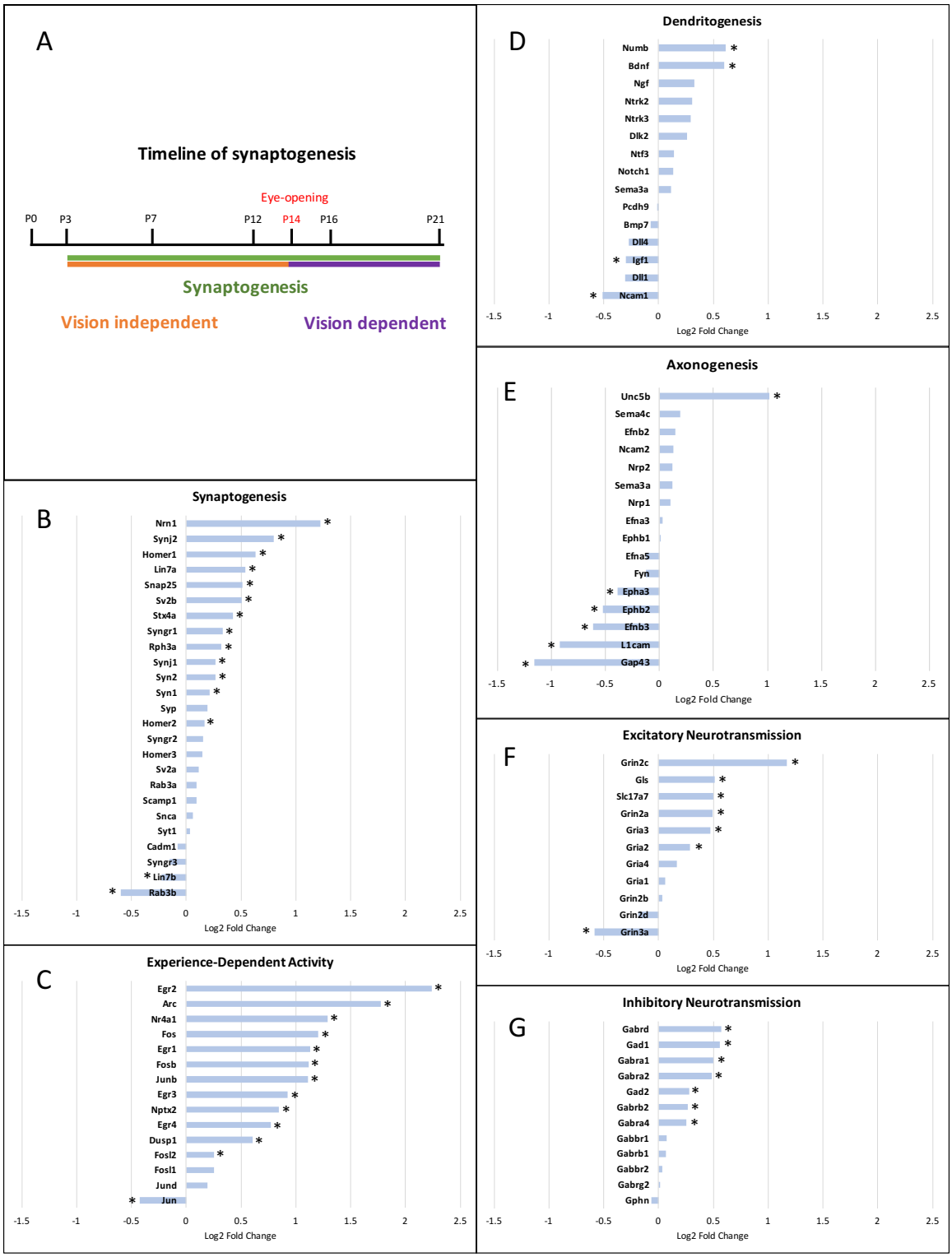

Figure 7. Genes involved in neurotransmission, activity, and synaptogenesis are upregulated with eye opening.
(A) Schematic representing the time-period of synaptogenesis analyzed.

(B) The expression levels of select genes (Fertuzinhos et al., 2014) involved in synaptogenesis are upregulated with eye opening. *Rab3b* is the only gene significantly downregulated from this category after eye opening.
(C) With the exception of *Jun*, the expression levels of genes associated with experience-dependent activity (Fertuzinhos et al., 2014) are upregulated with eye opening.
(D) The expression levels of genes involved in dendritogenesis (Fertuzinhos et al., 2014) are not strongly developmentally regulated with eye opening, with the exceptions of *Bdnf* and *Numb*, which are upregulated, and *Ncam1*, which is downregulated.
(E) Genes associated with axonogenesis (Fertuzinhos et al., 2014) are largely downregulated with eye opening.
(F) With the exception of *Grin3a*, genes involved in excitatory neurotransmission (Fertuzinhos et al., 2014) are upregulated with eye opening.
(G) The expression levels of many genes involved inhibitory neurotransmission (Fertuzinhos et al., 2014) are upregulated with eye opening.

Names	**Fold change**	**DESeq padj**	**Publication**	**Biological Regulation**
Nr4a1	3.64	6.43E-39	Yang et al., 2009	Continuously increased P0-P45
S100b	2.23	1.13E-11	Yang et al., 2009	Continuously increased P0-P45
Pygm	2.17	7.48E-09	Yang et al., 2009	Continuously increased P0-P45
Ntsr2	1.99	5.06E-11	Yang et al., 2009	Continuously increased P0-P45
Apod	1.97	1.54E-08	Yang et al., 2009	Continuously increased P0-P45
Nptx1	1.78	1.17E-08	Yang et al., 2009	Continuously increased P0-P45
Vamp1	1.63	1.72E-05	Yang et al., 2009	Continuously increased P0-P45
Rnase4	1.44	0.025	Yang et al., 2009	Continuously increased P0-P45
Sorcs2	0.66	0.00011	Yang et al., 2009	Continuously decreased P0-P45
Met	0.54	9.09E-09	Yang et al., 2009	Continuously decreased P0-P45
Dpysl3	0.14	9.04E-83	Yang et al., 2009	Continuously decreased P0-P45
Arc	7.24	4.14E-79	Yang et al., 2009	Continuously increased P0-P45
Mal	7.80	1.65E-70	Lyckman et al., 2008	Expression peaks at P28 in V1 relative to P14
Tnnc1	7.53	2.88E-17	Lyckman et al., 2008	Expression peaks at P28 in V1 relative to P14
Plp1	5.05	2.20E-45	Lyckman et al., 2008	Expression peaks at P28 in V1 relative to P14
Pdlim2	2.87	1.02E-10	Lyckman et al., 2008	Expression peaks at P28 in V1 relative to P14

Fn3k	2.14	4.02E-07	Lyckman et al., 2008	Expression peaks at P28 in V1 relative to P14
Cmtm5	1.92	4.42E-06	Lyckman et al., 2008	Expression peaks at P28 in V1 relative to P14
Ccdc28a	1.67	0.0061	Lyckman et al., 2008	Expression peaks at P28 in V1 relative to P14
Penk	1.61	0.0011	Lyckman et al., 2008	Expression peaks at P28 in V1 relative to P14
Josd2	1.53	0.0050	Lyckman et al., 2008	Expression peaks at P28 in V1 relative to P14
Gng13	1.48	0.032	Lyckman et al., 2008	Expression peaks at P28 in V1 relative to P14
Sdc4	1.34	0.035	Lyckman et al., 2008	Expression peaks at P28 in V1 relative to P14
Csrp2bp	1.29	0.093	Lyckman et al., 2008	Expression peaks at P28 in V1 relative to P14
Mobp	5.59	1.14E-60	Lyckman et al., 2008; Majdan & Shatz, 2006	Expressed highly at P28, Increased D/ND ratio at P46 only with DR.
Bdnf	1.64	1.65E-05	Majdan & Shatz, 2006	Decreased D/ND ratio unchanged with DR at P24, but decreased magnitude with DR at P46.
Fos	2.98	7.88E-26	Majdan & Shatz, 2006	Decreased D/ND ratio with decreased magnitude after DR at P24 and P46.
Fosb	2.95	1.18E-06	Majdan & Shatz, 2006	Decreased D/ND ratio unaffected by dark rearing.
Egr1	2.68	6.05E-23	Majdan & Shatz, 2006	Decreased D/ND ratio unchanged with DR at P24, but decreased magnitude with DR at P46.
Dusp6	1.84	2.65E-09	Majdan & Shatz, 2006	Decreased D/ND ratio unchanged with DR at P24, but decreased magnitude with DR at P46.
Matn2	1.69	6.19E-06	Majdan & Shatz, 2006	Increased D/ND ratio at P24 unaffected by DR.
Dbp	1.60	0.00089	Majdan & Shatz, 2006	Increased D/ND ratio at P46 with normal vision. No regulation with DR.
Gadd45b	1.49	0.046	Majdan & Shatz, 2006	Decreased D/ND ratio at P46 with normal vision. No regulation with DR.
Olfm1	1.46	0.00033	Majdan & Shatz, 2006	Decreased D/ND ratio at P24 with normal vision. No regulation with DR.
Ier2	1.27	0.095	Majdan & Shatz, 2006	Decreased D/ND ratio unchanged with DR at P24, but decreased magnitude with DR at P46.
Evl	0.78	0.067	Majdan & Shatz, 2006	Increased D/ND ratio at P18. Not regulated at other ages.
Igfbp2	0.66	0.00017	Majdan & Shatz, 2006	Decreased D/ND ratio at P24 with normal vision. No regulation with DR.

Table 1. Genes shown to be developmentally regulated in previous transcriptomic studies of visual cortex development.
In this table, we identify: gene name, fold change from P12–P16, DESeq adjusted p-value (significance set at padj < 0.1), previous publication describing developmental regulation, and what biological regulation was identified in this previous publication. Genes shown to be continuously increased or decreased with age from Yang et al., 2009 (time points P0, P10, P20, P45) were also regulated with eye opening, as expected. Many genes from Lyckman et al. 2008 found to have expression levels that peaked at P28 relative to P14 were also shown to have increased expression levels between P12 and P16. Also shown are select genes from Majdan and Shatz (2006) found to have regulated expression with monocular deprivation (MD) and/or dark rearing (DR) either before (P18), during (P24), or after (P45) the critical period for ocular dominance plasticity. A decrease in the deprived over non-deprived ratio (D/ND) indicates the gene is being positively regulated with monocular deprivation (non-deprived cortex has high expression relative to deprived cortex). Many genes in this study were also examined to determine whether regulated expression during MD was dependent on normal visual development by dark rearing animals until a few days before the MD manipulation. Here we show that several of these genes are also regulated during the normal onset of vision.

Cell-type composition of visual cortex appears to transform from P12 to P16

To determine whether the cell-type composition of V1 may be changing over eye opening, we surveyed genes enriched at P12 or P16 for transcripts expressed in neuronal and non-neuronal cell types, identified using an online database (Cahoy et al., 2008) (Figure 8). At P12, a significant enrichment of genes from neuronal and oligodendrocyte progenitor cell types was observed (significance determined using a statistical resampling method, Supplementary Table 1). At P16, genes highly expressed in neurons, astrocytes, endothelial cells, and both newly formed and myelinating oligodendrocytes were found to be significantly enriched. It should be noted that significance in this case is not related to differences between groups, but rather indicates whether the degree of overlap between cell-type enriched and time-point enriched genes is greater than expected by chance. Though our test of statistical significance is not directly comparing P12 and P16, the transcriptional contributions of various non-neuronal cell types appear to differ between

these time points. The observed differences indicate a maturation of oligodendrocytes and an increase in the number of endothelial and astrocytic support cells in V1, coinciding with the increased neuronal activity observed after eye opening.

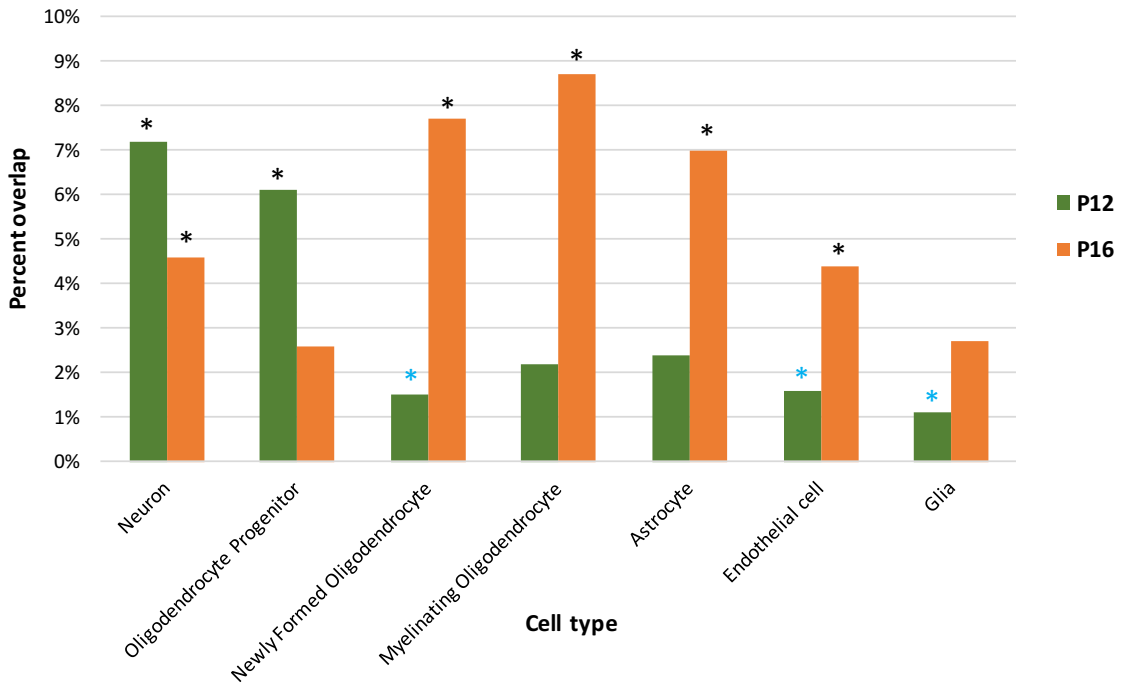

Figure 8. Cell-type composition of V1 changes between P12 and P16.
The 500 most enriched genes in neuronal and non-neuronal cell types were obtained from an online database (https://web.stanford.edu/group/barres_lab/brain_rnaseq.html) (Cahoy et al., 2008). We used neuronal genes from this database that were enriched in neurons when compared to all other non-neuronal cell types. We used microglial, astrocytic, and endothelial genes from this database that were enriched in these cell types when compared to neurons. Genes from this database associated with myelinating oligodendrocytes, newly formed oligodendrocytes, or oligodendrocyte progenitor cells, were each enriched as compared to both neurons and the other two types of oligodendrocytes. Database genes enriched in each cell type were compared to genes differentially expressed in V1 between P12 and P16. Proportionally (as indicated by percent overlap), genes expressed in neurons and oligodendrocyte progenitor cells decreased from P12 to P16, while genes expressed in all other non-neuronal cell types increased.

Developmentally regulated genes in L2/3 cortical neurons fall into distinct gene ontology categories

Since TU-samples are a combination of cell-type specific tagged RNA and to a lesser degree, background 'untagged' RNA from the rest of cortex, comparisons made between sample types need to be considered carefully. Because expression patterns and cell-type composition in all of cortex differ greatly between P12 and P16, the background 'noise' from unlabeled RNAs would likely be very different between Sepw1-pure samples prepared at P12 and P16, and could drive differential expression unrelated to cell type. We concluded that a direct comparison of Sepw1-pure samples prepared at P12 and P16 would be difficult to interpret, so we utilized an alternative method for identifying developmentally regulated genes in L2/3 neurons.

For this analysis, we searched for genes that were both Sepw1-enriched (compared to Nr5a1-pure samples) and developmentally regulated in all V1 with eye opening. Since L2/3 enrichment at a particular developmental time point does not necessarily indicate whether a gene is developmentally regulated (changing expression level over time), a combined dataset of genes enriched at both P12 (Tomorsky et al., 2017) (Chapter II) and P16 in L2/3 cortical neurons was examined for changing expression levels with eye opening. Here we searched for genes that were both Sepw1-enriched and downregulated (enriched at P12 in V1) or upregulated (enriched at P16 in V1) with eye opening (Figure 9A, C). Gene ontology analysis was then performed on overlapping developmentally regulated genes in L2/3 cortical neurons (princeton.go.edu), and visualized using REVIGO tree maps (Boyle et al., 2004; Supek et al., 2011) (Figure

9B, D). From this analysis, genes with decreased expression in L2/3 neurons after eye opening were classified as having roles in neuron projection development and genes with increased expression fell into synaptic transmission and developmental regulation GO categories.

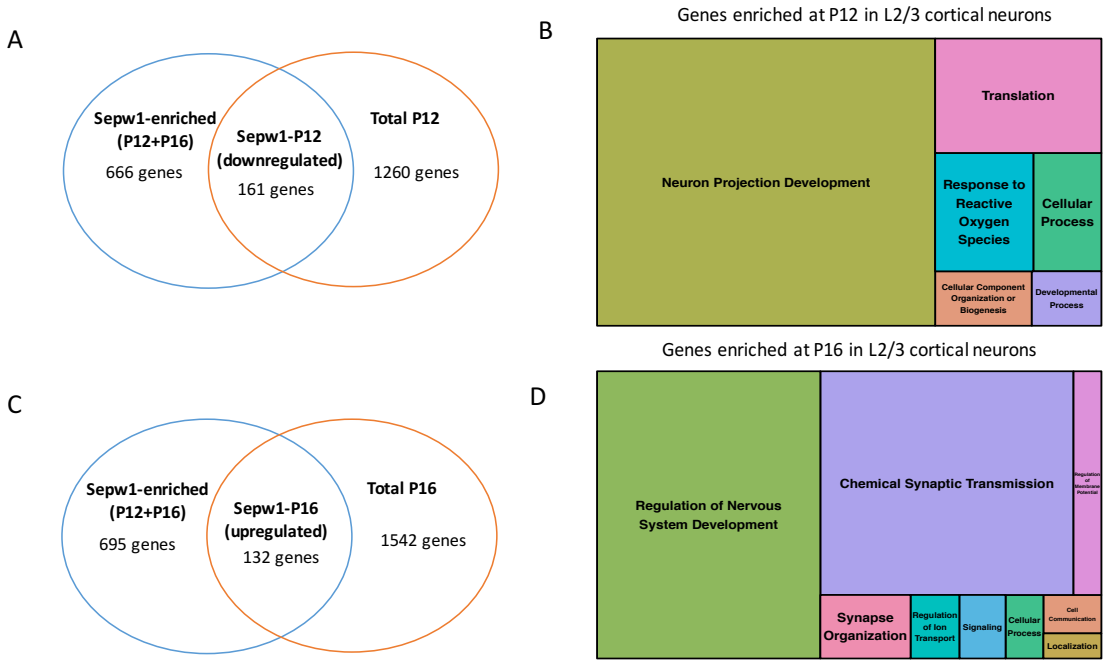

Figure 9. Examination of genes both enriched in *Sepw1-cre* neurons and developmentally regulated between P12 and P16.
(A) 161 genes were found to overlap between Sepw1-enriched genes (P12 and P16) and genes enriched at P12 in all of cortex (compared to P16).
(B) Genes assumed to be downregulated with eye opening in L2/3 cortical neurons largely fell into 'neuron projection development' categories after gene ontology analysis.
(C) 132 genes were found to overlap between Sepw1-enriched genes (P12 and P16) and genes enriched at P16 in all of cortex (compared to P12).
(D) Genes assumed to be upregulated with eye opening in L2/3 cortical neurons largely fell into 'regulation of nervous system development' and 'chemical synaptic transmission' gene ontology categories.

DISCUSSION

Previous studies of gene expression in visual cortex have focused on the critical period for ocular dominance plasticity (ODP), often examining ages separated by large

developmental time periods. These studies have indicated neuronal gene expression is tightly regulated during the critical period for ODP, but have not closely examined gene expression during the developmental onset of vision. Here, we examine changes in gene expression over a four-day period surrounding eye opening (~P14) from P12 to P16. In addition, we identify genes enriched in a population of excitatory L2/3 neurons in V1 (labeled by the *Sepw1-cre* mouse line) at P16, a time point just following eye opening when many synapses are forming. We used the TU-tagging technique to prepare samples from both *Sepw1-cre; CA>GFP-stop>HA-UPRT* and *Nr5a1-cre;CA>GFP-stop>HA-UPRT* transgenic crosses to identify Sepw1-enriched genes by differential expression analysis, as previously described (Figures 2–4) (Tomorsky et al., 2017). Finally, we identified genes that were both L2/3 enriched and developmentally regulated in all V1, and used these genes to distinguish processes important for the development of L2/3 neuronal cell types.

In this study, we add to a previous TU-tagging study that identified genes enriched in L2/3 cortical neurons at P12 (Chapter II), by examining genes enriched in the same neurons at P16. Genes enriched at P16 in Sepw1-pure samples compared to Nr5a1-pure samples overlapped significantly with L2/3 and L4 genes from an online database (Belgard et al., 2011). When compared to genes that were Sepw1-enriched at P12 (Nr5a1-pure comparison), approximately half overlapped, and those that did not had unique functions depending on whether they were found exclusively at P12 or P16 (Figure 4). Unexpectedly, genes with functions related to ion transport and synaptic signaling were Sepw1-enriched at P12 but not P16. It is possible the expression of these genes increases in Nr5a1-neurons relative to Sepw1-neurons between P12 and P16,

decreasing the observed Sepw1-enrichment at P16. It is important to keep in mind that Sepw1-enriched genes are enriched relative to samples containing RNA purified from a different neuronal cell type and do not necessarily represent a complete transcriptomic profile from these cells.

Several of the genes demonstrating unique enrichment at P16 in L2/3 neurons were involved in transcriptional regulation and metabolism, specifically oxidative phosphorylation. Cytochrome oxidase, two subunits of which were Sepw1-enriched at P16 and not P12 (*Cox6c* and *Cox7c*), is a protein involved in oxidative phosphorylation and redox balance which has been previously used as an indicator of neuronal activity (Wong-Riley, 1989). Interestingly, a previous study found that a large degree of oxidative phosphorylation, as measured by *Cox* enrichment, occurs in dendrites (Wong-Riley, 1989). Since TU-tagging preserves RNAs enriched in the dendrites, this developmental enrichment of metabolic genes may not have been identified using transcriptomic techniques requiring dissection or cell isolation. This also indicates that the level of activity in L2/3 neurons may be high relative to the L4 neuronal cells used as a comparison here. This demonstrates an aspect of the TU-tagging technique that can be beneficial or detrimental, depending on the biological question, since metabolic genes are not necessarily 'specific' to L2/3 neurons, but are likely enriched in these cells after eye opening. This finding is consistent with other lines of evidence indicating that L2/3 neurons increase their activity with the onset of sensory experience (Fertuzinhos et al., 2014; Shen & Colonnese, 2016).

Previous studies of auditory and somatosensory cortices have found that the onset of sensory information can have profound effects on gene expression in these areas

(Fertuzinhos et al., 2014; Hackett et al., 2015). Similarly, gene expression in V1 appeared highly regulated with eye opening, with thousands of genes found differentially expressed between P12 and P16. Gene categories enriched at P12 relative to P16 were overwhelmingly classified as extracellular matrix, cytoskeletal, or cell division genes. On the other hand, genes enriched at P16 relative to P12 fell into synaptic, cell membrane, signaling, and ion transport functional categories (Figure 3). This pattern of gene regulation appears to describe the structural wiring of the cortical circuit at P12, with the expression of extracellular matrix and cytoskeletal components. At P16 we see increased transmission through this newly constructed circuit with the enrichment of genes important for neuronal activity (synaptogenesis, excitatory and inhibitory neurotransmission and experience dependent genes, Figure 3). A previous study indicated that the expression of genes involved in synaptogenesis were downregulated between P14 and P28, but was unable to resolve when this downregulation takes place relative to eye opening. Here we show a robust increase in the expression of genes involved in synaptogenesis from P12 to P16, which is consistent with functional studies also indicating synapse formation increases at eye opening in V1 (Desai et al., 2002; W. Lu & Constantine-Paton, 2004).

Genes enriched in neuronal and non-neuronal cell types also appear to change their degree of expression in visual cortex over this developmental period. At P12 genes enriched in neurons and oligodendrocyte progenitors are dominant, while at P16 we observe increased enrichment of genes expressed in astrocytes and newly formed and mature oligodendrocytes. This appears to describe an influx of astrocytes and the maturation of oligodendrocytes, coinciding with the onset of visually driven activity in

V1. It would be interesting to see if a similar shift in cell type would occur after dark rearing or whether the maturation of these non-neuronal cells is linked to activity. While observing differences in the expression of cell-type enriched genes with eye opening may indicate changes in the cell-type composition of V1, it is not a direct measure of this process, and should be interpreted cautiously.

Several other studies have indicated that neuronal gene expression may be under tight regulation during the critical period for ODP (Benoit et al., 2015; Lyckman et al., 2008; Majdan & Shatz, 2006; Tropea et al., 2006). Here we find that genes modulated with the normal onset of visual activity overlap with many genes found to have developmental and/or activity dependent regulation during the critical period. Many genes associated with the critical period for ODP, due to their strong enrichment at P28 relative to P14 (Lyckman et al., 2008), were also strongly upregulated between P12 and P16. This indicates that the regulation of these genes may not be uniquely associated with the critical period since developmental onset of vision alone can drive differences in expression. The gene cardiac troponin B (*Tnnc1*), for example, was found to be most significantly increased at P28 relative to P14 and, due to its association with actin, was singled out for its potential as a novel plasticity gene (Lyckman et al., 2008). Here we find this gene is also very highly enriched (7.5 fold) with the onset of vision, indicating this gene may not be uniquely important for ocular dominance plasticity during the critical period. By comparing genes regulated between P12 and P16 to those also enriched during the critical period, we can begin to identify patterns of expression that may be important during either or both developmental window (Table 1).

Majadan and Shatz (2006) performed an extensive study of genes regulated with monocular deprivation (MD) and examined how normal or deprived visual experience with dark rearing (DR) changes the regulation of gene expression at time points spanning the critical period for ODP. Many genes found to have expression regulated by monocular deprivation (change in relative expression between deprived and non-deprived cortical hemispheres), were also regulated with the developmental onset of vision. One notable gene from this study, Ena-VASP-like protein (Evl) increases its expression in deprived cortex relative to non-deprived cortex with MD at P18, but not at other ages (Majdan & Shatz, 2006). Evl encodes a protein that regulates actin dynamics by linking signaling pathways to actin remodeling (Kwiatkowski, Gertler, & Loureiro, 2003; Majdan & Shatz, 2006). This gene also decreases expression with the onset of vision from P12 to P16, indicating that the normal onset of visual input also negatively regulates its expression. Insulin-like growth factor binding protein 2 (Igfbp2) is another notable gene from this study that decreases its expression in deprived cortex relative to non-deprived cortex with MD at P24, but was not regulated after DR (Majdan & Shatz, 2006). Igfbp2 encodes a protein that is associated with neurite outgrowth (Jeong et al., 2013). This gene was also regulated with eye opening, decreasing its expression from P12 to P16, possibly initiating the signaling cascades necessary for flexible regulation of this gene during the critical period. Overall, the gene specific patterns of regulation observed with MD and DR were highly variable with respect to changes in gene expression with eye opening. Understanding the how genes are regulated after the normal onset of vision can provide context for understanding gene regulation during the critical period for ocular dominance plasticity. By providing expression data for the important developmental time

point of eye opening, we can better understand the complex system of gene regulation governing the development of postnatal visual cortex.

Interestingly, most of the genes found to change their expression level over development from P14 to P28, reversed the direction of this change with monocular deprivation. This again indicates there is strict developmental regulation of ODP-associated plasticity genes (Lyckman et al., 2008). Here we show many genes associated with developmental or transcriptional regulation have enriched expression after eye opening, particularly in L2/3 neurons. We identified genes that were regulated with eye opening (all of V1) that also overlapped with Sepw1-enriched genes at P12 or P16. Using this method, we found 161 downregulated and 132 upregulated genes with eye opening that were also enriched in L2/3 cortical neurons. Downregulated genes were largely involved in neuron projection development and upregulated genes were largely involved in developmental regulation and synaptic transmission. This is consistent with other studies finding L2/3 neurons increase activity with sensory input and may be expressing regulatory genes important for normal visual development and later plasticity (Benoit et al., 2015; Fertuzinhos et al., 2014).

In this study, we identify many genes developmentally regulated with eye opening both in all visual cortex and in a subset of excitatory neurons enriched in L2/3. We found that genes upregulated with the developmental onset of vision are largely involved in synaptic transmission and synaptogenesis, while downregulated genes are largely structural (cytoskeletal and extracellular matrix associated). In addition, we find that genes expressed in specific neuronal and non-neuronal cell types are changing their patterns of expression during this time, indicating the cell-type composition of V1 may be

changing with eye opening. We also searched for genes that may be important for the development of L2/3 neurons at eye opening, and identified several Sepw1-enriched genes that changed their expression level from P12 to P16. L2/3 enriched genes upregulated with eye opening from this analysis were largely involved in synaptic transmission and regulation, and genes downregulated with eye opening were largely involved in neuron projection development. The regulatory genes identified as being enriched in L2/3 neurons after eye opening may be important for the development of plasticity in these neurons. Here we add to previous transcriptomic studies of visual cortex development, which largely focused on the critical period for ODP, by providing a comprehensive analysis of genes regulated both in all V1 and a subset of upper cortical layer neurons at eye opening, a period of intense gene regulation in this region.

BRIDGE TO CHAPTER V

In Chapter IV, I discussed the regulation of gene expression during a period of intense synaptogenesis around eye opening (~P14). I found that between P12 and P16, many genes important for synapse formation are up regulated and many genes important for neuron projection development are down regulated in layer 2/3 (L2/3) cortical neurons. A subset these 'neuron project development' genes downregulated in cortex are cytoskeletal molecules or molecules with links to the cytoskeleton. Some molecules found to be downregulated concurrent with eye opening, are upregulated with monocular deprivation in non-dominant cortex. This indicates a complex system of gene regulation that is differentially modulated by activity at different developmental stages. In Chapter V, I examine how manipulating the expression of an Ig-domain cell adhesion molecule,

nectin-3, affects the development of L2/3 neurons in post-natal visual cortex. The nectins are a family of Ig-domain cell adhesion molecules that bind *in trans* at a number of cell–cell junctions (Rikitake et al., 2012). Nectin-3 is located at post-synaptic sites and interacts *in trans* with pre-synaptic nectin-1 to stabilize synapse between hippocampal neurons. In Chapter II, both nectin-1 and nectin-3 were found to have enriched expression in L2/3 neurons (Tomorsky et al., 2017), but their function in synapse formation during the development of these neurons is unknown.

In the next chapter, I examine how manipulating nectin-3 expression in layer 2/3 neurons affects dendritic spine densities at eye opening (P14), one week after eye opening (P21), and at the close of the critical period for ocular dominance plasticity (ODP) at P35. I discovered that in the week after eye opening, the developmental increase in synaptic densities is amplified with nectin-3 knockdown and diminished with nectin-3 overexpression. I also found that spines are pruned from P21 to P35, consistent with previous literature, and that this pruning occurs regardless of whether nectin-3 is knocked down or overexpressed. This suggests that nectin-3 is not necessary for synaptic pruning during the critical period for ODP, but may have a regulatory role in spine formation and maturation in the week following eye opening. Nectin molecules are known to interact with f-actin through a linker molecule, afadin, which interacts with the cytoplasmic tail of nectins. Here I propose that the reciprocal interaction between nectin and actin through afadin may help facilitate the increased spine formation observed between P14 and P21. Regulation of cell adhesion molecules during this developmental period of high synaptogenesis is relatively unknown, and here I discuss reasons a balance of stability and plasticity may be necessary for normal development.

CHAPTER V

THE ROLE OF NECTINS IN SYNAPSE FORMATION IN DEVELOPING CORTICAL LAYER 2/3 NEURONS

INTRODUCTION

Developing neurons are required to find and stabilize the connections necessary for circuit function, first through the extension of axonal and dendritic processes, and then through the development of synapses (Niell et al., 2004). Synapses are composed of at least two different types of cell-cell junctions: synaptic and puncta adherentia junctions (Mizoguchi et al., 2002; Rikitake et al., 2012). Synaptic junctions (SJs) are the first to form, and are sites of neurotransmission consisting of synaptic vesicles at the axonal/presynaptic side, and calcium channels and neurotransmitter receptors at the dendritic/postsynaptic side (Figure 1A) (Mizoguchi et al., 2002). As synapses develop, they are stabilized by the formation of puncta adherentia junctions (PAJs), distinct regions surrounding synaptic junctions composed of a variety of cell adhesion molecules (Mizoguchi et al., 2002). PAJs are formed and remodeled over development in an activity dependent manner, and have a role in synaptic plasticity that may vary depending on cell type and developmental stage (Mizoguchi et al., 2002).

The nectins are a family of Ig-domain cell adhesion molecules found at PAJs that form cis-dimers and bind *in trans* through their third and first extracellular Ig-domains, respectively (Honda et al., 2006; Rikitake et al., 2012; Tachibana et al., 2000; Takai & Nakanishi, 2003). The cytoplasmic C-terminus of nectin proteins interacts with afadin, which in turn connects nectins to actin and cadherin molecules (Ikeda et al., 1999;

Tachibana et al., 2000; Takai & Nakanishi, 2003). Nectins and cadherins co-localize at PAJs through an interaction between the nectin bound molecule, afadin, and the cadherin associated molecule, α-catenin (Rikitake et al., 2012; Tachibana et al., 2000). Ig-domain binding of nectin proteins occurs independently of its intracellular binding to afadin, but the cytoplasmic C-terminus of nectin proteins is necessary for both their interactions with cadherins and the actin cytoskeleton (Tachibana et al., 2000). Pre-synaptic nectin-1, localized at the axonal boutons of dentate granule cells, has been shown to interact *in trans* with post-synaptic nectin-3 on the dendrites of CA3 principal neurons at the stratum lucidum in hippocampus (Figure 1A) (Honda et al., 2006; Mizoguchi et al., 2002). The co-localization of pre-synaptic nectin-1, post-synaptic nectin-3, and their associated PAJ proteins, has been shown at P7 at immature SJs in the stratum lucidum (Mizoguchi et al., 2002). By P14, nectin-1 and nectin-3 localize specifically at PAJs but not at SJs (Mizoguchi et al., 2002). This indicates that nectin-1 and nectin-3 may be involved in both the formation and maturation (stabilization) of synapses in hippocampus and the segregation of SJ and PAJ domains (Mizoguchi et al., 2002).

Disrupting the binding of nectin-1 to nectin-3 in hippocampus through knockdown, knockout, or pharmacological blockade, produces a variety of effects on synapse morphology, density, and function depending on the system studied and the age of knockdown (Honda et al., 2006; Mizoguchi et al., 2002; Wang et al., 2013; Wang et al., 2017). Disrupting the trans-binding of nectin-1 and nectin-3 in cultured developing hippocampal neurons through the application of glycoprotein D (a nectin-1 inhibitor), resulted in a decrease in size and increase in number of synapses (Mizoguchi et al., 2002). Nectin-$1^{-/-}$ and nectin-$3^{-/-}$ knockout mice had an overextended mossy fiber

infrapyramidal bundle and significantly fewer PAJs (Honda et al., 2006). However, the morphological characteristics of dendritic spines and synaptic transmission at mossy fiber synapses were indistinguishable from WT mice at the age of assay (6-12 weeks) (Honda et al., 2006). Eliminating nectin proteins throughout the development of an animal by genetic 'knockout' may lead to the recruitment of compensatory mechanisms to normalize synaptic function in the absence of these proteins (Gil-Sanz et al., 2013). Indeed, several studies have found different phenotypes with genetic 'knockout' vs 'knockdown', a phenomenon previously attributed to genetic compensation (El-Brolosy & Stainier, 2017). Consistent with this, shRNA knockdown of nectin-3 in adult hippocampus decreases dendritic spine densities in CA3 or dentate granule cells, corresponding with deficits in long term memory formation (Wang et al., 2013; Wang et al., 2017). In addition, overexpression of nectin-3 in hippocampal neurons prevented the decrease in spine densities normally associated with early life stress (Wang et al., 2013). These studies and others linking nectin binding to a variety of biological and disease states, including stress, taopathy, and mental retardation, indicate that nectins may have different functions in the development, aging, and maintenance of a number of different systems (Gong et al., 2018; Maurin et al., 2013; Van der Kooij et al., 2014; Wang et al., 2013; Wang et al., 2017).

While a great deal of work has been done examining the function of nectins in adult and developing hippocampus, fewer studies have examined the role of nectin binding in cortex. Mammalian cortex has a conserved laminar structure, and nectin-1 and nectin-3 have been shown by us and others to have distinct laminar expression patterns with enriched expression in upper cortical layers of post-natal mouse cortex (Allen

Developing Mouse Brain Atlas (2008), Maurin et al., 2013; Tomorsky et al., 2017) (Figure 1B, Figure 2). One study found that coincidence detection between nectin-1 expressing Cajal-Retzius cells in L1 and newly born deep layer neurons expressing nectin-3 was important for guiding the migration of these neurons between embryonic day 12.5 (E12.5) and E16.5 (Gil-Sanz et al., 2013). The migration of deep layer neurons, however, occurs via different mechanisms than that of upper layer neurons; the former are glial independent and the later are glial dependent (Gil-Sanz et al., 2013; Hirota & Nakajima, 2017; Nadarajah et al., 2003). It is unclear if the mechanisms governing the migration L2/3 neurons would also depend on nectin expression. In addition, the function of nectin-1 to nectin-3 binding in post-natal cortical development is unknown.

To identify potential roles of nectin-3 and nectin-1 in the development of upper layer cortical neurons, we used *in utero* electroporation to deliver nectin-1 and nectin-3 shRNA constructs to mouse L2/3 cortical neurons at E15.5. No migration deficit was observed at P21 when both nectins were knocked down in newly born L2/3 cortical neurons, but we did observe an increase in dendritic spine densities as compared to control neurons receiving a scramble shRNA. Since nectin-3 is localized to dendritic spines in hippocampus, we hypothesized that knocking down nectin-3 alone may replicate the spine density phenotype observed with double knockdown. To determine the function of nectin-3 alone, we knocked down, overexpressed, and introduced a dominant negative form of nectin-3 (lacking a C-terminus) to developing L2/3 neurons and examined synaptic densities at P14, P21, and P35. Again, we found that nectin-3 knockdown increased spine densities, while overexpression decreased spine densities. Dominant negative expression of nectin-3 appeared prevent the developmental increase

in spine densities normally observed between P14 and P21. We also show that the phenotypic increase in dendritic spine densities after eye opening does not depend on the early developmental knockdown (E15.5–P14) of nectin-3 expression. These results correspond best to the pharmacological blockade of nectin binding in culture, and indicate that the intra and extracellular domains of nectin-3 may mediate different aspects of post-natal synapse formation in L2/3 of visual cortex.

MATERIALS AND METHODS

Immunohistochemistry

Tissue preparation for immunohistochemistry (IHC) was performed as previously described (Piscopo, Weible, Rothbart, Posner, & Niell, 2018). Briefly, brains were prepared for IHC by first fixing perfused brains overnight in 4% PFA (1 x PBS), after which brains were immersed in 30% sucrose (1 x PBS) for 24–48 hours. Brains were then sliced on a vibratome to a thickness of 80 µm, placed in cryoprotectent solution (30% sucrose, 1% polyvinyl-pyrrolidone, 30% ethylene glycol in 0.1 M PB), and stored at -20 ºC. IHC was performed on free floating sections as previously described (Piscopo et al., 2018). Briefly, sections were washed 3 x 10 min in 0.7% glycine solution in PBS, and blocked for 1–3 h in a solution of 5% goat and 5% donkey serum in PBT. Slices were then transferred to a primary antibody solution of 1.5 µL/mL of Anti-RFP rabbit (Rockland Cat# 600-401-379, RRID:AB_2209751) and 2 µL/mL of Anti-GFP chicken (Aves Labs Cat# GFP-1020, RRID:AB_10000240) and incubated overnight at 4 ºC. The next day slices were washed 1 x 10 min in PBST and 3 x 10 min in PBS and transferred to a solution of 4 µL/mL of rabbit-555 (Thermo Fisher Scientific Cat# A-21429,

RRID:AB_2535850) and 4 µL/mL chick-488 (Jackson ImmunoResearch Labs Cat# 703-545-155, RRID:AB_2340375) secondary antibodies in PBT. Slices were incubated in secondary for 3 h at room temperature, then washed for 10 min in PBT at room temperature, followed by an overnight wash in PBS at 4 ºC. The next day, slices were washed an additional 2 x 10 min in PBS, placed on slides, treated with DAPI (4′, 6-diamidino-2-phenylindole), and mounted with VECTASHIELD mounting media (Vector Labs).

In situ hybridization

The expression patterns of nectin-1 and nectin-3 were assayed by nonradioactive colorimetric RNA *in situ* hybridization, using solutions and probes as previously described (Lein et al., 2007; Oh et al., 2014; Tomorsky et al., 2017; Wehr et al., 2009). Briefly, animals were perfused, and brains were fixed (4% PFA) and cryoprotected in a 30% sucrose solution, as described. Brains were then cryosectioned to a thickness of 30 µm, placed onto Superfrost Plus slides (Fisherbrand), and stored at -80 °C until use. 30 µm sections were brought to room temperature, washed in PBS and acetylated (Lein et al., 2007). Slides were then pre-hybridized in hybridization solution in a humidity chamber for 2 h at 70 °C. The riboprobes to *Pvrl1* and *Pvrl3* (the genes encoding nectin-1 and nectin-3 proteins) were diluted in hybridization solution to a concentration of 1–2 ng/µL, and were generated with dig-labeled nucleotides and SP6 RNA polymerase using probe sequences and protocols described by the Allen Brain Institute (Allen Mouse Brain Atlas (2004); Allen Developing Mouse Brain Atlas (2008); Lein et al., 2007). Slides were hybridized overnight at 70 °C with each probe. Slides were

then washed (at 70 °C) and blocked before incubating overnight at 4 °C in Anti-dig sheep Fab fragments conjugated to alkaline phosphatase (AP) (Roche No. 11093274910) diluted 1:2500 in blocking solution. Slices were then washed at room temperature with MABT buffer and then AP staining buffer, after which 3.5 µL/mL NBT, 2.6 µL/mL BCIP, and 80 µL/mL levamisole in AP staining buffer was applied. The AP colorimetric reaction was observed closely as it developed for 3–48 h at 37 °C, and was stopped by washing twice with PBS (0.1% Tween-20) and twice with deionized H_2O. Slides were then dehydrated in graded ethanols and mounted (Permount).

Design of Cre-dependent nectin-1 and nectin-3 shRNA plasmids

Nectin-3 shRNA was designed using previously used siRNA sequences (Gil-Sanz et al., 2013). These 19bp sequences were used to design shRNA hairpin sequences for cloning into a pSico vector as previously described (Gil-Sanz et al., 2013, Ventura et al., 2004). The siRNA sequence to nectin-1 was designed using an online tool and similarly used to construct an shRNA hairpin sequence for cloning into pSico (Ventura et al., 2004). The nectin-3, nectin-1, and scramble shRNA oligos used for cloning were as follows:

Pvrl3 shRNA1 sense oligo:

TGGCCGGATTCTTTAATTGATTCAAGAGTCAATTAAAGAATCCGGCCTTTTTTC

Pvrl3 shRNA1 antisense oligo:

TCGAGAAAAAAGGCCGGATTCTTTAATTGACTCTTGAATCAATTAAAGAATCCGGCC A

Pvrl3 shRNA2 sense oligo:

TGTTTATTGGCGTCAGATAATTCAAGAGATTATCTGACGCCAATAAACTTTTTTC

Pvrl3 shRNA2 antisense oligo:

TCGAGAAAAAAGTTTATTGGCGTCAGATAATCTCTTGAATTATCTGACGCCAATAAACA

Scr sense oligo:

TGCTACACTATCGAGCAATTTTCAAGAGAAATTGCTCGATAGTGTAGCTTTTTTC

Scr antisense oligo:

TCGAGAAAAAAGCTACACTATCGAGCAATTTCTCTTGAAAATTGCTCGATAGTGTAGCA

Pvrl1 shRNA1 sense oligo:

TGCATTGTCAACTATCACCTTTCAAGAGAGGTGATAGTTGACAATGCTTTTTTC

Pvrl1 shRNA1 antisense oligo:

TCGAGAAAAAAGCATTGTCAACTATCACCTCTCTTGAAAGGTGATAGTTGACAATGCA

Cloning into pSico was modified from methods previously described (Ventura et al., 2004). Briefly, restriction enzymes XhoI and HpaI were used to digest the pSico vector (Addgene plasmid #11578). Digested vector RNA was then dephosphorylated using shrimp alkaline phosphatase (Roche) for 60 min at 37 °C to prevent re-ligation of the vector, followed by deactivation at 65 °C for 15 min. 1 µL of 100 µM sense and antisense shRNA oligos synthesized by IDT were then annealed and phosphorylated using T4 PNK (1µL 10X T4 Ligation Buffer (NEB), 6.5 µL H2O and 0.5 µL T4 PNK (NEB)). Annealing was performed in a thermocycler at 37 °C for 30 min and then 95 °C for 5 min, followed by a ramp down to 25 °C at 5 °C/min. Vector and insert were the ligated with Quick Ligase (NEB) using manufacturers protocols. Ligated plasmid was then treated with PlasmidSafe exonuclease to prevent unwanted recombination products and used to transform NEB Stable Competent *e. coli*. Positive colonies were grown in LB + amp., after which plasmid DNA was extracted (QIAprep Spin Miniprep Kit) and sequenced using the pSico sequencing primer: CAAACACAGTGCACACAACGC (Ventura et al., 2004). Plasmid DNA verified to contain the shRNA insert was then

prepped for electroporation from 200–400 µL of cultured *e. coli* using a NucleoBond Midi or Maxi EF kit (Clontech) and eluted to a concentration of 5–10 µg/µL in TE.

Design of nectin-3 overexpression construct

A nectin-3 overexpression vector was created by modifying a pCag-iCre expression vector (Addgene plasmid # 89573). Nectin-3 alpha was PCR amplified (KOD hot start DNA polymerase) from a mouse brain cDNA library using the forward primer: GTTGAGGACACGCGCG and reverse primer: CTGTTAGACATACCACTCCCTCC. Amplified DNA was run on a gel and a band of the approximate length of nectin-3 (~1800bp) was cut from the gel and purified (Quiaquick Gel Extraction Kit). Sequences were then amplified (KOD hot start DNA polymerase) using nested primers with and without a flag tag and containing restriction sites for MluI and Not1. Primer sequences were as follows (restriction sites are bold):

Nectin-3 F: TAAGCA-ACGCGT-GCCACCATGGCGCGGACCCCG

Nectin-3 R: TGCTTA-GCGGCCGC-TTA-GACATACCACTCCCTCCTG

Nectin-3 R Flag: TAAGCA-GCGGCCGC-TTA-CTTGTCGTCATCGTCTTTGTAGTC-GACATACCACTCCCTCCTG

Amplified DNA was then gel purified, and digested using the same restriction sites. The pCAG-iCre plasmid was also digested with MluI and NotI to remove the iCre sequence from the vector and gel purified. Digested vector and nectin-3 were then ligated, used to transform *e. coli*, and prepped for electroporation, as for pSico shRNA vectors. Positive clones were sequenced using a pCag F: GCAACGTTGCTGGTTATTGT, and Bglob-pA R: TTTTTGGCAGAGGGAAAAGAT sequencing primers.

A previously published dominant negative construct for nectin-3 was kindly gifted by Dr. Gil Sanz and Dr. Mueller (Gil-Sanz et al., 2013). FLEX-tdTomato constructs were purchased from Addgene (plasmid #51509 and #51505), and the Cre plasmid was also from Addgene (plasmid #51904).

In utero electroporation of plasmid DNA

All experimental protocols were approved by the University of Oregon Institutional Animal Care and Use Committees, in compliance with the National Institutes of Health guidelines for the care and use of experimental animals. *In utero* electroporation was performed at E15.5 to target L2/3 pyramidal neurons, as previously described (Harwell et al., 2012). For shRNA knockdown using pSico, a solution of ~2 µg/µL of pSico-shRNA vector, ~1.5 µg/µL of FLEX-tdTomato and ~0.02 µg/µL Cre plasmids were prepped in PBS (pH 7.2 for injections). In addition, 0.1% Fast Green dye was used to visualize plasmid DNA as it entered the ventricle with injection. For overexpression (OE) and dominant negative (DN) experiments, a solution of ~0.5 µg/µL DN or OE expression vector, ~1ug/µL FLEX-tdTomato, and ~0.01 µg/µL Cre plasmids was prepared in PBS and 0.1% Fast Green. For double knockdown using both nectin-3 and nectin-1 shRNA, 1.5 µg/µL of each shRNA expression vector was combined in solution.

Timed pregnancies were set up overnight between a hybrid strain (F1 cross of C57BL/6J and 129S1/SvlmJ, Jax) of WT female mice and either the same strain of WT male mice or *CaMKII-Cre* homozygous transgenic male mice (Jax 005359). The day the plug was observed was designated embryonic day 0.5 (E0.5). 15.5 day pregnant mice

were anesthetized with 2% isofluorane (0.8% O_2) for the duration of the surgery. A small incision was made in the abdomen of pregnant females and the uterus was pulled out of the abdominal cavity. ~1 µL of plasmid solution was injected into the ventricle of E15.5 pup brains through the uterus. Visual cortex was then targeted with an electrical pulse through tweezer-type electrodes using five, 45 V, 100 ms pulses at a 1 s interval. The uterus was then placed back in the abdominal cavity, the mouse was sutured, and allowed to recover. Animal health was monitored daily after surgery until pups were born (~4 days later). Electroporated mice were perfused as previously described (Piscopo et al., 2018) at P14, P21, or P35, and brains were prepared for immunohistochemistry.

Microscopy and spine counting

In situ hybridizations were imaged using an EC Plan-NEOFLUAR 5x/0.16 objective on a Zeiss Axio Imager.A2 wide field epifluorescence microscope having an X-Cite 120Q LED excitation lamp and a Zeiss AxioCam MRm 1.4 megapixel camera. ZEN lite imaging software (2012) was used to view images, and Adobe Photoshop CS6 was used for the background removal and color processing of images.

Electroporated sections were checked for fluorescent neurons in V1 using the Zeiss Axio Imager.A2 microscope and an EC Plan-NEOFLUAR 2.5x/0.085 objective. Immunohistochemistry was performed on sections confirmed to have successful electroporations. Neurons identified as being located V1 L2/3 using DAPI staining and a mouse brain atlas (Paxinos & Franklin, 2013) were imaged on a ZeissLSM700 confocal microscope using Zen software. Images of secondary (at least one branching away from the soma) apical and basal dendrites were taken for double knockdown and CKII-

experiments (Figures 3–5). The analysis of knockdown (KD), overexpression (OE), dominant negative (DN), and scramble neurons over multiple ages was performed using basal dendrites only (Figure 6 and Figure 7). High resolution images of dendrites for spine counting were taken using a Plan-Apochromat 63x/1.40 Oil DIC objective with 1.1–1.3x zoom, a speed of 8, averaging of 2, z-resolution of 0.3 μm, and variable laser intensities to capture dendritic spines. Spines in high resolution images of dendrites were counted manually using the open source FIJI image analysis software and the multipoint tool. Neurite lengths were measured using the 'simple neurite tracer' plugin

Statistical analysis

ANOVA analyses (either type 3 or with Tukey's HD post-hoc test) were performed in R to determine the effects of age, condition, and cortical location on dendritic spine densities. A statistics table is provided as Supplementary Table 1 describing all statistical analyses and p-values found. Select p-values are also listed in figure legends. Dendritic spine densities in different brain areas (V1M, V1B, or V2) at P21 and P35 were examined using data from nectin-3 overexpression, knockdown, and scramble conditions (Figure 7). Neurons with measured spine densities at P21 or P35 were mapped to V1M, V1B, or V2 cortical regions using a brain atlas (Paxinos & Franklin, 2013) and 2.5x images of brain sections (Zeiss Axio Imager.A2 microscope). For age and condition comparisons, V2 neurons were limited to 1–2 per condition. A minimum of 12 basal dendrites for each condition/age pairing were analyzed (exception: V2-P35, N = 6, Figure 7, Supplementary Table 1).

RESULTS

Nectin-1 and nectin-3 have enriched expression in L2/3 visual cortex

To determine the expression patterns of nectin-1 and nectin-3 just after eye opening, we performed an *in situ* hybridization (ISH) to *Pvrl3* and *Pvrl1* (the genes encoding nectin-3 and nectin-1 proteins) in post-natal visual cortex at P16 (Figure 1B). We also examined *in situ* data available at allenbrain.org (Allen Developing Mouse Brain Atlas (2008)) to both nectins at a variety of developmental time points (Figure 2). Our ISHs revealed both genes have enriched expression in L2/3 of visual cortex at P16 (Figure 1B). Developmental data from Allen Brain Atlas shows L2/3 enriched expression of nectin-3 first appears at E18.5, and nectin-3 remains highly expressed in these neurons throughout development (Figure 2). Nectin-1 begins to show enriched expression in L2/3 and L5 at P4 and remains enriched in these layers between P14 and P28 (Figure 2). This indicates the functional role of nectin-1 and nectin-3 in cortical development may change depending on developmental stage.

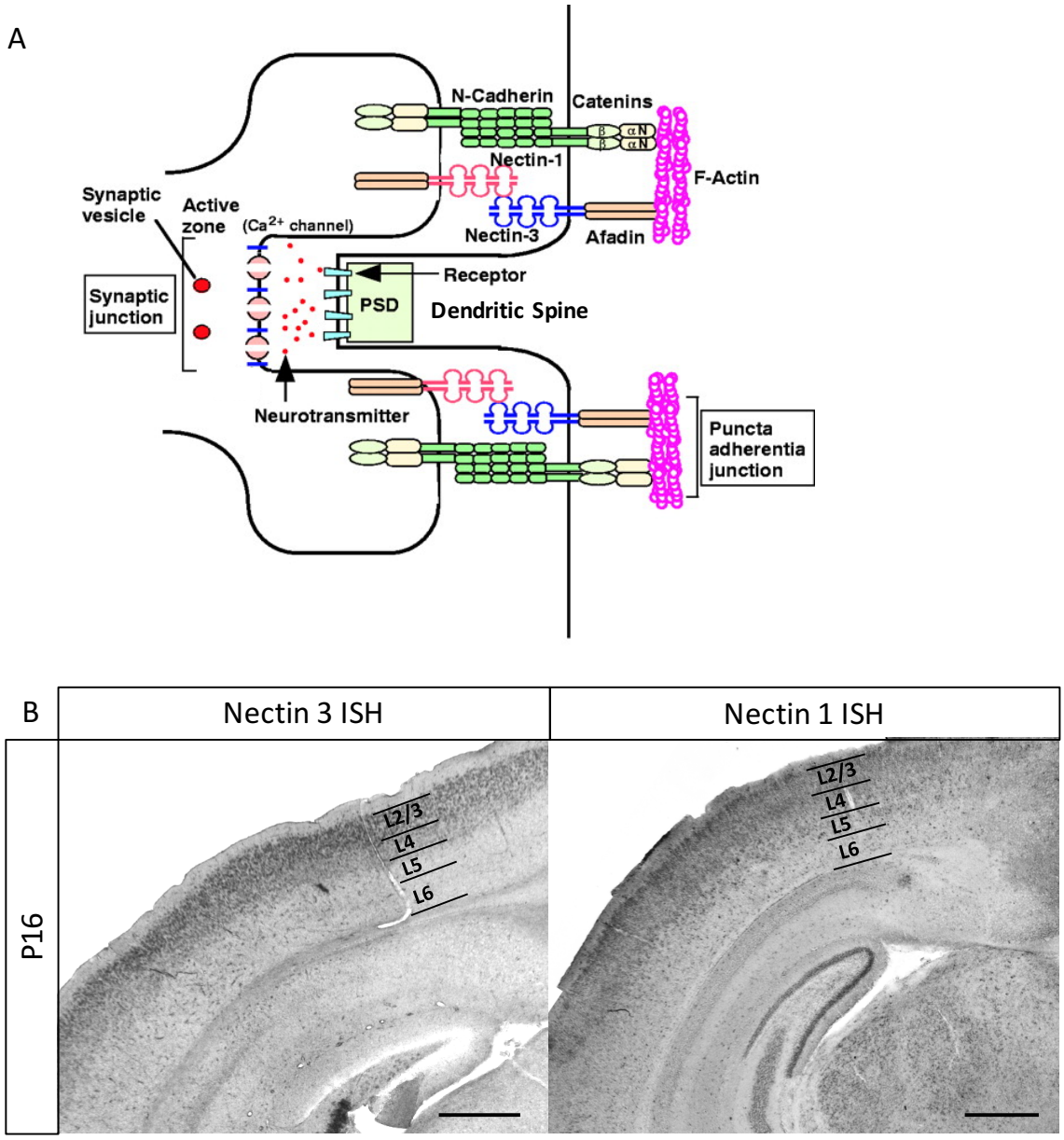

Figure 1. Nectin-1 and nectin-3 are binding partners with enriched expression in layer 2/3 of visual cortex at P16.
(A) Nectin-1 and nectin-3 have been shown to bind *in trans* at puncta adherentia junctions (PAJs) in hippocampus and interact with actin secondarily through their binding partner afadin (Honda et al., 2006; Mizoguchi et al., 2002). Nectin and afadin have also been shown to interact with N-cadherin at PAJs (Honda et al., 2006; Mizoguchi et al., 2002; Rikitake et al., 2012; Satoh-Horikawa et al., 2000). N-cadherin binds β-catenin, which in turn binds α-catenin, which associates with afadin to co-localize nectins and cadherins (Rikitake et al., 2012; Tachibana et al., 2000; Takai & Nakanishi, 2003). PAJs are found at synapses and are stabilizing sites of adhesion between axons and dendrites. PAJs are distinct from synaptic junctions (SJs), which are the sites of neurotransmission. SJs incorporate neurotransmitter receptors at post-synaptic densities

on dendritic spines, and synaptic vesicles at presynaptic active zones (Mizoguchi et al., 2002; Takai & Nakanishi, 2003). Schematic diagram is modified from Takai & Nakanishi, 2003.
(B) *In situ* hybridizations (ISH) to nectin-3 and nectin-1 demonstrate enriched expression in upper cortical layer neurons in V1 at P16 (5x objective, scale bar = 500 µm).

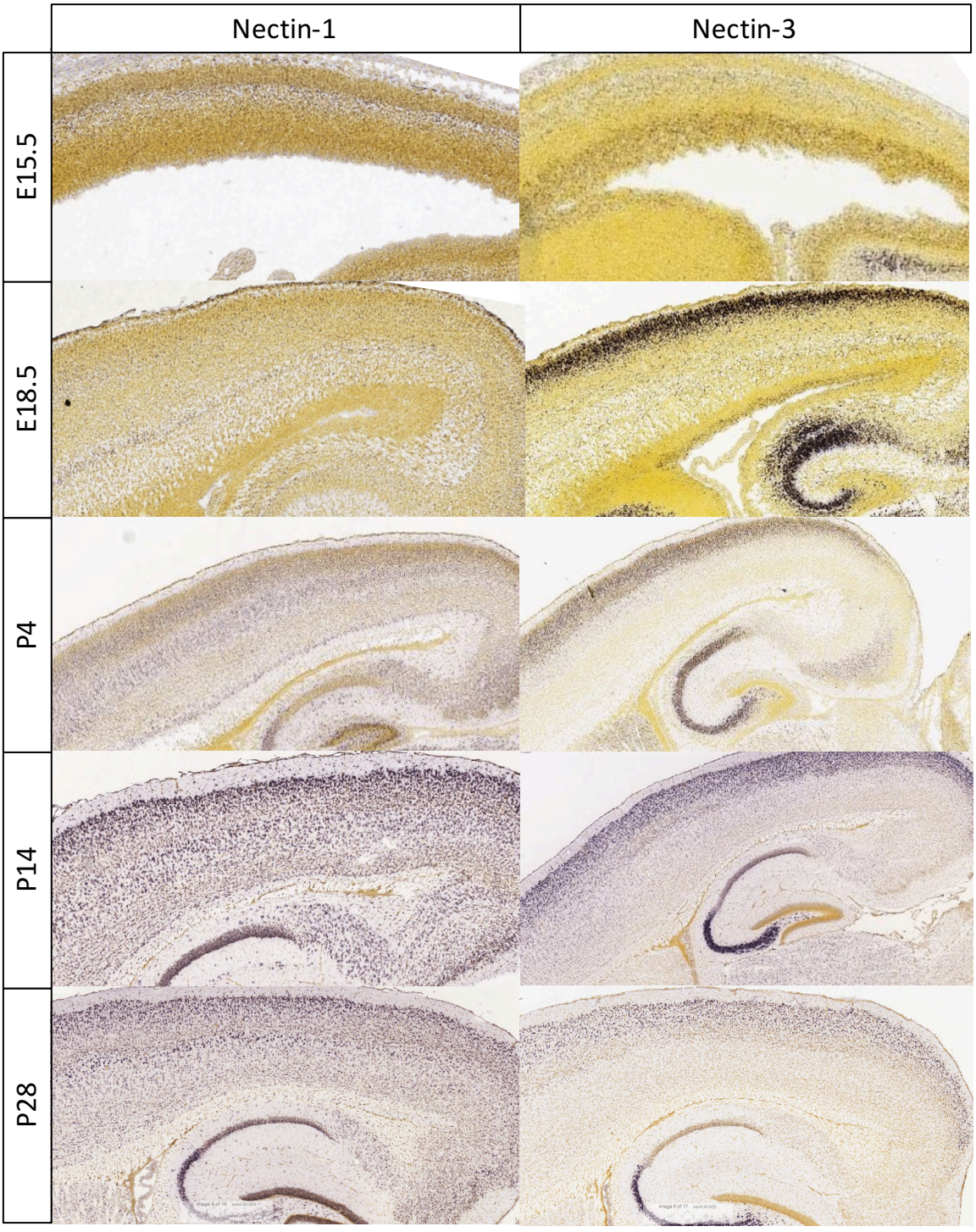

Figure 2. Nectin-1 and nectin-3 expression over development.
Allen brain atlas *in situ* data collected at various developmental time points for nectin-1 and nectin-3 (Image credit: Allen Institute) (Allen Developing Mouse Brain Atlas (2008)). Both nectins change their expression patterns over development, but have relatively consistent postnatal laminar segregation.

Double knockdown of nectin-1 and nectin-3 increase spine densities at P21

To determine whether nectin-1 and nectin-3 may influence synapse formation in postnatal visual cortex, we knocked down both proteins in developing layer 2/3 cortical neurons. To manipulate gene expression in developing layer 2/3 neurons, we used *in utero* electroporation to introduce plasmid DNA to dividing cortical cells *in vivo*. *In utero* electroporation uses an electrical pulse to draw injected DNA into specific developing cell types, depending on the placement of the electrodes and the developmental time point at which the manipulation takes place (Langevin et al., 2007; LoTurco, Manent, & Sidiqi, 2009). We designed Cre-dependent shRNA constructs targeting nectin-1 and nectin-3 using the pSico vector, which contains a loxP flanked GFP-stop sequence that prevents the expression of shRNA in the absence of Cre. Nectin-1 and nectin-3 shRNA constructs were co-electroporated at E15.5 with both a Cre-dependent tdTomato construct (also expressing synaptophysin-EGFP) and a low concentration of a pCag-Cre vector for sparse knockdown of both nectin proteins (Figure 3A, C). In this system, Cre-negative neurons express GFP and Cre-positive neurons express tdTomato (Figure 3B). Both GFP and tdTomato expressing neurons showed normal migration (Figure 3B and 3C).

To assess the potential effects of nectin-1 and nectin-3 on synapse formation in L2/3 neurons, we identified tdTomato expressing neurons in V1 and imaged one apical and one basal dendrite at 63x (Figure 3D). Dendritic spines were manually counted to

obtain measurements of dendritic spine density in both knockdown neurons and in control neurons expressing a scramble shRNA. Control scramble shRNA animals and constructs were prepared identically to those receiving shRNA to nectin-1 and nectin-3. Dendritic spine densities were significantly greater in neurons electroporated with nectin-1 and nectin-3 shRNA expressing plasmid vectors (Figure 4A) than in those expressing scramble shRNA (Figure 4B) at P21 (Figure 4C). Both apical and basal dendrites were similarly affected by nectin knockdown (Figure 4C). From this we conclude that nectin binding may regulate dendritic spine densities one week after eye opening.

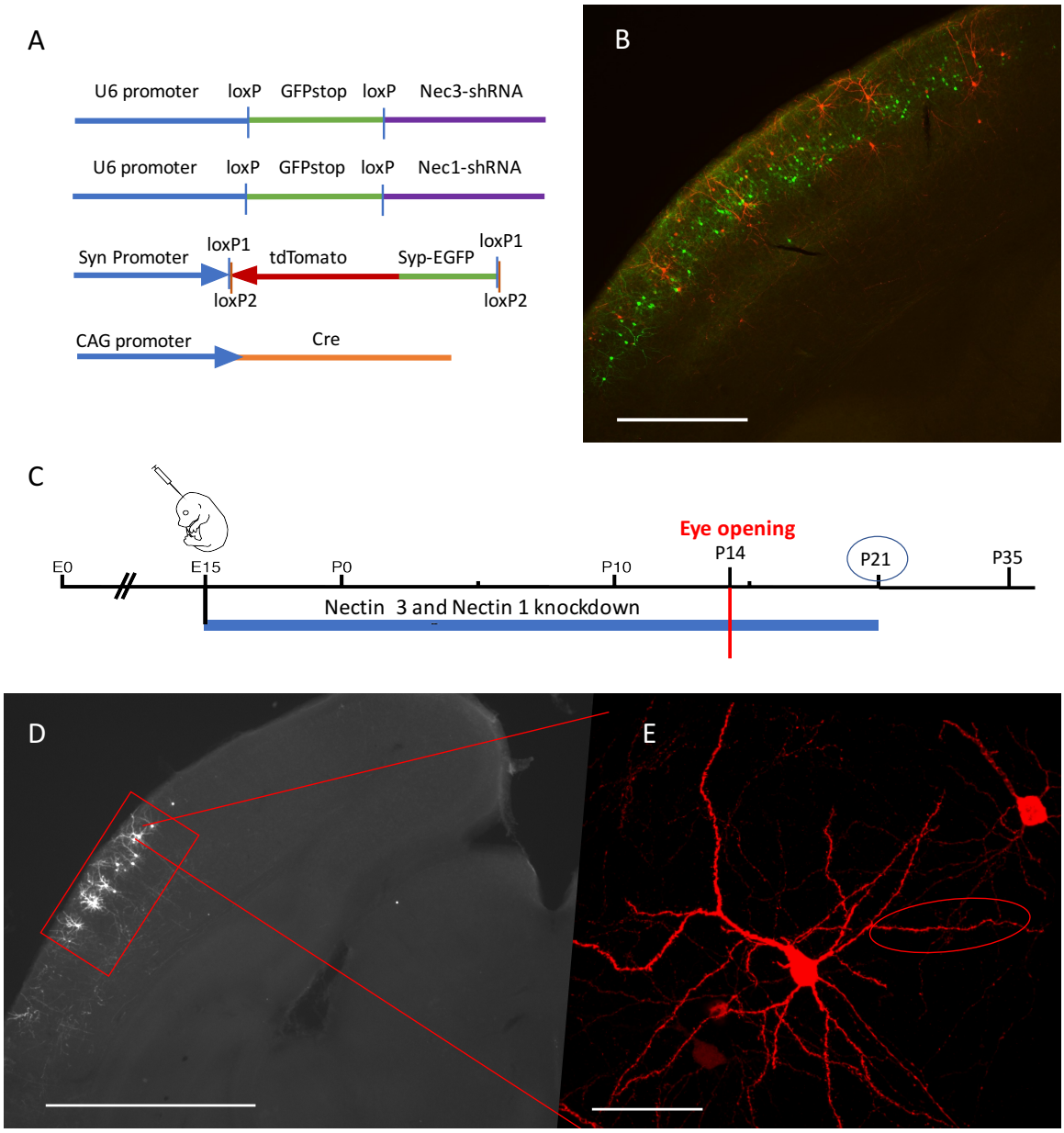

Figure 3. Knocking down nectin-1 and nectin-3 at P21 in developing L2/3 cortical neurons.

(A) Cre-dependent shRNA constructs to nectin-1 and nectin-3 were designed using the pSico vector containing a loxP flanked GFP-stop sequence to prevent the expression of shRNA in the absence of Cre. In this system, GFP-positive cells are Cre-negative. As a control, a scramble shRNA construct was designed using the same pSico plasmid vector. A Cre-dependent FLEX tdTomato plasmid also expressing synaptophysin-EGFP was co-electroporated with shRNA constructs. Cre-positive cells also positive for this plasmid expressed cytoplasmic tdTomato and pre-synaptic EGFP. A Cre-plasmid was also co-electroporated at a low concentration for immediate and sparse Cre-mediated expression of shRNA and tdTomato.

(B) 10x image of nectin-1 and nectin-3 knockdown neurons at P21 in visual cortex. Cre-positive RFP-expressing cells assumed positive for nectin shRNA can be observed surrounded by Cre-negative GFP-expressing cells. All cells migrated normally to L2/3 (scale bar = 500 µm).
(C) Animals were electroporated at E15.5 when L2/3 neurons are born at the ventricle. Co-electroporation with a Cre-plasmid immediately initiated shRNA expression in Cre-positive cells. Dendritic spine densities were assayed at P21.
(D) RFP-expressing cells in V1 at P21 were identified (2.5x image, scale bar = 1 mm).
(E) One apical and one basal dendrite, at least one branch away from the soma, were imaged at 63x for spine counting. At least 12 cells were used per condition (nectin knockdown or control scramble) (40x image, scale bar = 50 µm).

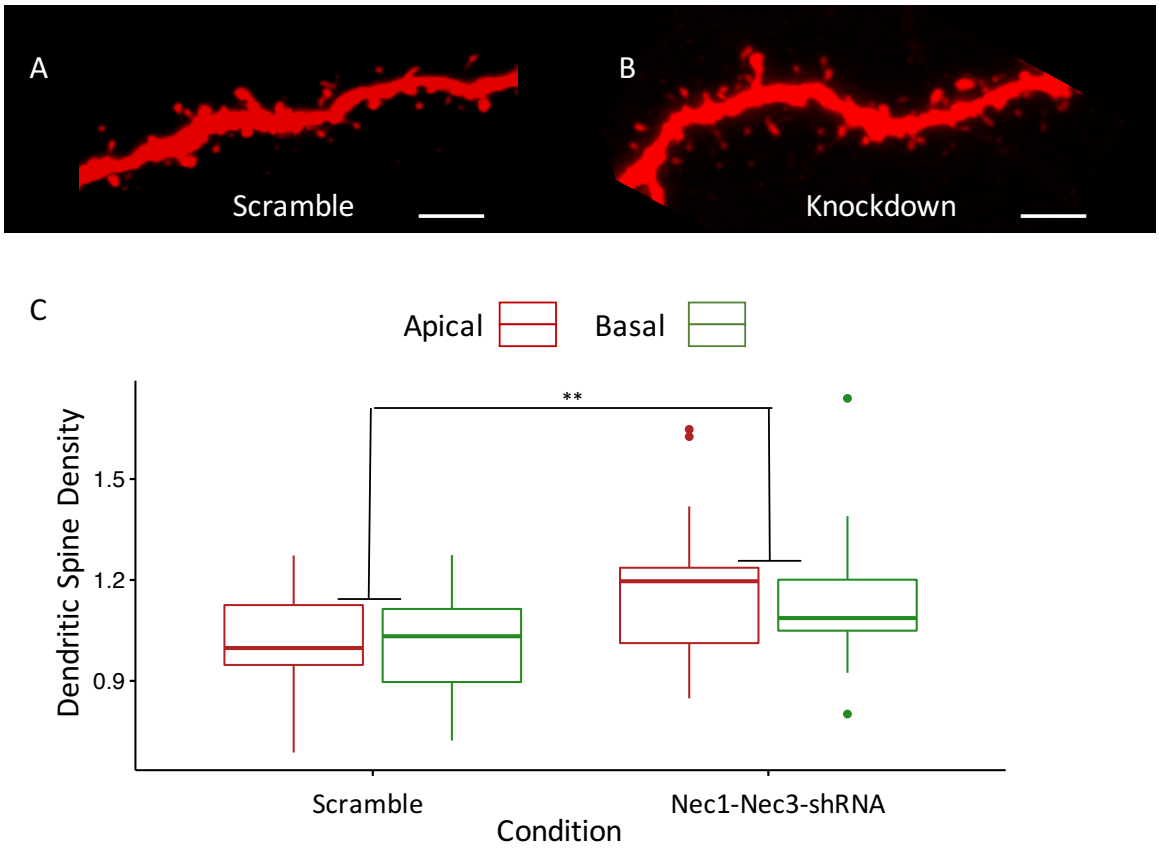

Figure 4. Spine density is increased in nectin-1 nectin-3 double knockdown and similar effects are seen in apical and basal dendritic spines.
(A) Representative image of a dendrite from a neuron expressing a scrambled shRNA construct at P21 (scale bar = 5 µm).
(B) Representative image of a dendrite from a neuron expressing shRNA to nectin-3 and nectin-1 at P21 (scale bar = 5 µm).
(C) Nectin-3 and nectin-1 shRNA expressing neurons exhibited increased dendritic spine densities (number of spines / µm) as compared to neurons expressing scramble shRNA. Differences between apical and basal dendrites were not significant for either condition

(2-way ANOVA, type 3: Scramble vs Nec1-Nec3-shRNA, $p = 0.0066^{**}$; Apical vs Basal, $p = 0.666$).

Nectin-3 knockdown from P14 onwards increases dendritic spine densities at P35

While knockdown of nectin-3 and nectin-1 from E15.5 to P21 produced an increase in dendritic spine densities, this phenotype could have been attributed to multiple factors. It was unclear which protein was driving this phenotype or during which developmental period knockdown was critical. Nectin-3 was previously shown to be localized at post-synaptic sites along dendrites in hippocampal neurons, while nectin-1 was localized at axonal pre-synaptic sites. For this reason, we hypothesized that reduced nectin-3 may be mediating the dendritic spine effect observed, and limited our future experiments to exclusively manipulate nectin-3 expression. In addition, since developmental processes from E15.5 onward might have been affected in the previous experiment, the effects observed at P21 may have depended on the knockdown of nectin proteins before eye opening. In this case, the increased spine densities observed at P21 may have been a compensatory rebound after nectin-3 knockdown decreased spine densities early in development. To examine this possibility, we knocked down nectin-3 alone after eye opening, and spine densities were assayed at P35.

For this experiment, we co-electroporated the same Cre-dependent Nec3-shRNA construct (or control scramble shRNA) with a Cre-dependent tdTomato construct also expressing synaptophysin-EGFP into transgenic *CaMKII-Cre* mice at E15.5. *CaMKII-Cre* does not drive Cre expression in layer 2/3 neurons until after P14, allowing neurons to develop normally until this time (Figure 5A, C). Dendritic spine densities were then analyzed for both apical and basal dendrites at P35, to allow time for full expression of

Cre/shRNA in layer 2/3 cortical neurons (Figure 5B, C). Here we found dendritic spine densities in knockdown neurons were significantly increased compared to control scramble neurons at P35 (Figure 5D). This increase in spine density was not specific to apical or basal dendrites (Figure 5D). From this we conclude that the increase in dendritic spine densities observed after eye opening with nectin-3 knockdown is not dependent on the disruption of early developmental mechanisms.

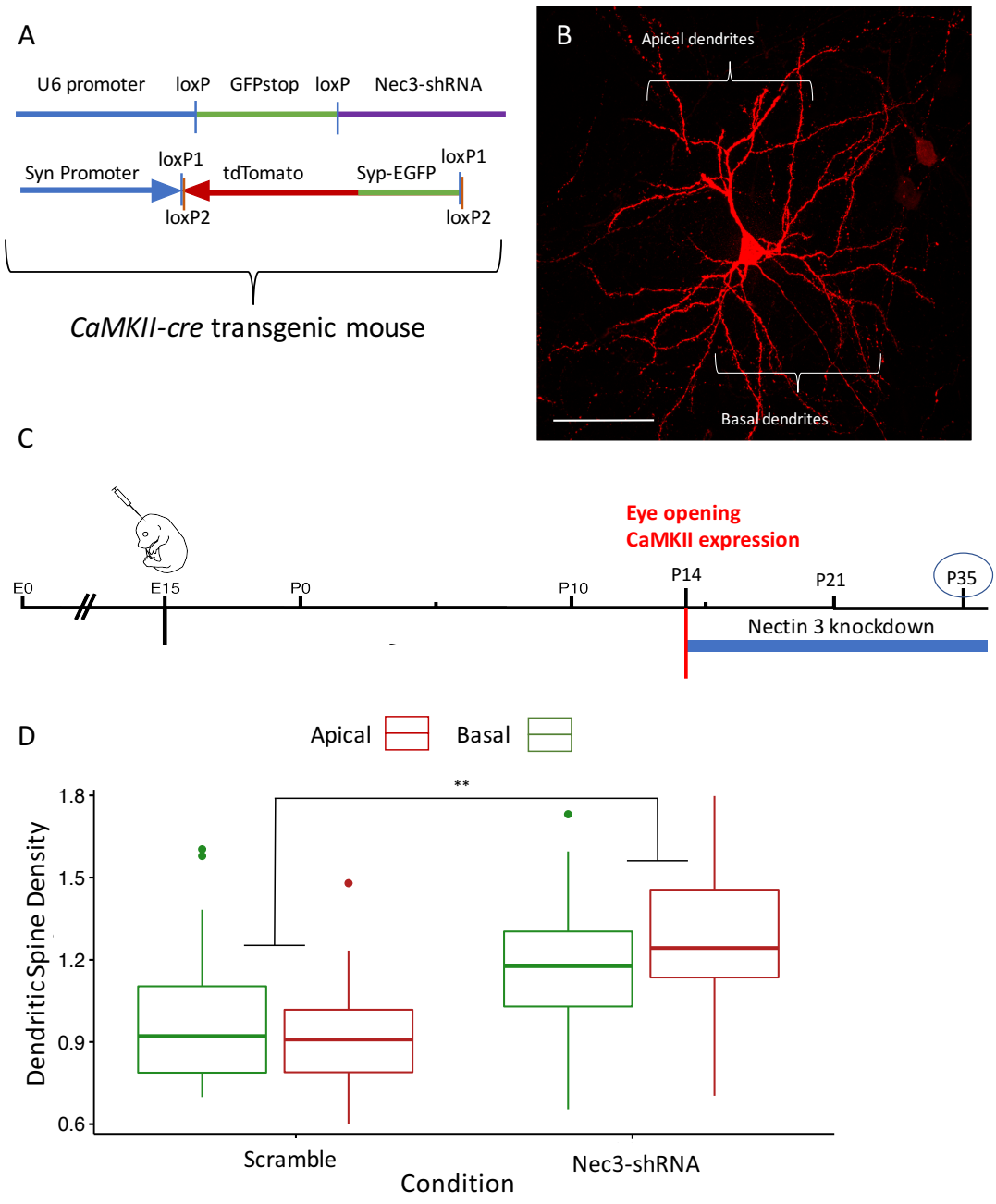

Figure 5. Nectin-3 knockdown at ~P14 results in increased spine densities at P35.
(A) A Cre-dependent shRNA construct to nectin-3 (or scramble shRNA construct) was co-electroporated with a Cre-dependent FLEX tdTomato plasmid (also expressing synaptophysin-EGFP) into developing *CaMKII-cre* transgenic mice.
(B) Both apical and basal dendrites on *CaMKII-cre*/shRNA/tdTomato positive neurons were imaged at P35 (40x image, scale bar = 50 µm).
(C) Mice were electroporated at E15.5 to target developing L2/3 neurons, but Cre expression does not turn on until ~P14 in the *CaMKII-cre* mouse line used. For this

experiment, neurons develop normally until nectin-3 knockdown at ~P14. Mice were sacrificed and neurons were imaged at P35.
(D) Dendritic spine densities (number of spines / μm) at P35 were higher for nectin-3 knockdown neurons than for neurons receiving the scramble shRNA. A similar effect was observed for both apical and basal dendrites (Two-way ANOVA type 3: Nec3-shRNA vs Scramble, $p = 0.00160$; Apical vs Basal, $p = 0.464$).

Knocking down or overexpressing nectin-3 in L2/3 cortical neurons increases and decreases spine densities on basal dendrites, respectively

To gain further insight into the role of nectin-3 in developing L2/3 cortical neurons, we sought to bi-directionally manipulate the expression of nectin-3 in developing L2/3 cortical neurons and examine changes in dendritic spine densities at multiple time points. To accomplish this, we electroporated either an shRNA plasmid (nectin-3 shRNA or control scramble shRNA), overexpression plasmid, or dominant negative (lacking a C-terminus) overexpression plasmid into dividing neurons at E15.5. All shRNA and expression constructs were co-electroporated with a Cre dependent tdTomato construct and a low concentration of a pCag-Cre plasmid (Figure 6A). Dendritic spine densities were assayed for nectin-3 shRNA (Nec3-shRNA), control scramble shRNA (Scramble), nectin-3 overexpression (Nec3-OE), or dominant negative nectin-3 expression (Nec3-DN) neurons at eye opening (P14), one week after eye opening (P21), and at the close of the critical period for ocular dominance plasticity (P35) (Figure 6B, C). As before, tdTomato expressing neurons were identified in V1, but for these experiments, only basal dendrites were assayed (Figure 6C).

Here we found that manipulating nectin-3 expression levels in L2/3 neurons affected the developmental increase and then decrease in dendritic spine densities normally observed after eye opening. Between, P14 and P21 there was a ~37% increase

in spine densities overall. This increase was amplified when nectin-3 was knocked down and diminished when nectin-3 was overexpressed. Expression of a dominant negative nectin-3 eliminated the increase in spine densities normally observed between P14 and P21 (Figure 7A, B). The increase in spine densities between P14 and P21 was significant for all conditions except Nec3-DN (Figure 7B). Between P21 and P35, developmental pruning produced an overall decrease in dendritic spine densities by ~16%. This decrease in spine densities was significant for Nec3-shRNA and Scramble conditions (Figure 7B).

We also found that the observed differences in dendritic spine densities between nectin-3 knockdown and overexpression neurons were dependent on the time point assayed (Figure 7A). At P14 and P35, no significant differences were observed between conditions, though it is possible that statistical significance might be achieved with higher sampling, particularly at P35 (Figure 7A, Supplementary Table 1). At P21, however, dendritic spine densities were significantly different between Nec3-shRNA and Nec3-OE or Nec3-DN conditions as well as between scramble and Nec3-DN conditions (Figure 7A). As expected, the effect of nectin-3 manipulation was found to depend on age, and a significant interaction effect was shown by two-way ANOVA (Figure 7B). From this we conclude that nectin-3 may have a significant role in regulating the developmental increase in dendritic spines observed between P14 and P21.

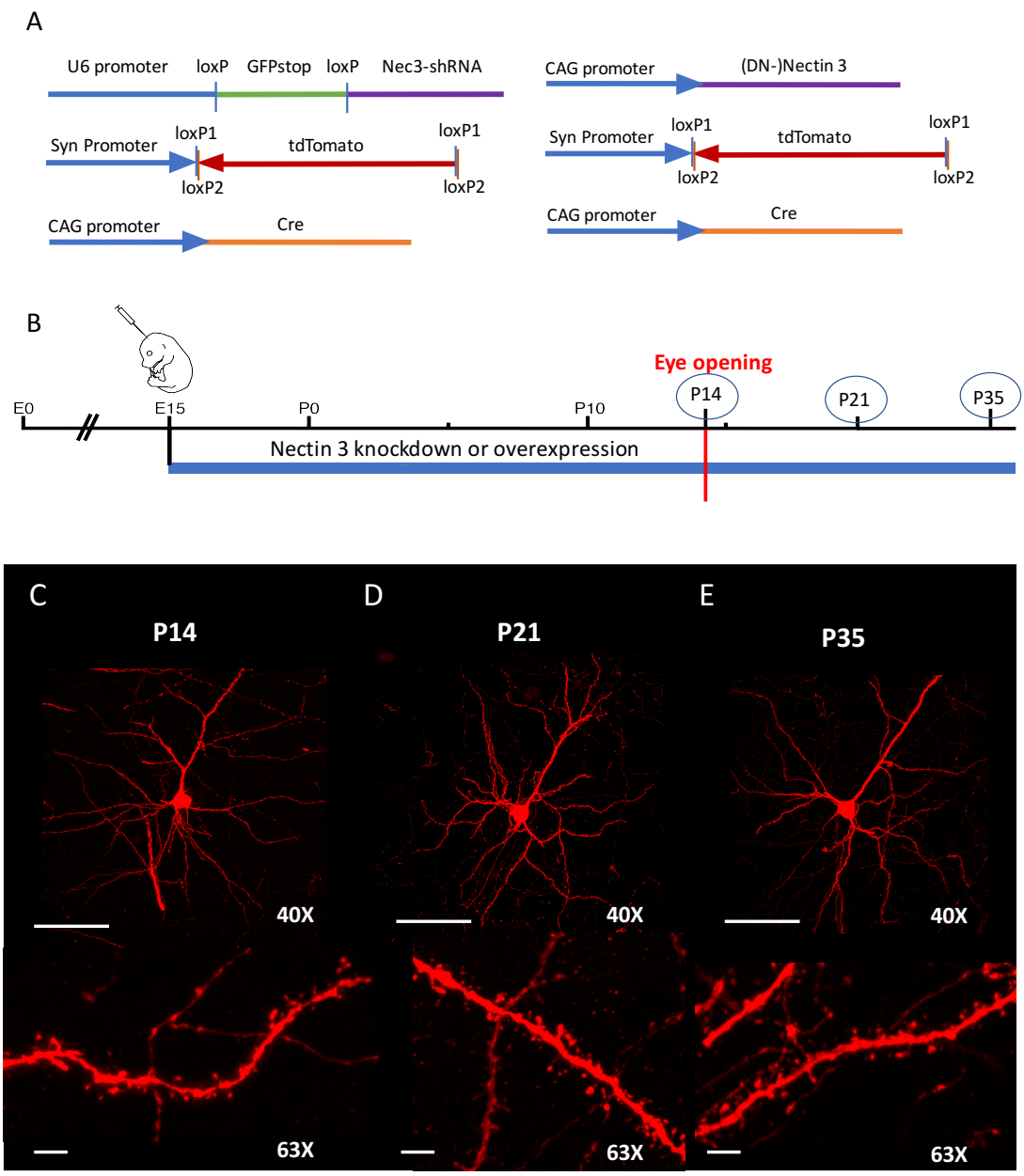

Figure 6. Increasing or decreasing nectin-3 expression by *in utero* electroporation and assaying spine densities at P14, P21 and P35.
(A) For shRNA knockdown, a Cre-dependent shRNA construct to nectin-3 was used containing a loxP flanked GFP-stop sequence to prevent the expression of shRNA in the absence of Cre. As a control, a scramble shRNA construct was designed using the same vector. In addition, a Cre-dependent FLEX tdTomato plasmid was co-electroporated with the nectin-3-shRNA construct. A Cre-plasmid was also co-electroporated at a low concentration for the immediate and sparse Cre mediated expression of shRNA and tdTomato. For the nectin-3 expression experiments, constructs driving the expression of either full length (OE) or truncated (DN, lacking cytoplasmic tail) nectin-3 were co-

electroporated with the same Cre-dependent tdTomato construct and Cre plasmid used for the knockdown experiment.
(B) Dendritic spine densities were measured at three time points: eye opening (P14), one week after eye opening (P21), or at the closing of the critical period for ODP (P35).
(C-E) RFP-expressing cells in V1 were identified, and basal dendrites, at least one branch away from the soma, were imaged at 63x for spine counting. At least 12 cells were used per condition. Representative 40x images of neurons (scale bar = 50 µm) and 63x images of dendrites (scale bar = 5 µm) are shown for the three time points assayed (C: P14, D: P21 and E: P35).

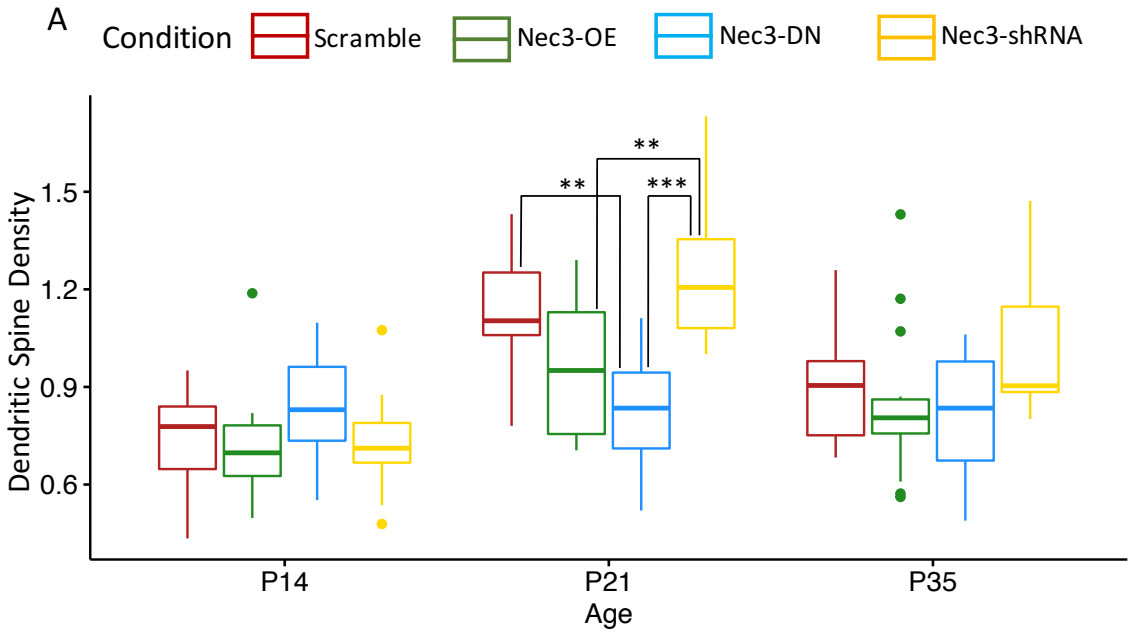

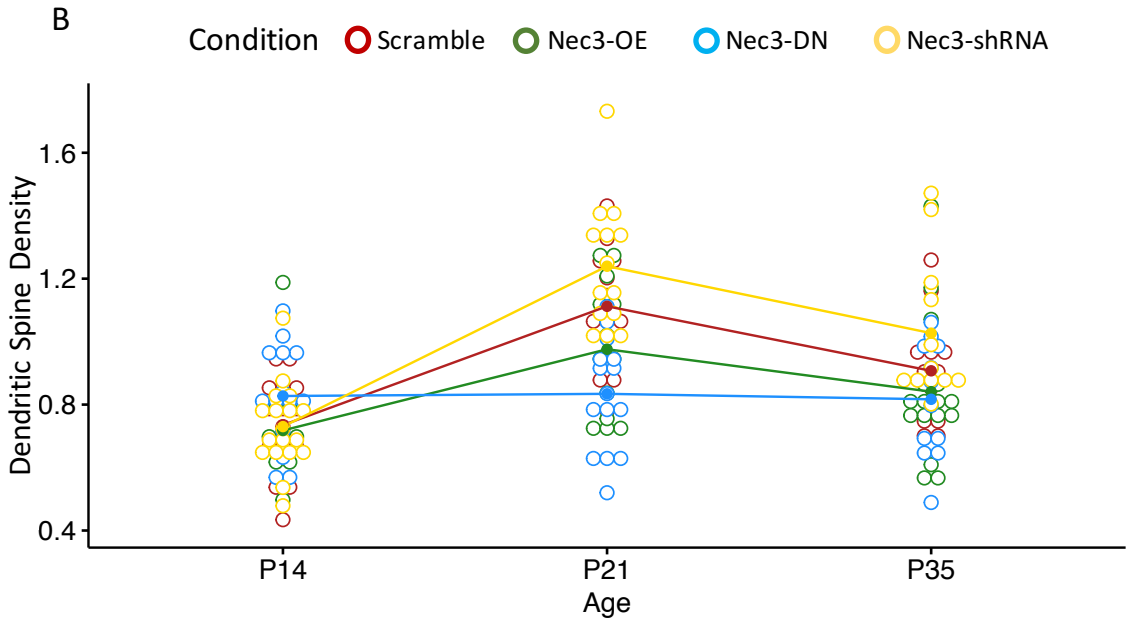

Figure 7. Nectin-3 manipulation significantly impacts spine densities.
(A) To identify significant differences in dendritic spine densities (number of spines / μm) with nectin-3 manipulation, each age group was isolated and a one-way ANOVA was performed over all conditions. At P14 no significant differences were observed between conditions (One-way ANOVA with Tukey HSD: Nec3-OE vs Nec3-DN, p = 0.287; Nec3-shRNA vs Nec3-DN, p = 0.303; Scramble vs Nec3-DN, p = 0.384, Nec3-shRNA vs Nec3-OE, p = 0.997, Scramble vs Nec3-OE, p = 0.992; Scramble vs. Nec3-shRNA, p = 1.0). At P21 significant differences were observed between Nec3-shRNA and Nec3-OE, Nec3-shRNA and Nec3-DN, as well as between scramble and Nec3-DN conditions (One-way ANOVA with Tukey HSD: Nec3-OE vs Nec3-DN, p = 0.23; Nec3-shRNA vs Nec3-DN, p = 4.7e-6; Scramble vs Nec3-DN, p = 0.00225, Nec3-shRNA vs Nec3-OE, p = 0.00480, Scramble vs Nec3-OE, p = 0.288; Scramble vs. Nec3-shRNA, p = 0.332). Finally, at P35, differences between groups were again insignificant (One-way ANOVA with Tukey HSD: Nec3-OE vs Nec3-DN, p = 0.99; Nec3-shRNA vs Nec3-DN, p = 0.0704; Scramble vs Nec3-DN, p = 0.702, Nec3-shRNA vs Nec3- OE, p = 0.095, Scramble vs Nec3-OE, p = 0.831; Scramble vs. Nec3-shRNA, p = 0.486).
(B) Age and nectin-3 manipulation were found to interact producing observable differences between groups at P21, but not at other ages (Two-way ANOVA, type 3, with interaction: Condition:Age, p = 3.638e-12). Significant increases in dendritic spine densities (number of spines / μm) between P14 and P21 were observed for Nec3-shRNA, Scramble, and Nec3-OE conditions, but not for Nec3-DN (One-way ANOVA with Tukey HSD, P14-P21: Scramble, p = 3.46e-6; Nec3-shRNA, p = <1e-7; Nec3-OE, p = 0.00927; Nec3-DN, p = 0.994). Significant decreases in dendritic spine densities were observed between P21 and P35 for Nec3-shRNA and Scramble conditions but not Nec3-OE or Nec3-DN conditions (One-way ANOVA with Tukey HSD, P21-P35: Scramble, p = 0.0136; Nec3-shRNA, p = 0.0151; Nec3-OE, p = 0.20; Nec3-DN, p = 0.964).

Spine densities are pruned between P21 and P35 in V1M and V1B but not V2

Differences in synaptic plasticity between V1M and V1B neurons have previously been observed during critical periods in the development of visual cortex (Nataraj & Turrigiano, 2011). Here we examine whether the developmental regulation of synaptic densities on L2/3 neurons may differ between functional regions of visual cortex. To accomplish this, we determined the approximate cortical locations of neurons with dendritic spine density data at P21 or P35. We examined 2.5x images of cortical sections containing the neurons assayed to identify anatomical markers characteristic of location. Using a brain atlas (Paxinos & Franklin, 2013), the approximate coordinates of each

neuron within visual cortex were determined, and neurons were identified as belonging to V1M, V1B, or V2 cortical areas. We assayed changes in dendritic spine densities with age in these areas using density data from all conditions except Nec3-DN, since this condition appeared to eliminate the developmental changes in dendritic spine densities normally observed between P14 and P35 (Figure 7). We found that V2 neurons had overall higher dendritic spine densities than neurons in V1M or V1B, though this difference is only significant at P35, after V1M and V1B neurons undergo developmental synaptic pruning (Figure 8). V2 neurons did not appear to undergo the same degree of developmental pruning as was observed in V1M and V1B (Figure 8). From this we conclude that developmental synaptic pruning in L2/3 neurons may be differentially regulated between V2 and V1, while neurons in V1M and V1B both experience significant levels of dendritic spine loss between P21 and P35.

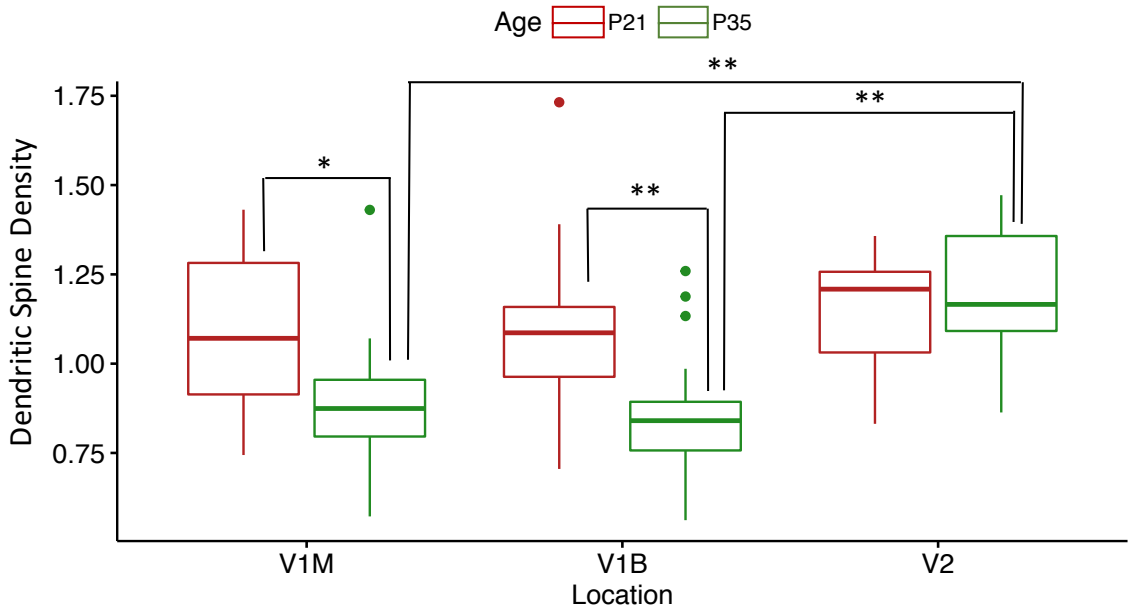

Figure 8. Spine densities in V2 are higher than V1M and V1B and developmental pruning is less evident in V2.
At P21 and P35 cells with dendritic spine density data were mapped to V1M, V1B, or V2 cortical regions using a mouse brain atlas. For this analysis, dominant negative data was

excluded. We found that cells located in V2 had overall greater spine densities (number of spines / µm) than cells located in V1M and V1B at P35 (One-way ANOVA with Tukey HSD at P35: V1M vs V1B, p = 0.928; V2 vs V1B, p = 0.00157; V2 vs V1M, p = 0.00439). This appears to be due to a lack of developmental pruning in V2 as compared to V1M and V1B, which both had significantly decreased spine densities at P35 as compared to P21 (One-way ANOVA, type 3, P21–P35: V1M, p = 0.0204; V1B, p = 0.00132; V2, p = 0.732).

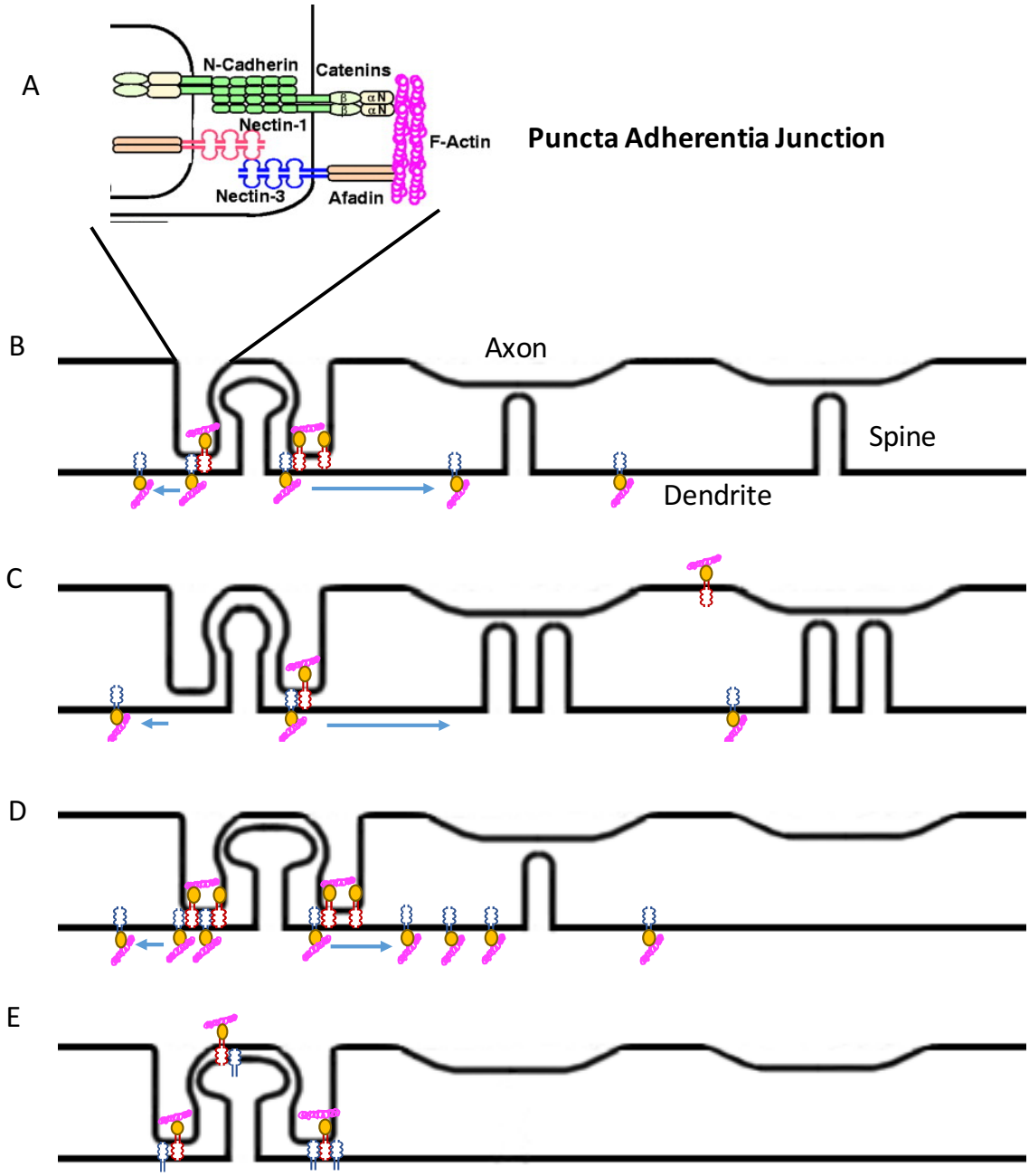

Figure 9. Proposed model for nectin-3 – actin interaction as a facilitator for spine formation from P14-P21.
In this model, synaptic strength in developing L2/3 neurons is inversely related to synapse number. Here I propose that changing actin dynamics with eye opening allows the dispersal of nectin-3 away from synaptic sites. This leads to a decrease in synaptic strength and an increase in synapse number.
A) Diagram of nectins and cadherins at a synaptic puncta adherentia junction, modified from Figure 1A (Takai & Nakanishi, 2003).
B) Normally developing axon and dendrite between L2/3 neurons where nectin-3 levels help balance synapse strength and number. In this condition, an interaction with the actin cytoskeleton facilitates the mobility of nectin-3 both towards and away from PAJs depending on developmental condition. After eye-opening, the strength of synapses is decreased to compensate for increases in synapse number. In this case, the interaction of nectin-3 with the actin cytoskeleton facilitates homeostatic synaptic plasticity. As the system matures, this process reverses. In this case, the binding of nectin-3 to nectin-1 (and association with N-cadherin at PAJs) leads to the strengthening/maturation of active spines, and the loss of inactive spines.
C) With nectin-3 knockdown, synaptic strength is decreased relative to control neurons, leading to increased synaptogenesis. Reduced nectin-3 binding at PAJs decreases the strength of individual synaptic connections. The increase in synapse number normally observed between P14 and P21 is even less restricted by previous cell adhesion, facilitating an even greater increase in synapse density. In addition, the activity guided maturation of synapses may be delayed, since the stabilization and strengthening of spines is hindered.
D) With nectin-3 overexpression, synaptic strength is increased relative to control neurons. Since nectin-3 is still able to interact with the actin cytoskeleton, some plasticity remains, facilitating an increase in synapse number after eye opening. This increase, however, is reduced compared to nectin-3 shRNA or scramble control conditions. This may be due to reduced plasticity during post-eye opening synaptogenesis. Alternatively, the accelerated maturation and stabilization of active spines may also accelerate the pruning of weak/inactive spines.
E) In the final condition, we expressed a dominant negative (DN) nectin-3 lacking its C-terminus. Theoretically, this modified nectin should exhibit disrupted intracellular signaling and interaction with actin. However, the intact Ig-domain of this protein still functions to form cis-dimers and bind *in trans* to nectin-1. It is uncertain where or if bound nectin-1 and nectin-3 would localize at synapses. Since nectin-1 is still able to interact with the pre-synaptic cytoskeleton, it is possible that bound nectin-1 and DN nectin-3 would still exhibit some localization to PAJs. In the model presented here, expression of DN nectin-3 prevents synaptic plasticity and growth between P14 and P21 by preventing actin-mediated dispersal of nectin-3 away from existing spines. In our study, this appeared to prevent the increase in synapse number usually observed between P14 and P21.

DISCUSSION

Cell adhesion molecules (CAMs) have a variety of roles in neuronal development and function including roles in the guidance of axons and dendritic processes, the initiation of contact between pre- and post-synaptic sites, as well as the maturation and stabilization of synapses (Biederer et al., 2002; Kitt & Nelson, 2011; Mizoguchi et al., 2002; Ooshio et al., 2004; Rikitake et al., 2012; Tachibana et al., 2000). Many CAMs are expressed in specific cell types during development and in the mature brain, indicating they may have roles in developing the specific connections and functional properties of different neuronal cell types (Hertel & Redies, 2011; Krishna-K, Hertel, & Redies, 2011). Here we examine the potential role of two CAMs, nectin-1 and nectin-3, in the development of layer 2/3 cortical neurons. The nectins are a family of Ig-domain cell-adhesion molecules that bind *in trans* through their extracellular Ig domains and interact with afadin, a PDZ-domain containing protein, through their cytoplasmic tail. In hippocampus, post-synaptic nectin-3 and pre-synaptic nectin-1 have been shown to interact at synaptic puncta adherentia junctions to help guide the formation and maturation/stabilization of synaptic connections (Honda et al., 2006; Sakamoto et al., 2006; Satoh-Horikawa et al., 2000; Wang et al., 2017). Here we show that nectin-3 and nectin-1 are enriched in L2/3 excitatory neurons in post-natal mouse cortex and examine how manipulating the expression of these nectins, particularly nectin-3, affects dendritic spine densities in L2/3 neurons at P14, P21, and P35.

In this study, we examined the developmental changes in dendritic spine densities on L2/3 cortical neurons both during normal postnatal development and after manipulating nectin expression levels. Consistent with previous studies (Blue &

Parnavelas, 1983; Chen et al., 2014; Cruz-Martín et al., 2010; Zuo et al., 2005), we found that dendritic spine densities increase in V1 L2/3 cortical neurons from P14 to P21. Over the course of the critical period for ODP (P21-P35) many spines are pruned, reducing the spine densities of L2/3 neurons in V1M and V1B. In this study, V2 neurons did not appear to undergo the same level of developmental pruning as was seen in V1M and V1B, though it is possible pruning in these neurons happens later in development (Figure 8). We also found that the knockdown of nectin-1 and nectin-3 together (Figure 4), or nectin-3 alone (Figure 5 and Figure 7), increased the dendritic spine densities of V1 L2/3 neurons after eye opening. These increased spine densities were observed after early (E15.5) or late (P14) nectin knockdown, indicating that the phenotype observed after eye opening was not compensatory for an early (E15.5 – P14) disruption in spine formation. In addition, overexpression of full length nectin-3 or a dominant negative nectin-3 lacking a C-terminus, decreased the spine densities of L2/3 neurons at P21. Interestingly, disrupting the cytoplasmic signaling of nectin-3 by expressing a truncated protein lacking its C-terminus, appeared to prevent the developmental increase in spine densities usually observed after eye opening. Our results indicate that decreasing or increasing nectin-3 Ig-binding after eye opening, facilitates or reduces, respectively, the normal developmental increase in dendritic spine densities observed between P14 and P21. The combination of increased Ig-binding while simultaneously eliminating C-terminus signaling, prevented the normal developmental increase in spine densities observed after eye opening. From these data, we conclude that nectin-3 may normally function to limit the developmental increase in dendritic spine densities that occurs after eye opening, and that the extent of this regulation may depend on an interaction between nectin-3 and actin.

There are a number of challenges associated with using electroporation to manipulate the expression of a protein in developing neurons. The amount of plasmid taken up by any given electroporated neuron can vary greatly, potentially leading to increased phenotypic variability within a single condition. We found that spine densities varied greatly among L2/3 neurons within a single condition, making it difficult to achieve the level of statistical significance desired between groups. For example, at P35 dendritic spine densities on nectin-3 knockdown and scramble neurons were significantly different when nectin-3 knockdown was initiated at P14 using *CaMKII-Cre* transgenic mice (Figure 5), but were not significantly different when knockdown was initiated at E15.5 (Figure 7). In the first experiment, we sampled a greater number of dendrites (Nec3-shRNA: n=35 vs n=12, Scramble: n=27 vs n=12) and included apical dendrites in the analysis, which may explain the different results (Figure 7D). It is also possible that compensatory mechanisms are more pronounced when nectin-3 is knocked down at E15.5 than when knockdown occurs at P14, increasing the effect observed with knockdown at the later time point (Figure 5D). In addition, the overexpression or knockdown of any protein in a developing cell, could lead to unhealthy phenotypes independent of the specific manipulation taking place. Again, since the amount of plasmid DNA taken up by any given cell can vary, it is possible that sick and healthy cells may appear side by side in electroporated cortex. To address this, we selectively imaged healthy looking cells with clear apical dendrites and limited the concentration of plasmid used for our overexpression and dominant negative experiments to below that used in previous experiments (Gil-Sanz et al., 2013). Despite the limits of the assay used, our confidence in the results obtained is increased by the consistent finding of increased

spine densities with nectin-3 knockdown after eye opening, even when time of knockdown, co-expression with nectin-1 shRNA, or time of assay are varied.

The developmental increase in spine densities found here with nectin-3 knockdown is in contrast to the decreased spine densities observed in hippocampal and dentate granule cells when nectin-3 was knocked down in adult mice (> 8 weeks) (Wang et al., 2013; Wang et al., 2017). This may be explained by innate differences in hippocampal and cortical neuron function and regulation, or may be due to differences in the developmental stage of the neurons examined. Consistent with this, it was previously shown that blocking nectin-1 and nectin-3 binding in developing hippocampal neurons in culture increased spine formation concomitant with a decrease in spine size. Here, for the first time, we were able to replicate this result in a developing system *in vivo*. These previous studies combined with our results indicate that the functional role of nectin-1 and nectin-3 in synapse formation and maintenance may change as neurons develop.

The ability of dendritic spines to regulate their shape and content in response to synaptic activity is vital for their function (Cerri et al., 2011; Chen et al., 2014; Duman et al., 2015; Shen & Cowan, 2010). The signaling and regulation of cell adhesion molecules has previously been shown to influence spine morphology, plasticity, and function (Arikkath & Reichardt, 2008). The long-term maintenance of synaptic plasticity requires that CAMs are continuously regulated at synapses, and multiple studies have shown this regulation can depend on activity (Arikkath & Reichardt, 2008; Bailey, Chen, Keller, & Kandel, 1992; Schuman & Murase, 2003; Tai et al., 2007). N-cadherin, for example, has been shown to stabilize at synapses with increased NMDA receptor signaling, and the continued stabilization of this CAM at synapses prevented LTD (Tai et al., 2007). While

many studies have shown that an increase in cell-adhesion molecules with activity can strengthen individual synapses, early work has also suggested that an abundance of adhesion molecules can restrict the morphological changes necessary for plasticity. One such study found that the application of serotonin to *Aplysia* neurons stimulated the endocytosis of apCAM, an *Aplysia* specific cell adhesion molecule, while also stimulating new synaptic growth in *Aplysia* sensory neurons (Bailey et al., 1992). It was suggested endocytosis may allow the redistribution of membrane components to sites where new synapses form (Bailey et al., 1992). Here, I suggest that the inability to destabilize existing synaptic contacts through the redistribution of nectin cell adhesion molecules may inhibit the synaptic growth normally observed the first week after eye opening.

Many developmental changes in synapse structure and function have been observed during the unique developmental period following eye opening. Between P16 and P23, it was found that mEPSC amplitudes decreased while frequencies increased in L2/3 neurons, concomitant with increased spine formation (Desai et al., 2002). Sensory experience was found to be necessary for the decrease in mEPSC amplitude, but the increase in frequency was also observed in dark reared animals (Desai et al., 2002). Increased mEPSC frequency is likely a result of the dramatic increase in new synapses formed between P14 to P21. Decreased amplitude is likely a homeostatic reaction to increased mEPSC frequencies in an active system. A form of non-Hebbian synaptic plasticity is necessary keep activity levels within a working range, as neurons are likely required to compensate for the increased spine formation. My results indicate that decreasing nectin binding *in vivo* may facilitate an increase spine formation, possibly by

enabling the concomitant decrease in synaptic strength required to maintain functional activity levels.

The formation of PAJs themselves may restrict an overproduction of spines by stabilizing and strengthening existing spines. The trans-interaction of nectin-1 and nectin-3 is an important facilitator of the co-localization of PAJ proteins (Tachibana et al., 2000). By prohibiting this binding through pharmacological blockade or shRNA knockdown, spines continue to form SJs, but PAJs are weakened, potentially making spines less stable (Honda et al., 2006; Mizoguchi et al., 2002). This may facilitate an overproduction of smaller/weaker spines in the system. Over normal development, we see an increase in spine densities in the first week after eye opening from P14 to P21. At P21, knockdown of nectin-3 further increased dendritic spine densities, while overexpressing nectin-3 had the opposite effect. It is possible that an increase in nectin-3 mediated PAJ formation may hinder synaptogenesis at this time by over stabilizing existing spines (Figure 9). While expression of full-length nectin-3 reduced spine densities at P21, it did not prevent a developmental increase in spine densities between P14 and P21. However, when nectin-3 intracellular signaling was disrupted by expressing a truncated protein lacking its cytoplasmic tail, this normal developmental increase in spine densities was prevented (Figure 7). It is unclear whether the dominant negative nectin-3 protein, by competing with endogenous nectins for space at the cell membrane, would prevent the formation of PAJs entirely. It is possible that the intact intracellular signaling of nectin-1 is enough to localize bound nectin-1 and nectin-3 to PAJs. Though we are unable to resolve the location of dominant negative nectin-3 at the cell membrane, our results indicate that the normal developmental increase in spine densities that occurs

after eye opening may require afadin or other intracellular signaling mechanisms if nectin-3 is present (Figure 9).

In the model presented in Figure 9, the regulation of spine plasticity by nectin-3 requires a connection to the actin cytoskeleton. Nectin-3 has been shown to regulate actin dynamics through afadin binding and Rho-GTPase signaling (Rap1, Rac1, and Cdc42) (Fukuhara, Shimizu, Kawakatsu, Fukuhara, & Takai, 2003; Kitt & Nelson, 2011; Ogita & Takai, 2006; Takai & Nakanishi, 2003). Cytoskeletal components and their modulators are under tight regulatory control in developing cortical neurons and it is unclear how modified nectin levels would interfere with this system (Azzarelli et al., 2014; Cerri et al., 2011; Duman et al., 2015; Tolias, Duman, & Um, 2011). Though nectin binding is usually associated with increased Rho-GTPase signaling and subsequent filopodia development (Duman et al., 2015), one study found nectin and cadherin binding first increased Rac1 signaling, followed by a rapid down regulation of the activated form of the protein below baseline in endothelial cells (Kitt & Nelson, 2011). A homeostatic downregulation of Rac1 may be necessary to prevent the overproduction of spines in a developing system, and nectin binding may mediate part of this regulatory process (Duman et al., 2015). In addition, Ig-domain CAMs have been shown to both regulate and be regulated by the cytoskeletal components they interact with (Leshchyns'ka & Sytnyk, 2016). Nectin-1, for example was shown to disperse along the cell membrane with actin depolymerization, a phenomenon with potential functions in synaptic plasticity (Lim, Lim, Giuliano, & Federoff, 2008). It is possible that a developmentally regulated change in actin dynamics causes the dispersal of nectin-3 away from PAJs, which is necessary for the dispersal of not only nectin-3 but other cell-adhesion components across

the cell membrane. The destabilization of PAJs and/or the dispersion of cell adhesion molecules across the cell membrane may be important for the increased spine formation observed after eye opening.

Here, we show that the cell adhesion molecules nectin-1 and nectin-3 are important mediators of spine formation during a period of intense synaptogenesis after eye opening from P14–P21. I propose a model for developmental synapse formation that requires the dispersal of nectins and nectin associated synaptic cell adhesion molecules away from synaptic sites to facilitate the plasticity necessary for large increases in dendritic spine density. In this model, an overabundance of nectin-3 restricts plasticity and reduces the number of new spines that can form after eye opening, whereas decreasing nectin-3 facilitates increased plasticity and dendritic spine formation. Dominant negative expression of nectin-3 prevented the developmental increase in synapse formation usually observed after eye opening, indicating the interaction of nectin-3 with afadin or other intracellular signaling molecules may be important for the normal development of L2/3 neurons at this time. The functional effect of increased spine densities with nectin-3 knockdown is unknown, and more work will need to be done to understand whether overall firing rates, or visual response properties (orientation selectivity, receptive field properties, spatial frequency responses, or surround suppression) change with nectin-3 knockdown or overexpression. It would also be interesting to see whether the same effect is observed with dark rearing, or mis-expression of nectin-3 in deep layer neurons. Though more work is necessary, we identify what may be a unique mechanism for the homeostatic scaling of synaptic

strength after eye opening, which requires nectin-3–actin signaling to reduce synaptic stabilization at PAJs.

CHAPTER VI

CONCLUSIONS

Neurons located in different layers of visual cortex (V1) exhibit unique functional properties that develop in response to visual input in the weeks following eye opening (Hoy & Niell, 2015; Niell & Stryker, 2008). The development of these properties requires the coordinated expression of a series of molecular factors, which are only beginning to be understood. Recently, the use of transcriptomics to identify genes expressed in developing systems has allowed the identification of many molecular factors whose expression levels change in V1 with development (Benoit et al., 2015; Lyckman et al., 2008; Majdan & Shatz, 2006; Tropea et al., 2006). However, few studies have attempted to isolate specific cell types, and most have examined developmental time points separated by large periods of development (Benoit et al., 2015; Lyckman et al., 2008; Majdan & Shatz, 2006; Tropea et al., 2006). This makes identifying genes important for specific developmental processes difficult. In addition, there is much work to be done linking gene expression data to function in developing systems. Here, I identified genes expressed and regulated in a subset of layer 2/3 excitatory neurons over eye opening, and manipulated two of those genes in developing layer 2/3 neurons to establish their function *in vivo*.

TU-tagging for temporal and layer-specific gene profiling

Excitatory neurons in layer 2/3 of visual cortex exhibit low firing rates, high stimulus selectivity, and a high degree of activity regulated synaptic structural plasticity over development (Bear & Rittenhouse, 1999; Feldman et al., 1999; Hoy & Niell, 2015;

Majewska & Sur, 2003; Niell & Stryker, 2008; Trachtenberg et al., 2000). Eye opening is a time of high synapse formation, structural motility, and plasticity in upper layer cortical neurons (Cruz-Martín et al., 2010; Desai et al., 2002; Majewska & Sur, 2003). It is largely unknown, however, how gene regulation drives the unique morphological and functional properties of neurons at this time. To identify potential molecular mechanisms important for the development of the unique functional properties of L2/3 neurons, I used a modified TU-tagging technique to identify genes expressed in these neurons at eye opening. TU-tagging allows the study of gene expression in developing systems with both spatial and temporal specificity. After newly transcribed RNAs are thiol-labeled in genetically characterized cell types *in vivo*, labeled transcripts can be isolated through streptavidin/biotin purification of RNAs isolated from whole tissue homogenates (Gay et al., 2014, 2013). This technique does not require cell dissociation or dissection, preserving RNAs found in delicate neuronal processes. In Chapters II–IV of this dissertation, I described using this technique to identify a number of genes enriched in upper-layer neuronal cell types at time points immediately before (P12) and after (P16) eye opening (Majewska & Sur, 2003; Tomorsky et al., 2017).

TU-tagging technical considerations

We were the first to use the TU-tagging technique, combined with a transgenic mouse system, to isolate neuronal RNAs (Tomorsky et al., 2017). This approach presented a number of challenges addressed in Chapters II and III. Unfortunately, the streptavidin-biotin purification technique used to isolate tagged RNAs thiol-labeled *in vivo* was unable to completely remove all background unlabeled RNAs from our

'purified' samples. This is most problematic when working with sparse cell types, when tagged RNAs are a very small subset of the total RNA extracted. In Chapters II and III, we describe the preparation and use of a new sample type, which consisted exclusively of purified 'background' RNAs extracted from wild-type tissue where thiol-labeling should have been absent (WT-pure). We used this sample type as a 'control' comparison to identify genes enriched in L4 neurons thiol-labeled using the sparse expressing Cre line, *Nr5a1-cre* (Nr5a1-pure), or L2/3 neurons thiol-labeled using the dense expressing Cre line, *Sepw1-cre* (Sepw1-pure). In Chapter III, I compare genes identified as enriched using the Sepw1–WT and Nr5a1–WT comparisons. As expected, genes Nr5a1-enriched compared to WT-pure samples were more likely to be classified as genes found outside upper layer cortical neurons (enriched expression in endothelial cells and deep layer neurons), than Sepw1-enriched genes identified using the same comparison. This indicates that, proportionally, background unlabeled RNA is more highly represented in samples purified from sparse expressing cell types than dense expressing cell types.

Due to varying levels of background RNA represented in Nr5a1-pure and Sepw1-pure sample types, we used a direct comparison of these two sample types to identify Sepw1-enriched genes, but not Nr5a1-enriched genes. When purification techniques are required to isolate labeled RNAs for analysis, the comparisons used to identify gene enrichments should be carefully considered to account for the quality of purification and cell types being compared. When two genetically identified cell types are to be compared, the genes found to be enriched in a sparse expressing line as compared to a dense expressing line should be interpreted cautiously. Indeed, genes enriched in the Nr5a1-pure sample type did not appear L4 enriched when Sepw1-pure was used as a

comparison, but rather L2/3 depleted (classified as endothelial cell and deep layer enriched). On the other hand, purified RNA from a sparsely expressed cell type could be uniquely useful for isolating genes enriched in a more densely expressed cell type. The *Sepw1-cre* line used here demonstrated enriched expression in L2/3 neurons, but also exhibited some sparse expression in L4. In this study, utilizing the sparse expressing L4 line, *Nr5a1-cre*, as a comparison for *Sepw1-cre* isolated RNAs, may have allowed us to identify a greater number of genes specific to L2/3 neurons while reducing the number of L4 enriched genes identified.

The functional role of genes with regulated expression at eye opening

Eye opening is a developmental turning point marking the initial receipt and processing of visually evoked activity by developing neurons in visual cortex. In Chapter IV, we examined the set of genes regulated in all visual cortex with eye opening by comparing RNA-seq data prepared from V1 cortical tissue collected at P12 and P16. Gene-ontology and functional annotation analyses of genes enriched and depleted over eye opening in V1 revealed that genes upregulated were important for synaptogenesis and synaptic transmission while genes down regulated encoded cytoskeletal, extracellular matrix, and cell-cycle components. We also found that the cell-type composition of visual cortex is likely changing over eye opening, based on the changing expression levels of genes enriched in neurons, astrocytes, oligodendrocytes, or microglia (Cahoy et al., 2008). At P12, genes enriched in neurons and oligodendrocyte-progenitors were significantly overrepresented, while at P16, genes enriched in neurons, mature and newly formed oligodendrocytes, astrocytes and endothelial cells were significantly

overrepresented. This influx of non-neuronal support cells into cortex correlates with the increased neural activity experienced with the onset of visual input.

Many previous studies of gene expression and regulation over the development of visual cortex have carefully examined the critical period for ocular dominance plasticity (ODP, P21–P35). In Chapter IV, we also examined how genes regulated over eye opening compared to genes previously identified as enriched or activity regulated during the critical period. As expected, many genes found to be upregulated between P14 and P28, or continuously upregulated between P0 and P45, were also upregulated with eye opening. We also identified several genes regulated with eye opening that were previously found to modify their expression with dark rearing or monocular deprivation (MD) during the critical period for ODP. Interestingly, the direction of regulation at eye opening could not be predicted by the direction of regulation with MD. This indicates the complex system of gene regulation with eye opening may interact with visual experience to prepare cortical neurons for later developmental plasticity.

The identification of genes enriched in L2/3 excitatory neurons at P12 or P16 provides a snapshot into the developmental processes that may be important for these neurons either before or after eye opening. L2/3 enriched genes with changing expression levels over eye opening may be important for regulating the adaptation of these neurons to the onset of visually driven activity. A gene's enrichment in L2/3, however, does not necessarily reflect developmental regulation, and a separate assay was required to identify which L2/3 enriched genes were changing their expression levels with eye opening. To accomplish this, we combined the list of genes identified as L2/3 enriched at P12 and P16 and determined which of these genes were also significantly modulated in

visual cortex between these ages. In Chapter IV, I identified several genes both highly expressed and regulated in layer 2/3 neurons between P12 and P16. Layer 2/3 enriched genes falling into 'neuron projection development' gene ontology categories were largely downregulated with eye opening, likely reflecting the downregulation of genes involved in axonogenesis and dendritogenesis. Up regulated genes were largely involved in synaptic transmission and developmental regulation. Genes upregulated in L2/3 neurons with eye opening may have functions in the synaptic scaling, plasticity, and growth associated with developmental onset of visual input (Cruz-Martín et al., 2010; Desai et al., 2002; Majewska & Sur, 2003). Through this approach, we identified overall changes in gene expression required for layer 2/3 neuronal development as neurons first experience visually driven activity.

Manipulating nectin-1 and nectin-3 expression in developing L2/3 cortical neurons affects dendritic spine densities

Cell adhesion molecules (CAMs) have previously been implicated as important for circuit connectivity and synapse formation in developing systems (Arikkath & Reichardt, 2008; Biederer et al., 2002; Frei, Andermatt, Gesemann, & Stoeckli, 2014; Kitt & Nelson, 2011; Leshchyns'ka & Sytnyk, 2016; Osterhout et al., 2011; Rikitake et al., 2012; Williams et al., 2011). The TU-tagging study described in Chapter II identified two L2/3 enriched cell adhesion molecules, nectin-1 and nectin-3, which had previously been studied for their involvement in hippocampal synapse formation (Wang et al., 2013; Wang et al., 2017). In Chapter V, I manipulated the expression of these CAMs in developing L2/3 neurons and examined their role in synapse formation by examining

dendritic spine densities at three time points: P14, P21, and P35. Dendritic spines are a good proxy for excitatory synapse formation, since the vast majority of glutamatergic dendritic spines contain the required molecular components for synaptic signaling (Mizoguchi et al., 2002). We found that dendritic spine densities were increased in the week(s) following eye opening when nectin-1 and nectin-3, or nectin-3 alone, were knocked down in developing layer 2/3 neurons. This increase was most dramatic at P21 when knockdown was initiated at the time the neurons were born, but was also significant at P35 when knockdown was initiated at P14. Overexpressing either full length nectin-3 or a truncated version of this protein lacking its C-terminus, appeared to decrease spine densities at P21. This decrease was most dramatic when the overexpressed nectin-3 lacked a C-terminus. From this I conclude that dendritic spine formation on L2/3 cortical neurons may be restricted by nectin-3 in the weeks following eye opening.

Model for nectin involvement in synapse formation and refinement in developing L2/3 neurons

The nectins are a family of Ig-domain proteins that bind *in trans* through their extracellular Ig-domain and interact with the actin cytoskeleton through intracellular C-terminus binding to afadin (Rikitake et al., 2012). Nectins and cadherins interact through their intracellular components to localize at puncta adherent junctions (PAJs), stabilizing structures at synapses distinct from synaptic junctions, which are the sites of neurotransmission (Mizoguchi et al., 2002). While nectin localization and interaction with actin and cadherin are dependent on intracellular signaling, the trans binding of nectins through their extracellular Ig-domains occurs independent of the proteins' C-

termini (Takai & Nakanishi, 2003). Reciprocal interactions between Ig-domain CAMs and the cytoskeletal components they interact with, has previously been demonstrated (Leshchyns'ka & Sytnyk, 2016). It has been shown that the de-polymerization of actin distributes nectin-1 along cell membranes, a process previously implicated in synaptic plasticity (Lim et al., 2008). It has also been previously shown that nectin-3 and nectin-1 are present at immature synaptic junctions in developing synapses, but re-localize to puncta adherent junctions (PAJs) as synapses mature (Mizoguchi et al., 2002). Blocking nectin-1 to nectin-3 binding in culture decreases synapse size while increasing synapse number, an effect thought to be driven by reduced PAJ formation. Here, I propose that nectin-3 is important for stabilizing spines during development, but that overstabilization after eye opening reduces plasticity and synaptogenesis.

A developmental feature of many brain regions is an overproduction of synapses followed by 'refinement' whereby weak inactive synapses are removed through synaptic pruning (Benoit et al., 2015). In visual cortex, an 'overproduction' of spines appears to occur in the week after eye opening, from P14 to P21, followed by developmental 'pruning' over the critical period from P21 to P35. Pruning is thought to be activity dependent during the normal development of visual cortex, leading to the strengthening of some spines and subsequent elimination of weak spines (Espinosa & Stryker, 2012). At the end of the critical period, the remaining un-pruned synaptic contacts are more stable and less 'plastic' than earlier in development (end of ODP). It has also been shown that periods of dark rearing can delay the maturation of cortical circuits, increasing plasticity and extending the critical period for ODP (Erchova, Vasalauskaite, Longo, & Sengpiel, 2017). Decreasing cortical activity may prevent neurons from strengthening

existing spines, resulting in a delayed loss of the weaker spines. In developing neurons, plasticity and stability may be opposing mechanisms, i.e. the more plastic an individual spine the less stable and vice versa. Since nectin has been shown to participate in the formation of PAJs, stabilizing structures at synapses, it is likely nectin has a role in increasing the stability of spines over development. In addition, preventing the accumulation of nectin at synapses may be necessary to facilitate synaptic plasticity and synaptogenesis early in development.

In Chapter V, I propose the interaction of nectin-3 with actin through intracellular signaling at the C-terminus, helps to distribute nectin-3 away from synapses at eye opening, facilitating increased synaptogenesis. In Chapter IV, we found that actin and other cytoskeletal components are down regulated with eye opening. This indicates that the actin cytoskeleton at synapses may be dynamically regulated at this time. This model predicts that the interaction of nectin with actin is necessary for the increased synaptogenesis observed with eye opening. Indeed, we find that the overexpression of a truncated version of nectin-3, incapable of interacting with actin, prohibits the increased synaptogenesis normally observed between P14 and P21. On the other hand, shRNA knockdown of nectin-3 facilitates an increased production of weak spines by reducing the overall accumulation of nectin-3 at synapses. The overexpression of full-length nectin-3 does not eliminate the increase is spine density observed between P14 and P21, since its ability to interact with actin is intact. It does, however, reduce overall spine densities at P21, compared to the condition where nectin-3 is eliminated, likely due to an overall reduction in plasticity.

It is also possible that nectins are important for the stabilization of synapses with activity over the critical period for ODP. The trans interactions of nectins have been shown to facilitate the accumulation of cadherins to different types of cell-cell junctions (Takai & Nakanishi, 2003). N-cadherin interacts with nectins at synapses, and has further been shown to regulate the stability of synapses with activity, accumulating at spines with NMDA receptor activation (Mizoguchi et al., 2002; Tai et al., 2007). N-cadherin also interacts with β-catenin, which, through its interaction with α-catenin, indirectly connects N-cadherin to both the actin cytoskeleton and nectins (Arikkath & Reichardt, 2008). β-catenin knockdown was found to reduce spine stability, while stabilizing β-catenin at synapses was found to reduce spine number (Ochs et al., 2015; Okuda, Yu, Cingolani, Kemler, & Goda, 2007). Preventing the formation of PAJs through nectin knockdown may prevent the stabilization and strengthening of spines over the critical period for ODP, increasing spine number to compensate (Mizoguchi et al., 2002). On the other hand, overexpressing nectin-3 might lead to increased PAJ formation and activity dependent stabilization of spines. This accelerated stabilization and strengthening of active spines over the critical period may facilitate the removal of weak, inactive synapses, reducing overall synapse number at an earlier developmental time point.

Unanswered questions and future directions

The model proposed here generates several testable hypotheses that can be explored in future studies. First, it suggests that nectin-3 localization at PAJs might decrease after eye opening, facilitating increased dendritic spine density, motility, and plasticity. This redistribution of nectin-3 is dependent on its ability to interact with actin,

and is eliminated with the expression of a dominant negative form of nectin-3 lacking a C-terminus. It is unclear how expression of the dominant negative nectin-3 might affect the localization of nectin-3 in developing and mature synapses. Examining normal and dominant-negative nectin distribution at synapses in developing cortical neurons by electron microscopy (EM) could resolve this. I also propose that nectin-3 facilitates the strengthening of synapses through its association with N-cadherin at PAJs. Again, EM could be used to identify whether PAJ formation is reduced in nectin-3 knockdown neurons and increased in nectin-3 overexpression neurons at P21. It would also be informative to examine N-cadherin expression and distribution at synapses with nectin-3 knockdown, overexpression, and dominant negative expression to identify how nectin binding and signaling affects this CAM at different stages of development.

It would also be interesting to determine whether the synaptic phenotypes observed with nectin-3 manipulation are activity dependent. A balance of genetically encoded and activity dependent processes guide the development of V1 neurons (Espinosa & Stryker, 2012; Mower et al., 1981). Activity can have variable effects on developing systems, depending on developmental stage (Desai et al., 2002; Toyoizumi, Kaneko, Stryker, & Miller, 2014). During the critical period for ODP, activity is thought to guide circuit maturation through the modification of synaptic strengths (Majdan & Shatz, 2006; Toyoizumi et al., 2014). In the week after eye opening, activity has been shown to drive homeostatic synaptic scaling, decreasing mEPSC amplitudes (a measure of synaptic strength) to compensate for the large increase in synapse number (and mEPSC frequency) observed at this time (Desai et al., 2002). It is possible that activity affects the distribution of nectin-3 at synaptic junctions and PAJs both at eye opening and

during the critical period for ODP. If activity is necessary for the nectin-3 dependent strengthening of synapses and concomitant decreases in synapse number, the differences in synaptic densities observed here between nectin-3 knockdown and overexpression neurons should be eliminated in dark reared animals.

Final Remarks

In this dissertation, I first identified genes with enriched expression in a subset of upper layer cortical neurons in V1 at eye opening. I then examined how two of the genes identified, nectin-1 and nectin-3, influenced synapse formation in developing L2/3 neurons. I determined that knocking down these nectins in L2/3 neurons increased the number of dendritic spines formed by these neurons after eye opening. I proposed that the distribution of nectin-3 away from synapses after eye opening facilitates spine formation, while the accumulation of nectin-3 at PAJs during the critical period facilitates the maturation of strong/active spines and concomitant pruning of weak/inactive spines. Disrupting the interaction of nectin-3 with actin through expression of a dominant negative nectin-3 lacking a C-terminus, eliminated the developmental increase in dendritic spine density observed in the week after eye opening. We found in Chapter IV that actin expression is regulated with eye opening, suggesting the interaction of nectin-3 with actin may facilitate nectin distribution during synaptogenesis.

Our results are unique with respect to previous studies on the role of nectin binding in synapse formation. Increased spine densities were also previously observed when nectin-3 was knocked down in developing neurons in culture, but this result had not previously been replicated in a developing system *in vivo* (Mizoguchi et al., 2002). In

adult hippocampus, nectin-3 knockdown was shown to have the opposite effect, decreasing spine densities and disrupting long-term memory formation (Wang et al., 2013; Wang et al., 2017). The results presented here suggest that nectin-3 dependent synaptic stabilization may have different roles in developing and adult systems. In addition, the specific expression pattern of nectin-3 in L2/3 of visual cortex indicates it may have unique roles in the functional development these neurons. Over the course of my studies, I linked transcriptomic data to molecular function in developing visual cortex and suggested a potential molecular mechanism regulating synapse formation and maturation in L2/3 neurons.

APPENDIX A

SUPPLEMENTARY INFORMATION FOR CHAPTER II

Tissue type	Standard deviation	Estimate	Lower_CI	Upper_CI	Experimental value	P-value
Sepw1-Pure to WT-Pure Comparison, 1907 Enriched Genes						
Layer 2/3	5.83	39.93	28.26	51.59	117*	< 0.001
Layer 4	5.13	31.72	21.46	41.98	59*	< 0.001
Layer 5	6.47	50.47	37.53	63.41	55	0.429
Layer 6	5.87	42.17	30.43	53.92	45	0.613
Layer 6b	5.84	43.51	31.84	55.18	47	0.534
Unpatterned	6.53	47.22	34.15	60.28	40	0.26
Sepw1-Pure to Nr5a1-Pure Comparison, 634 Sepw1-Enriched Genes						
Layer 2/3	3.63	13.35	6.07	20.61	103*	< 0.001
Layer 4	3.18	10.48	4.11	16.84	37*	< 0.001
Layer 5	3.85	16.6	8.90	24.31	6*	0.002
Layer 6	3.58	14.02	6.85	21.18	12	0.501
Layer 6b	3.71	14.48	7.06	21.89	15	0.786
Unpatterned	3.86	15.66	7.93	23.38	11	0.180

Supplementary Table 1. Resampling estimates for number of database genes overlapping with DESeq Sepw1-enriched genes.
List of standard deviations, estimates, confidence intervals, and p-values calculated using a resampling method to estimate expected values for the number of layer enriched database genes that overlap with either 1907 (Sepw1-WT) or 634 (Sepw1-Nr5a1) randomly selected genes. The number of genes randomly selected was equal to the number of Sepw1-enriched genes identified using either WT-pure or Nr5a1-pure sample type comparisons. P-values were calculated using resampled estimates and experimental values. Asterisks indicate experimental values that fell outside the upper or lower 95% confidence limits.

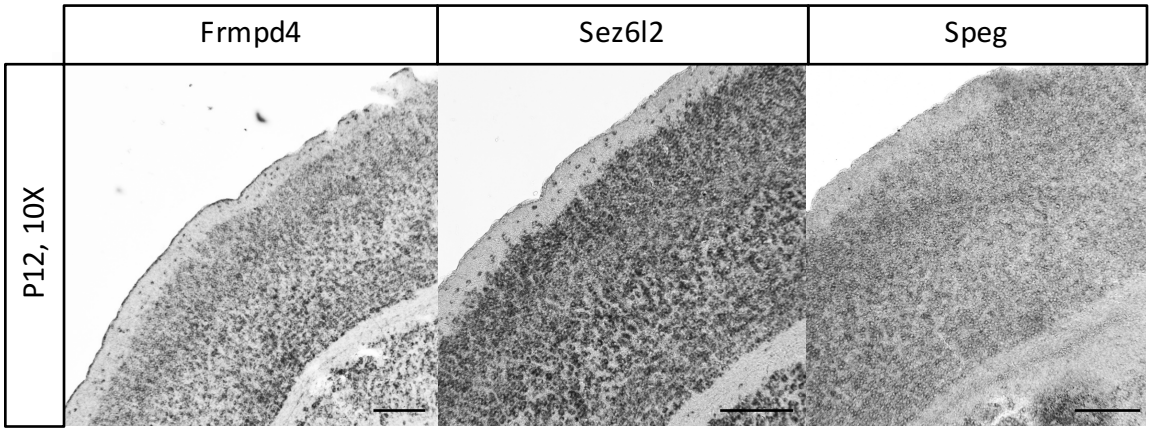

Supplementary Figure 1. *In situ* hybridizations showing pan-neuronal expression of three genes of interest.
In situ hybridization showing pan-neuronal expression of three genes shown to be enriched in Sepw1-pure samples when compared to Nr5a1-pure samples at P12. These three genes were chosen for analysis based on gene ontology (GO) categorization as cell-adhesion molecules or involvement in synapse formation (scale bar = 200 μm).

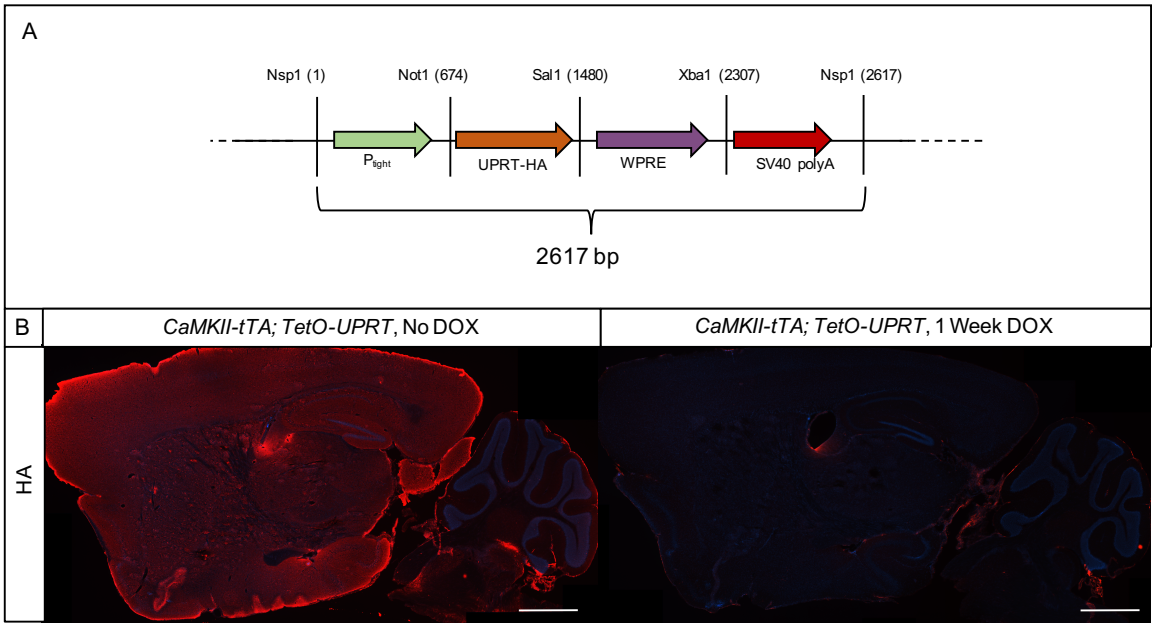

Supplementary Figure 2. Development of a *TetO-UPRT* mouse with neuronal expression responsive to DOX.
(A) Figure of the TetO-UPRT transgene.
(B) HA-staining for UPRT before and after DOX administration (scale bar = 1000 μm, 5x objective). Both images were taken with an exposure time of 150 ms and were

adjusted identically for brightness and contrast (Photoshop adjusted brightness = 30, contrast = 100). DAPI is also shown to highlight underlying cell structure. Mice were placed on high DOX (2 µg/ml administered in 1% sucrose water) for one week. The transgene was DOX responsive, with a substantial reduction in UPRT protein expression after one week of DOX administration, though a small amount of leaky expression remained. Placing mice on high DOX from birth may help with leaky expression.

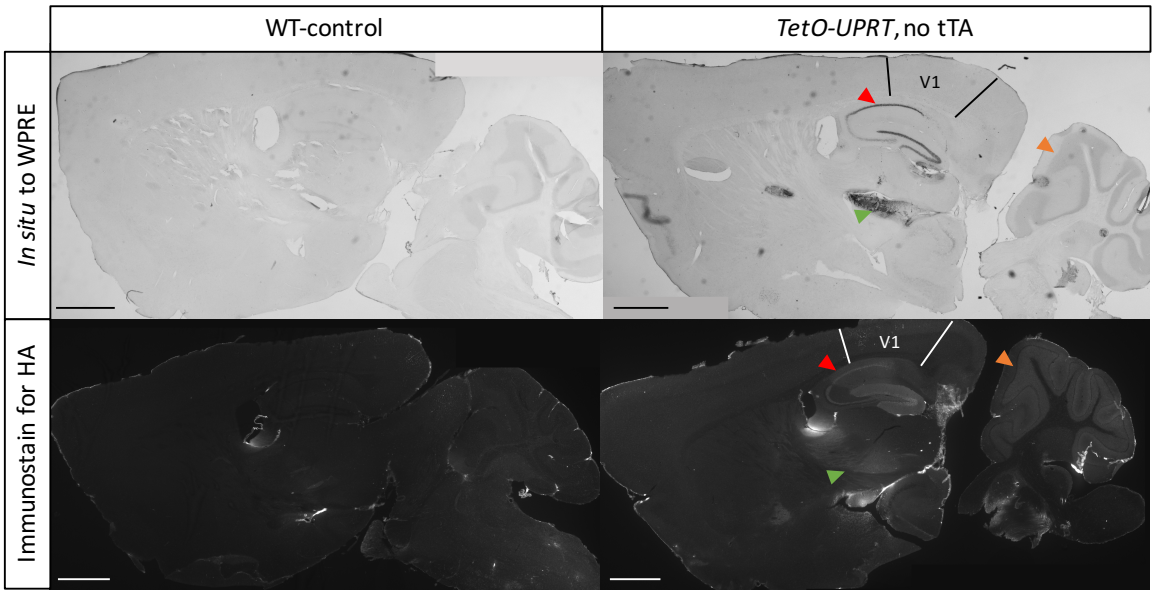

Supplementary Figure 3. Leaky expression of UPRT in a single positive *TetO-UPRT* mouse.
There is some 'leaky' UPRT expression even when no tTA is present in a single positive *TetO-UPRT* transgenic mouse. This leaky expression is mostly limited to hippocampus, though the cerebellum and thalamus also appear weakly positive for the UPRT protein (2.5x objective, scale bar = 1000 µm). Primary visual cortex (V1) and areas of potential leaky expression are labeled. Red arrow: hippocampus; Orange arrow: cerebellum; Green arrow: thalamus.

APPENDIX B

SUPPLEMENTARY INFORMATION FOR CHAPTER III

Tissue type	Standard deviation	Estimate	Lower_CI	Upper_CI	Experimental value	P-value
Nr5a1-Pure to WT-Pure Comparison, 1673 Enriched Genes						
Neuronal	7.07	53.77	39.63	67.91	93	< 0.001
Endothelial	6.60	47.82	34.62	61.02	30	0.007
Layer 2/3	5.52	35.05	24.02	46.09	76	< 0.001
Layer 4	4.85	27.89	18.19	37.60	37	0.052
Layer 5	6.05	43.82	31.71	55.93	53	0.12
Layer 6	5.68	37.29	25.94	48.64	52	0.007
Layer 6b	5.88	38.23	26.46	49.99	49	0.053
Unpatterned	6.16	42.37	30.04	54.69	43	0.87

Supplementary Table 1: Resampling estimates of the mean, standard deviation, confidence intervals, and p-values for number of database genes overlapping with DESeq Sepw1-or Nr5a1-enriched genes.
List of standard deviations, estimates, confidence intervals, and p-values obtained using a resampling method to estimate expected values for the number of neuronal, endothelial, or layer enriched database genes that overlap with a randomly selected number of genes listed in the comparison description (i.e. 1673 enriched genes). The number of genes to randomly select was taken from the number of Nr5a1-enriched genes identified when various comparisons were analyzed using DESeq. P-values were calculated using resampled estimates and experimental values (listed under the 'value' column).

APPENDIX C

SUPPLEMENTARY INFORMATION FOR CHAPTER IV

Tissue type	Standard deviation	Estimate	Lower_CI	Upper_CI	Experimental value	P-value
Sepw1-pure to Nr5a1-pure comparison, P16 (367 Sepw1-enriched)						
Neuron	3.2	11.8	2.1	21.6	19	0.062
Endothelial	3.1	10.2	4.0	16.4	14	0.184
L23	2.8	7.8	2.3	13.4	45	<0.001
L4	2.3	6.2	1.6	10.8	12	0.006
L5	3.1	9.8	3.6	16.0	4	0.048
L6	2.7	8.3	2.8	13.8	7	0.567
L6b	2.9	8.5	2.7	14.2	7	0.581
Unpatterned	3.0	9.2	3.3	15.2	4	0.062
P12 V1 to P16 V1 comparison (1674 P16 enriched)						
Neuron	6.5	49.9	30.5	69.3	77	<0.001
Glial	6.2	42.6	30.1	55.1	45	0.69
Astro	6.7	50.6	30.7	70.6	117	<0.001
Endo	6.5	48.8	35.9	61.8	73	0.001
Mye olig	6.3	47.0	28.2	65.7	145	<0.001
New olig	6.1	46.0	33.7	58.2	129	<0.001
Oligo progen	6.6	49.8	30.1	69.5	44	0.355
P12 V1 to P16 V1 comparison (1421 P12 enriched)						
Neuron	6.2	42.4	23.8	61.0	102	<0.001

Glial	5.5	35.9	24.9	46.8	15	<0.001
Astro	6.1	42.6	24.2	61.0	34	0.143
Endo	6.0	41.3	29.3	53.2	23	0.004
Mye olig	5.9	39.8	22.0	57.5	29	0.061
New olig	6.0	39.1	27.2	51.0	22	0.007
Oligo progen	6.4	42.4	23.2	61.5	86	<0.001

Supplementary Table 1: Resampling estimates of the mean, standard deviation, confidence intervals, and p-values for number of database genes overlapping with DESeq Sepw1-enriched genes or genes enriched at P12 or P16.
List of standard deviations, estimates, confidence intervals, and p-values obtained using a resampling method to estimate expected values for the number of cell type or layer enriched database genes that overlap with a randomly selected number of genes listed in the comparison description (i.e. 367, 1647, or 1421 enriched genes). The number of genes to randomly select was taken from the number of Sepw1- or Nr5a1-enriched genes identified when various comparisons were analyzed using DESeq. P-values were calculated using resampled estimates and experimental values (listed under the 'value' column).

APPENDIX D

SUPPLEMENTARY INFORMATION FOR CHAPTER V

Figure	Data structure	Test	N	P-value
Fig. 4C	Normal Distribution	Two-way ANOVA type 3	Nec1+Nec3-shRNA, N = 32; Scramble, N = 29; Apical, N = 30; Basal, N = 31	Nec1+Nec3-shRNA vs Scramble-shRNA, p = 0.0066; Apical vs Basal, p = 0.666
Fig 5D	Normal Distribution	Two-way ANOVA type 3	Nec3-shRNA, N = 35; Scramble, N = 27; Apical, N = 27; Basal, N = 35	Nec3_shRNA vs Scramble, p = 0.00160; Apical vs Basal, p = 0.464
Fig 7A, P21	Normal Distribution	One-way ANOVA type 3	Nec3-shRNA, N = 14; Nec3-OE, N = 13; Nec3-DN, N = 15; Scramble, N = 13	Nec3-shRNA vs Nec3-DN vs Nec3-OE vs Scramble, p = 6.379e-06
Fig 7A, P21	Normal Distribution	One-way ANOVA with Tukey HSD	Nec3-shRNA, N = 14; Nec3-OE, N = 13; Nec3-DN, N = 15; Scramble, N = 13	Nec3-OE vs Nec3-DN, p = 0.23; Nec3-shRNA vs Nec3-DN, p = 4.7e-6; Scramble vs Nec3-DN, p = 0.00225, Nec3-shRNA vs Nec3-OE, p = 0.00480, Scramble vs Nec3-OE, p = 0.288; Scramble vs. Nec3-shRNA, p = 0.332
Fig 7A, P14	Normal Distribution	One-way ANOVA type 3	Nec3-shRNA, N = 18; Nec3-OE, N = 12; Nec3-DN, N = 14; Scramble, N = 15	Nec3-shRNA vs Nec3-DN vs Nec3-OE vs Scramble, p = 0.23
Fig 7A, P14	Normal Distribution	One-way ANOVA with Tukey HSD	Nec3-shRNA, N = 18; Nec3-OE, N = 12; Nec3-DN, N = 14; Scramble, N = 15	Nec3-OE vs Nec3-DN, p = 0.287; Nec3-shRNA vs Nec3-DN, p = 0.303; Scramble vs Nec3-DN, p = 0.384, Nec3-shRNA vs Nec3-OE, p = 0.997, Scramble vs Nec3-OE, p = 0.992; Scramble vs. Nec3-shRNA, p = 1.0
Fig 7A, P35	Normal Distribution	One-way ANOVA type 3	Nec3-shRNA, N = 12; Nec3-OE, N = 16; Nec3-DN, N = 12; Scramble, N = 12	Nec3-shRNA vs Nec3-DN vs Nec3-OE vs Scramble, p = 0.0608

Fig 7A, P35	Normal Distribution	One-way ANOVA with Tukey HSD	Nec3-shRNA, N = 12; Nec3-OE, N = 16; Nec3-DN, N = 12; Scramble, N = 12	Nec3-OE vs Nec3-DN, p = 0.99; Nec3-shRNA vs Nec3-DN, p = 0.0704; Scramble vs Nec3-DN, p = 0.702, Nec3-shRNA vs Nec3-OE, p = 0.095, Scramble vs Nec3-OE, p = 0.831; Scramble vs. Nec3-shRNA, p = 0.486
Fig 7B, Nec3-shRNA	Normal Distribution	One-way ANOVA type 3	P14, N = 18; P21, N = 14 ; P35, N = 12	P14 vs P21 vs P35, p = 7.337e-09
Fig 7B, Nec3-shRNA	Normal Distribution	One-way ANOVA with Tukey HSD	P14, N = 18; P21, N = 14 ; P35, N = 12	P14 vs P21, p = <1e-7; P14 vs P35, p = 0.000289; P21 vs P35, p = 0.0151
Fig 7B, Nec3-OE	Normal Distribution	One-way ANOVA type 3	P14, N = 12 ; P21, N = 13 ; P35, N = 16	P14 vs P21 vs P35, p = 0.0128
Fig 7B, Nec3-OE	Normal Distribution	One-way ANOVA with Tukey HSD	P14, N = 12 ; P21, N = 13 ; P35, N = 16	P14 vs P21, p = 0.00927; P14 vs P35, p = 0.273; P21 vs P35, p = 0.20
Fig 7B, Nec3-DN	Normal Distribution	One-way ANOVA type 3	P14, N = 14; P21, N = 15; P35, N = 12	P14 vs P21 vs P35, p = 0.967
Fig 7B, Nec3-DN	Normal Distribution	One-way ANOVA with Tukey HSD	P14, N = 14; P21, N = 15; P35, N = 12	P14 vs P21, p = 0.994; P14 vs P35, p = 0.987; P21 vs P35, p = 0.964
Fig 7B, Scramble	Normal Distribution	One-way ANOVA type 3	P14, N = 15; P21, N = 13; P35, N = 12	P14 vs P21 vs P35, p = 6.276e-06
Fig 7B, Scramble	Normal Distribution	One-way ANOVA with Tukey HSD	P14, N = 15; P21, N = 13; P35, N = 12	P14 vs P21, p = 3.4e-6; P14 vs P35, p = 0.0351; P21 vs P35, p = 0.0136
Fig 7	Normal Distribution	Two-way ANOVA Type 3, with interaction	P14: Nec3-shRNA, N = 18; Nec3-OE, N = 12; Nec3-DN, N = 14; Scramble, N = 15; P21: Nec3-shRNA, N = 14; Nec3-OE, N = 13; Nec3-DN, N = 15; Scramble, N = 13; P35: Nec3-shRNA, N = 12; Nec3-OE, N = 16; Nec3-DN, N = 12; Scramble, N = 12	Condition, p = 0.377; Age, p = 0.97; Interaction of Condition:Age, p = 8.065e-05
Fig 8, P21	Normal Distribution	One-way ANOVA with Tukey HSD	V2, N = 13; V1M, N = 12; V1B, N = 22	V1M vs V1B, p = 0.997; V2 vs V1B, p = 0.567; V2 vs V1M, p = 0.692
Fig 8, P35	Normal Distribution	One-way ANOVA with Tukey HSD	V2, N = 6; V1M, N = 16; V1B, N = 20	V1M vs V1B, p = 0.928; V2 vs V1B, p = 0.00157; V2 vs V1M, p = 0.00439

Fig 8, V1M	Normal Distribution	One-way ANOVA type 3	P21, N = 12; P35, N = 16	P21 vs P35, p = 0.0204
Fig 8, V1B	Normal Distribution	One-way ANOVA type 3	P21, N = 22; P35, N = 20	P21 vs P35, p = 0.00132
Fig 8, V2	Normal Distribution	One-way ANOVA type 3	P21, N = 13; P35, N = 6	P21 vs P35, p = 0.732

Supplementary Table 1. Statistical information for all results presented

REFERENCES CITED

© 2004 Allen Institute for Brain Science. Allen Mouse Brain Atlas. Available from: mouse.brain-map.org.

© 2008 Allen Institute for Brain Science. Allen Developing Mouse Brain Atlas. Available from: developingmouse.brain-map.org.

© 2011 Allen Institute for Brain Science. Allen Mouse Brain Connectivity Atlas. Available from: connectivity.brain-map.org.

Anders, S., & Huber, W. (2012). Differential expression of RNA-Seq data at the gene level–the DESeq package. *Heidelberg, Germany: European Molecular …*.

Anders, S., Huber, W., Nagalakshmi, U., Wang, Z., Waern, K., Shou, C., … Salzberg, S. (2010). Differential expression analysis for sequence count data. *Genome Biology*, *11*(10), R106.

Anders, S., Pyl, P. T., & Huber, W. (2014). HTSeq - A Python framework to work with high-throughput sequencing data. *Bioinformatics (Oxford, England)*, 638.

Andrews, S. (2014). FastQC A Quality Control tool for High Throughput Sequence Data.

Arikkath, J., & Reichardt, L. F. (2008). Cadherins and catenins at synapses: roles in synaptogenesis and synaptic plasticity. *Trends in Neurosciences*, *31*(9), 487–494.

Azzarelli, R., Kerloch, T., & Pacary, E. (2014). Regulation of cerebral cortex development by Rho GTPases: insights from in vivo studies. *Frontiers in Cellular Neuroscience*, *8*, 445.

Bailey, C. H., Chen, M., Keller, F., & Kandel, E. R. (1992). Serotonin-mediated endocytosis of apCAM: an early step of learning-related synaptic growth in Aplysia. *Science (New York, N.Y.)*, *256*(5057), 645–649.

Balaram, P., & Kaas, J. H. (2014). Towards a unified scheme of cortical lamination for primary visual cortex across primates: insights from NeuN and VGLUT2 immunoreactivity. *Frontiers in Neuroanatomy*, *8*, 81.

Bear, M. F., & Rittenhouse, C. D. (1999). Molecular basis for induction of ocular dominance plasticity. *Journal of Neurobiology*, *41*(1), 83–91.

Belgard, T. G., Marques, A. C., Oliver, P. L., Abaan, H. O., Sirey, T. M., Hoerder-Suabedissen, A., … Ponting, C. P. (2011). A Transcriptomic Atlas of Mouse Neocortical Layers. *Neuron*, *71*(4), 605–616.

Benoit, J., Ayoub, A. E., & Rakic, P. (2015). Transcriptomics of critical period of visual cortical plasticity in mice. *Proceedings of the National Academy of Sciences of the United States of America*, *112*(26), 8094–8099.

Biederer, T., Sara, Y., Mozhayeva, M., Atasoy, D., Liu, X., Kavalali, E. T., & Südhof, T. C. (2002). SynCAM, a synaptic adhesion molecule that drives synapse assembly. *Science (New York, N.Y.)*, *297*(5586), 1525–1531.

Blue, M. E., & Parnavelas, J. G. (1983). The formation and maturation of synapses in the visual cortex of the rat. I. Qualitative analysis. *Journal of Neurocytology*, *12*(4), 599–616.

Bolger, A. M., Lohse, M., & Usadel, B. (2014). Trimmomatic: a flexible trimmer for Illumina sequence data. *Bioinformatics (Oxford, England)*, *30*(15), 2114–2120.

Boyle, E. I., Weng, S., Gollub, J., Jin, H., Botstein, D., Cherry, J. M., & Sherlock, G. (2004). GO::TermFinder--open source software for accessing Gene Ontology information and finding significantly enriched Gene Ontology terms associated with a list of genes. *Bioinformatics (Oxford, England)*, *20*(18), 3710–3715.

Cahoy, J. D., Emery, B., Kaushal, A., Foo, L. C., Zamanian, J. L., Christopherson, K. S., … Barres, B. A. (2008). A transcriptome database for astrocytes, neurons, and oligodendrocytes: a new resource for understanding brain development and function. *The Journal of Neuroscience : The Official Journal of the Society for Neuroscience*, *28*(1), 264–278.

Cembrowski, M. S., & Menon, V. (2018). Continuous Variation within Cell Types of the Nervous System. *Trends in Neurosciences*, *41*(6), 337–348.

Cerri, C., Fabbri, A., Vannini, E., Spolidoro, M., Costa, M., Maffei, L., … Caleo, M. (2011). Activation of Rho GTPases triggers structural remodeling and functional plasticity in the adult rat visual cortex. *The Journal of Neuroscience : The Official Journal of the Society for Neuroscience*, *31*(42), 15163–15172.

Chatzi, C., Zhang, Y., Shen, R., Westbrook, G. L., & Goodman, R. H. (2016). Transcriptional Profiling of Newly Generated Dentate Granule Cells Using TU Tagging Reveals Pattern Shifts in Gene Expression during Circuit Integration. *ENeuro*, *3*(1), ENEURO.0024-16.2016.

Chen, C.-C., Lu, J., & Zuo, Y. (2014). Spatiotemporal dynamics of dendritic spines in the living brain. *Frontiers in Neuroanatomy*, *8*, 28.

Chen, Y., Lun, A. T. L., & Smyth, G. K. (2014). Differential Expression Analysis of Complex RNA-seq Experiments Using edgeR *.

Cruz-Martín, A., Crespo, M., & Portera-Cailliau, C. (2010). Delayed stabilization of dendritic spines in fragile X mice. *The Journal of Neuroscience : The Official Journal of the Society for Neuroscience*, *30*(23), 7793–7803.

Cubelos, B., Sebastián-Serrano, A., Beccari, L., Calcagnotto, M. E., Cisneros, E., Kim, S., … Nieto, M. (2010). Cux1 and Cux2 Regulate Dendritic Branching, Spine Morphology, and Synapses of the Upper Layer Neurons of the Cortex. *Neuron*, *66*(4), 523–535.

Cubelos, B., Sebastián-Serrano, A., Kim, S., Redondo, J. M., Walsh, C., & Nieto, M. (2008). Cux-1 and Cux-2 control the development of Reelin expressing cortical interneurons. *Developmental Neurobiology*, *68*(7), 917–925.

Cui, P., Lin, Q., Ding, F., Xin, C., Gong, W., Zhang, L., … Yu, J. (2010). A comparison between ribo-minus RNA-sequencing and polyA-selected RNA-sequencing. *Genomics*, *96*(5), 259–265.

Cunningham, F., Amode, M. R., Barrell, D., Beal, K., Billis, K., Brent, S., … Flicek, P. (2014). Ensembl 2015. *Nucleic Acids Research*, *43*(D1), D662-669.

Desai, N. S., Cudmore, R. H., Nelson, S. B., & Turrigiano, G. G. (2002). Critical periods for experience-dependent synaptic scaling in visual cortex. *Nature Neuroscience*, *5*(8), 783–789.

Dölken, L., Ruzsics, Z., Rädle, B., Friedel, C. C., Zimmer, R., Mages, J., … Koszinowski, U. H. (2008). High-resolution gene expression profiling for simultaneous kinetic parameter analysis of RNA synthesis and decay. *RNA (New York, N.Y.)*, *14*(9), 1959–1972.

Doyle, J. P., Dougherty, J. D., Heiman, M., Schmidt, E. F., Stevens, T. R., Ma, G., … Heintz, N. (2008). Application of a translational profiling approach for the comparative analysis of CNS cell types. *Cell*, *135*(4), 749–762.

Duffy, E. E., Rutenberg-Schoenberg, M., Stark, C. D., Kitchen, R. R., Gerstein, M. B., & Simon, M. D. (2015). Tracking Distinct RNA Populations Using Efficient and Reversible Covalent Chemistry. *Molecular Cell*, *59*(5), 858–866.

Duman, J. G., Mulherkar, S., Tu, Y.-K., X Cheng, J., & Tolias, K. F. (2015). Mechanisms for spatiotemporal regulation of Rho-GTPase signaling at synapses. *Neuroscience Letters*, *601*, 4–10.

El-Brolosy, M. A., & Stainier, D. Y. R. (2017). Genetic compensation: A phenomenon in search of mechanisms. *PLoS Genetics*, *13*(7), e1006780.

Erchova, I., Vasalauskaite, A., Longo, V., & Sengpiel, F. (2017). Enhancement of visual cortex plasticity by dark exposure. *Philosophical Transactions of the Royal Society of London. Series B, Biological Sciences*, *372*(1715).

Erskine, L., & Herrera, E. (2014). Connecting the retina to the brain. *ASN Neuro*, *6*(6).

Espinosa, J. S., & Stryker, M. P. (2012). Development and plasticity of the primary visual cortex. *Neuron*, *75*(2), 230–249.

Feldman, D. E., Nicoll, R. A., & Malenka, R. C. (1999). Synaptic plasticity at thalamocortical synapses in developing rat somatosensory cortex: LTP, LTD, and silent synapses. *Journal of Neurobiology*, *41*(1), 92–101.

Fertuzinhos, S., Li, M., Kawasawa, Y. I., Ivic, V., Franjic, D., Singh, D., … Sestan, N. (2014). Laminar and temporal expression dynamics of coding and noncoding RNAs in the mouse neocortex. *Cell Reports*, *6*(5), 938–950.

Fishell, G., & Heintz, N. (2013). The Neuron Identity Problem: Form Meets Function. *Neuron*, *80*(3), 602–612.

Frei, J. A., Andermatt, I., Gesemann, M., & Stoeckli, E. T. (2014). The SynCAM synaptic cell adhesion molecules are involved in sensory axon pathfinding by regulating axon-axon contacts. *Journal of Cell Science*, *127*(Pt 24), 5288–5302.

Fukuhara, A., Shimizu, K., Kawakatsu, T., Fukuhara, T., & Takai, Y. (2003). Involvement of nectin-activated Cdc42 small G protein in organization of adherens and tight junctions in Madin-Darby canine kidney cells. *The Journal of Biological Chemistry*, *278*(51), 51885–51893.

García-Otín, A. L., & Guillou, F. (2006). Mammalian genome targeting using site-specific recombinases. *Frontiers in Bioscience : A Journal and Virtual Library*, *11*, 1108–1136.

Gärtner, A., Fornasiero, E. F., & Dotti, C. G. (2015). Cadherins as regulators of neuronal polarity. *Cell Adhesion & Migration*, *9*(3), 175–182.

Gay, L., Karfilis, K. V, Miller, M. R., Doe, C. Q., & Stankunas, K. (2014). Applying thiouracil tagging to mouse transcriptome analysis. *Nature Protocols*, *9*(2), 410–420.

Gay, L., Miller, M. R., Ventura, P. B., Devasthali, V., Vue, Z., Thompson, H. L., … Doe, C. Q. (2013). Mouse TU tagging: a chemical/genetic intersectional method for purifying cell type-specific nascent RNA. *Genes & Development*, *27*(1), 98–115.

Gerfen, C. R., Paletzki, R., & Heintz, N. (2013). GENSAT BAC cre-recombinase driver lines to study the functional organization of cerebral cortical and basal ganglia circuits. *Neuron*, *80*(6), 1368–1383.

Gil-Sanz, C., Franco, S. J., Martinez-Garay, I., Espinosa, A., Harkins-Perry, S., & Müller, U. (2013). Cajal-Retzius Cells Instruct Neuronal Migration by Coincidence Signaling between Secreted and Contact-Dependent Guidance Cues. *Neuron*, *79*(3), 461–477.

Gong, Q., Su, Y.-A., Wu, C., Si, T.-M., Deussing, J. M., Schmidt, M. V., & Wang, X.-D. (2018). Chronic Stress Reduces Nectin-1 mRNA Levels and Disrupts Dendritic Spine Plasticity in the Adult Mouse Perirhinal Cortex. *Frontiers in Cellular Neuroscience*, *12*, 67.

Hackett, T. A., Guo, Y., Clause, A., Hackett, N. J., Garbett, K., Zhang, P., … Mirnics, K. (2015). Transcriptional maturation of the mouse auditory forebrain. *BMC Genomics*, *16*(1), 606.

Harris, J. A., Hirokawa, K. E., Sorensen, S. A., Gu, H., Mills, M., Ng, L. L., … Huang, J. (2014). Anatomical characterization of Cre driver mice for neural circuit mapping and manipulation.

Harris, K. M. (1999). Structure, development, and plasticity of dendritic spines. *Current Opinion in Neurobiology*, *9*(3), 343–348.

Harwell, C. C., Parker, P. R. L., Gee, S. M., Okada, A., McConnell, S. K., Kreitzer, A. C., & Kriegstein, A. R. (2012). Sonic Hedgehog Expression in Corticofugal Projection Neurons Directs Cortical Microcircuit Formation. *Neuron*, *73*(6), 1116–1126.

Head, S. R., Komori, H. K., LaMere, S. A., Whisenant, T., Van Nieuwerburgh, F., Salomon, D. R., & Ordoukhanian, P. (2014). Library construction for next-generation sequencing: overviews and challenges. *BioTechniques*, *56*(2), 61–4, 66, 68.

Heiman, M., Schaefer, A., Gong, S., Peterson, J. D., Day, M., Ramsey, K. E., … Heintz, N. (2008). A translational profiling approach for the molecular characterization of CNS cell types. *Cell*, *135*(4), 738–748.

Hertel, N., & Redies, C. (2011). Absence of Layer-Specific Cadherin Expression Profiles in the Neocortex of the Reeler Mutant Mouse. *Cerebral Cortex*, *21*(5), 1105–1117.

Hida, N., Aboukilila, M. Y., Burow, D. A., Paul, R., Greenberg, M. M., Fazio, M., … Cleary, M. D. (2017). EC-tagging allows cell type-specific RNA analysis. *Nucleic Acids Research*, *45*(15), e138–e138.

Hirota, Y., & Nakajima, K. (2017). Control of Neuronal Migration and Aggregation by Reelin Signaling in the Developing Cerebral Cortex. *Frontiers in Cell and Developmental Biology*, *5*, 40.

Hirsch, J. A., & Martinez, L. M. (2006). Laminar processing in the visual cortical column. *Current Opinion in Neurobiology*, *16*(4), 377–384.

Honda, T., Sakisaka, T., Yamada, T., Kumazawa, N., Hoshino, T., Kajita, M., … Takai, Y. (2006). Involvement of nectins in the formation of puncta adherentia junctions and the mossy fiber trajectory in the mouse hippocampus. *Molecular and Cellular Neuroscience*, *31*(2), 315–325.

Honkura, N., Matsuzaki, M., Noguchi, J., Ellis-Davies, G. C. R., & Kasai, H. (2008). The Subspine Organization of Actin Fibers Regulates the Structure and Plasticity of Dendritic Spines. *Neuron*, *57*(5), 719–729.

Hooks, B. M., & Chen, C. (2007). Critical Periods in the Visual System: Changing Views for a Model of Experience-Dependent Plasticity. *Neuron*, *56*(2), 312–326.

Hoy, J. L., Haeger, P. A., Constable, J. R. L., Arias, R. J., McCallum, R., Kyweriga, M., … Washbourne, P. (2013). Neuroligin1 drives synaptic and behavioral maturation through intracellular interactions. *The Journal of Neuroscience : The Official Journal of the Society for Neuroscience*, *33*(22), 9364–9384.

Hoy, J. L., & Niell, C. M. (2015). Layer-specific refinement of visual cortex function after eye opening in the awake mouse. *The Journal of Neuroscience : The Official Journal of the Society for Neuroscience*, *35*(8), 3370–3383.

Huang, D. W., Sherman, B. T., & Lempicki, R. A. (2009). Bioinformatics enrichment tools: paths toward the comprehensive functional analysis of large gene lists. *Nucleic Acids Research*, *37*(1), 1–13.

Huber, W., Carey, V. J., Gentleman, R., Anders, S., Carlson, M., Carvalho, B. S., … Morgan, M. (2015). Orchestrating high-throughput genomic analysis with Bioconductor. *Nature Methods*, *12*(2), 115–121.

Ignacio, M. P., Kimm, E. J., Kageyama, G. H., Yu, J., & Robertson, R. T. (1995). Postnatal migration of neurons and formation of laminae in rat cerebral cortex. *Anatomy and Embryology*, *191*(2), 89–100.

Ikeda, W., Nakanishi, H., Miyoshi, J., Mandai, K., Ishizaki, H., Tanaka, M., … Takai, Y. (1999). Afadin: A key molecule essential for structural organization of cell-cell junctions of polarized epithelia during embryogenesis. *The Journal of Cell Biology*, *146*(5), 1117–1132.

Jeong, E. Y., Kim, S., Jung, S., Kim, G., Son, H., Lee, D. H., … Kim, H. J. (2013). Enhancement of IGF-2-induced neurite outgrowth by IGF-binding protein-2 and osteoglycin in SH-SY5Y human neuroblastoma cells. *Neuroscience Letters*, *548*, 249–254.

Kaas, J. H. (2011). Neocortex in early mammals and its subsequent variations. *Annals of the New York Academy of Sciences*, *1225*, 28–36.

Kamiguchi, H. (2007). The Role of Cell Adhesion Molecules in Axon Growth and Guidance. In *Axon Growth and Guidance* (Vol. 621, pp. 95–102). New York, NY: Springer New York.

Kawauchi, T. (2011). Regulation of cell adhesion and migration in cortical neurons: Not only Rho but also Rab family small GTPases. *Small GTPases*, *2*(1), 36–40.

Kitt, K. N., & Nelson, W. J. (2011). Rapid Suppression of Activated Rac1 by Cadherins and Nectins during De Novo Cell-Cell Adhesion. *PLoS ONE*, *6*(3), e17841.

Klopfenstein, D. R., & Vale, R. D. (2004). The lipid binding pleckstrin homology domain in UNC-104 kinesin is necessary for synaptic vesicle transport in Caenorhabditis elegans. *Molecular Biology of the Cell*, *15*(8), 3729–3739.

Krishna-K, K., Hertel, N., & Redies, C. (2011). Cadherin expression in the somatosensory cortex: evidence for a combinatorial molecular code at the single-cell level. *Neuroscience*, *175*, 37–48.

Kwan, K. Y., Sestan, N., & Anton, E. S. (2012). Transcriptional co-regulation of neuronal migration and laminar identity in the neocortex. *Development (Cambridge, England)*, *139*(9), 1535–1546.

Kwiatkowski, A. V., Gertler, F. B., & Loureiro, J. J. (2003). Function and regulation of Ena/VASP proteins. *Trends in Cell Biology*, *13*(7), 386–392.

Lachke, S. A., Higgins, A. W., Inagaki, M., Saadi, I., Xi, Q., Long, M., … Maas, R. L. (2012). The cell adhesion gene PVRL3 is associated with congenital ocular defects. *Human Genetics*, *131*(2), 235–250.

Lahens, N. F., Kavakli, I., Zhang, R., Hayer, K., Black, M. B., Dueck, H., … Lipman, D. (2014). IVT-seq reveals extreme bias in RNA sequencing. *Genome Biology*, *15*(6), R86.

Langevin, L. M., Mattar, P., Scardigli, R., Roussigné, M., Logan, C., Blader, P., & Schuurmans, C. (2007). Validating in utero electroporation for the rapid analysis of gene regulatory elements in the murine telencephalon. *Developmental Dynamics*, *236*(5), 1273–1286.

Larsen, D. D., & Callaway, E. M. (2006). Development of layer-specific axonal arborizations in mouse primary somatosensory cortex. *The Journal of Comparative Neurology*, *494*(3), 398–414.

Law, C. W., Alhamdoosh, M., Su, S., Smyth, G. K., & Ritchie, M. E. (2016). RNA-seq analysis is easy as 1-2-3 with limma, Glimma and edgeR. *F1000Research*, *5*, 1408.

Lein, E. S., Hawrylycz, M. J., Ao, N., Ayres, M., Bensinger, A., Bernard, A., … Jones, A. R. (2007). Genome-wide atlas of gene expression in the adult mouse brain. *Nature*, *445*(7124), 168–176.

Leshchyns'ka, I., & Sytnyk, V. (2016). Reciprocal Interactions between Cell Adhesion Molecules of the Immunoglobulin Superfamily and the Cytoskeleton in Neurons. *Frontiers in Cell and Developmental Biology*, *4*, 9.

Lim, S. T., Lim, K.-C., Giuliano, R. E., & Federoff, H. J. (2008). Temporal and spatial localization of nectin-1 and l-afadin during synaptogenesis in hippocampal neurons. *The Journal of Comparative Neurology*, *507*(2), 1228–1244.

Lin, Y.-C., & Koleske, A. J. (2010). Mechanisms of synapse and dendrite maintenance and their disruption in psychiatric and neurodegenerative disorders. *Annual Review of Neuroscience*, *33*, 349–378.

Liset, R., Sommeijer, J.-P., Levelt, C. N., & Heimel, J. A. (2012). Candidate genes in ocular dominance plasticity. *Frontiers in Neuroscience*, *6*, 11.

LoTurco, J., Manent, J.-B., & Sidiqi, F. (2009). New and improved tools for in utero electroporation studies of developing cerebral cortex. *Cerebral Cortex (New York, N.Y. : 1991)*, *19 Suppl 1*(Suppl 1), 20-5.

Lowenstein, P. R., Mandel, R. J., Xiong, W.-D., Kroeger, K., & Castro, M. G. (2007). Immune responses to adenovirus and adeno-associated vectors used for gene therapy of brain diseases: the role of immunological synapses in understanding the cell biology of neuroimmune interactions. *Current Gene Therapy*, *7*(5), 347–360.

Lu, B., Wang, K. H., & Nose, A. (2009). Molecular mechanisms underlying neural circuit formation. *Current Opinion in Neurobiology*, *19*(2), 162–167.

Lu, W., & Constantine-Paton, M. (2004). Eye Opening Rapidly Induces Synaptic Potentiation and Refinement. *Neuron*, *43*(2), 237–249.

Luo, L., Callaway, E. M., & Svoboda, K. (2008). Genetic Dissection of Neural Circuits. *Neuron*, *57*(5), 634–660.

Lyckman, A. W., Horng, S., Leamey, C. A., Tropea, D., Watakabe, A., Van Wart, A., … Sur, M. (2008). Gene expression patterns in visual cortex during the critical period: synaptic stabilization and reversal by visual deprivation. *Proceedings of the National Academy of Sciences of the United States of America*, *105*(27), 9409–9414.

Ma, L., Qiao, Q., Tsai, J.-W., Yang, G., Li, W., & Gan, W.-B. (2016). Experience-dependent plasticity of dendritic spines of layer 2/3 pyramidal neurons in the mouse cortex. *Developmental Neurobiology*, *76*(3), 277–286.

Majdan, M., & Shatz, C. J. (2006). Effects of visual experience on activity-dependent gene regulation in cortex. *Nature Neuroscience*, *9*(5), 650–659.

Majewska, A., & Sur, M. (2003). Motility of dendritic spines in visual cortex in vivo: changes during the critical period and effects of visual deprivation. *Proceedings of the National Academy of Sciences of the United States of America*, *100*(26), 16024–16029.

Manzini, M. C., & Walsh, C. A. (2011). What disorders of cortical development tell us about the cortex: one plus one does not always make two. *Current Opinion in Genetics & Development*, *21*(3), 333–339.

Martin, M. (2011, May 2). Cutadapt removes adapter sequences from high-throughput sequencing reads. *EMBnet.Journal*.

Maurin, H., Seymour, C. M., Lechat, B., Borghgraef, P., Devijver, H., Jaworski, T., … Van Leuven, F. (2013). Tauopathy Differentially Affects Cell Adhesion Molecules in Mouse Brain: Early Down-Regulation of Nectin-3 in Stratum Lacunosum Moleculare. *PLoS ONE*, *8*(5), e63589.

Mi, H., Muruganujan, A., Casagrande, J. T., & Thomas, P. D. (2013). Large-scale gene function analysis with the PANTHER classification system. *Nature Protocols*, *8*(8), 1551–1566.

Mi, H., Poudel, S., Muruganujan, A., Casagrande, J. T., & Thomas, P. D. (2016). PANTHER version 10: expanded protein families and functions, and analysis tools. *Nucleic Acids Research*, *44*(D1), D336-42.

Miller, M. R., Robinson, K. J., Cleary, M. D., & Doe, C. Q. (2009). TU-tagging: cell type-specific RNA isolation from intact complex tissues. *Nature Methods*, *6*(6), 439–441.

Mitchell, C., & Silver, D. L. (2018). Enhancing our brains: Genomic mechanisms underlying cortical evolution. *Seminars in Cell & Developmental Biology*, *76*, 23–32.

Miterko, L. N., Lackey, E. P., Heck, D. H., & Sillitoe, R. V. (2018). Shaping Diversity Into the Brain's Form and Function. *Frontiers in Neural Circuits*, *12*, 83.

Mizoguchi, A., Nakanishi, H., Kimura, K., Matsubara, K., Ozaki-Kuroda, K., Katata, T., … Takai, Y. (2002). Nectin: an adhesion molecule involved in formation of synapses. *The Journal of Cell Biology*, *156*(3), 555–565.

Mizutani, K., & Takai, Y. (2016). Nectin spot: a novel type of nectin-mediated cell adhesion apparatus. *Biochemical Journal*, *473*(18), 2691–2715.

Molyneaux, B. J., Goff, L. A., Brettler, A. C., Chen, H.-H., Brown, J. R., Hrvatin, S., … Arlotta, P. (2015). DeCoN: Genome-wide Analysis of In Vivo Transcriptional Dynamics during Pyramidal Neuron Fate Selection in Neocortex. *Neuron*, *85*(2), 275–288.

Moore, D. L., & Goldberg, J. L. (2011). Multiple transcription factor families regulate axon growth and regeneration. *Developmental Neurobiology*, *71*(12), 1186–1211.

Mower, G. D., Berry, D., Burchfiel, J. L., & Duffy, F. H. (1981). Comparison of the effects of dark rearing and binocular suture on development and plasticity of cat visual cortex. *Brain Research*, *220*(2), 255–267.

Nadarajah, B., Alifragis, P., Wong, R. O. L., & Parnavelas, J. G. (2003). Neuronal Migration in the Developing Cerebral Cortex: Observations Based on Real-time Imaging. *Cerebral Cortex*, *13*(6), 607–611.

Narayanan, R. T., Udvary, D., & Oberlaender, M. (2017). Cell Type-Specific Structural Organization of the Six Layers in Rat Barrel Cortex. *Frontiers in Neuroanatomy*, *11*, 91.

Nataraj, K., & Turrigiano, G. (2011). Regional and temporal specificity of intrinsic plasticity mechanisms in rodent primary visual cortex. *The Journal of Neuroscience : The Official Journal of the Society for Neuroscience*, *31*(49), 17932–17940.

Nguyen, D., & Xu, T. (2008). The expanding role of mouse genetics for understanding human biology and disease. *Disease Models & Mechanisms*, *1*(1), 56–66.

Niell, C. M. (2015). Cell Types, Circuits, and Receptive Fields in the Mouse Visual Cortex. *Annual Review of Neuroscience*, *38*(1), 413–431.

Niell, C. M., Meyer, M. P., & Smith, S. J. (2004). In vivo imaging of synapse formation on a growing dendritic arbor. *Nature Neuroscience*, *7*(3), 254–260.

Niell, C. M., & Stryker, M. P. (2008). Highly selective receptive fields in mouse visual cortex. *The Journal of Neuroscience : The Official Journal of the Society for Neuroscience*, *28*(30), 7520–7536.

Nieto, M., Monuki, E. S., Tang, H., Imitola, J., Haubst, N., Khoury, S. J., … Walsh, C. A. (2004). Expression of Cux-1 and Cux-2 in the subventricular zone and upper layers II-IV of the cerebral cortex. *The Journal of Comparative Neurology*, *479*(2), 168–180.

Ochs, S. M., Dorostkar, M. M., Aramuni, G., Schön, C., Filser, S., Pöschl, J., … Herms, J. (2015). Loss of neuronal GSK3β reduces dendritic spine stability and attenuates excitatory synaptic transmission via β-catenin. *Molecular Psychiatry*, *20*(4), 482–489.

Ogita, H., & Takai, Y. (2006). Activation of Rap1, Cdc42, and Rac by Nectin Adhesion System. In *Methods in enzymology* (Vol. 406, pp. 415–424).

Oh, S. W., Harris, J. A., Ng, L., Winslow, B., Cain, N., Mihalas, S., … Zeng, H. (2014). A mesoscale connectome of the mouse brain. *Nature*, *508*(7495), 207–214.

Okuda, T., Yu, L. M. Y., Cingolani, L. A., Kemler, R., & Goda, Y. (2007). beta-Catenin regulates excitatory postsynaptic strength at hippocampal synapses. *Proceedings of the National Academy of Sciences*, *104*(33), 13479–13484.

Ooshio, T., Irie, K., Morimoto, K., Fukuhara, A., Imai, T., & Takai, Y. (2004). Involvement of LMO7 in the association of two cell-cell adhesion molecules, nectin and E-cadherin, through afadin and alpha-actinin in epithelial cells. *The Journal of Biological Chemistry*, *279*(30), 31365–31373.

Osterhout, J. A., Josten, N., Yamada, J., Pan, F., Wu, S., Nguyen, P. L., … Huberman, A. D. (2011). Cadherin-6 mediates axon-target matching in a non-image-forming visual circuit. *Neuron*, *71*(4), 632–639.

Paxinos, G., & Franklin, K. (2013). *Paxinos and Franklin's the Mouse Brain in Stereotaxic Coordinates, Fourth Edition*. Academic Press.

Petersen, C. C. H., & Crochet, S. (2013). Synaptic Computation and Sensory Processing in Neocortical Layer 2/3. *Neuron*, *78*(1), 28–48.

Piscopo, D. M., Weible, A. P., Rothbart, M. K., Posner, M. I., & Niell, C. M. (2018). Changes in white matter in mice resulting from low-frequency brain stimulation. *Proceedings of the National Academy of Sciences of the United States of America*, *115*(27), E6339–E6346.

Poulin, J.-F., Tasic, B., Hjerling-Leffler, J., Trimarchi, J. M., & Awatramani, R. (2016). Disentangling neural cell diversity using single-cell transcriptomics. *Nature Neuroscience*, *19*(9), 1131–1141.

Prasad, S. ., Kojic, L. ., Li, P., Mitchell, D. ., Hachisuka, A., Sawada, J., … Cynader, M. . (2002). Gene expression patterns during enhanced periods of visual cortex plasticity. *Neuroscience*, *111*(1), 35–45.

Rikitake, Y., Mandai, K., & Takai, Y. (2012). The role of nectins in different types of cell-cell adhesion. *Journal of Cell Science*, *125*(16), 3713–3722.

Ritchie, M. E., Phipson, B., Wu, D., Hu, Y., Law, C. W., Shi, W., & Smyth, G. K. (2015). limma powers differential expression analyses for RNA-sequencing and microarray studies. *Nucleic Acids Research*, *43*(7), e47–e47.

Robinson, M. D., McCarthy, D. J., & Smyth, G. K. (2010). edgeR: a Bioconductor package for differential expression analysis of digital gene expression data. *Bioinformatics (Oxford, England)*, *26*(1), 139–140.

Ruff, C. A., Staak, N., Patodia, S., Kaswich, M., Rocha-Ferreira, E., Da Costa, C., … Raivich, G. (2012). Neuronal c-Jun is required for successful axonal regeneration, but the effects of phosphorylation of its N-terminus are moderate. *Journal of Neurochemistry*, *121*(4), 607–618.

Sakamoto, Y., Ogita, H., Hirota, T., Kawakatsu, T., Fukuyama, T., Yasumi, M., … Takai, Y. (2006). Interaction of integrin alpha(v)beta3 with nectin. Implication in cross-talk between cell-matrix and cell-cell junctions. *The Journal of Biological Chemistry*, *281*(28), 19631–19644.

Sanz, E., Yang, L., Su, T., Morris, D. R., McKnight, G. S., & Amieux, P. S. (2009). Cell-type-specific isolation of ribosome-associated mRNA from complex tissues. *Proceedings of the National Academy of Sciences of the United States of America*, *106*(33), 13939–13944.

Satoh-Horikawa, K., Nakanishi, H., Takahashi, K., Miyahara, M., Nishimura, M., Tachibana, K., … Takai, Y. (2000). Nectin-3, a new member of immunoglobulin-like cell adhesion molecules that shows homophilic and heterophilic cell-cell adhesion activities. *The Journal of Biological Chemistry*, *275*(14), 10291–10299.

Schuman, E. M., & Murase, S. (2003). Cadherins and synaptic plasticity: activity-dependent cyclin-dependent kinase 5 regulation of synaptic beta-catenin-cadherin interactions. *Philosophical Transactions of the Royal Society of London. Series B, Biological Sciences*, *358*(1432), 749–756.

Shapiro, E., Biezuner, T., & Linnarsson, S. (2013). Single-cell sequencing-based technologies will revolutionize whole-organism science. *Nature Reviews Genetics*, *14*(9), 618–630.

Shapiro, L., Love, J., & Colman, D. R. (2007). Adhesion Molecules in the Nervous System: Structural Insights into Function and Diversity. *Annual Review of Neuroscience*, *30*(1), 451–474.

Sharova, L. V, Sharov, A. A., Nedorezov, T., Piao, Y., Shaik, N., & Ko, M. S. H. (2009). Database for mRNA half-life of 19 977 genes obtained by DNA microarray analysis of pluripotent and differentiating mouse embryonic stem cells. *DNA Research : An International Journal for Rapid Publication of Reports on Genes and Genomes*, *16*(1), 45–58.

Shen, J., & Colonnese, M. T. (2016). Development of Activity in the Mouse Visual Cortex. *The Journal of Neuroscience : The Official Journal of the Society for Neuroscience*, *36*(48), 12259–12275.

Shen, K., & Cowan, C. W. (2010). Guidance molecules in synapse formation and plasticity. *Cold Spring Harbor Perspectives in Biology*, *2*(4), a001842.

Supek, F., Bošnjak, M., Škunca, N., & Šmuc, T. (2011). REVIGO Summarizes and Visualizes Long Lists of Gene Ontology Terms. *PLoS ONE*, *6*(7), e21800.

Tachibana, K., Nakanishi, H., Mandai, K., Ozaki, K., Ikeda, W., Yamamoto, Y., … Takai, Y. (2000). Two cell adhesion molecules, nectin and cadherin, interact through their cytoplasmic domain-associated proteins. *The Journal of Cell Biology*, *150*(5), 1161–1176.

Tai, C.-Y., Mysore, S. P., Chiu, C., & Schuman, E. M. (2007). Activity-Regulated N-Cadherin Endocytosis. *Neuron*, *54*(5), 771–785.

Takai, Y., & Nakanishi, H. (2003). Nectin and afadin: novel organizers of intercellular junctions. *Journal of Cell Science*, *116*(Pt 1), 17–27.

Tallafuss, A., Washbourne, P., & Postlethwait, J. (2014). Temporally and spatially restricted gene expression profiling. *Current Genomics*, *15*(4), 278–292.

Tien, N.-W., & Kerschensteiner, D. (2018). Homeostatic plasticity in neural development. *Neural Development*, *13*(1), 9.

Tolias, K. F., Duman, J. G., & Um, K. (2011). Control of synapse development and plasticity by Rho GTPase regulatory proteins. *Progress in Neurobiology*, *94*(2), 133–148.

Tomorsky, J., DeBlander, L., Kentros, C. G., Doe, C. Q., & Niell, C. M. (2017). TU-Tagging: A Method for Identifying Layer-Enriched Neuronal Genes in Developing Mouse Visual Cortex. *ENeuro*, *4*(5).

Tønnesen, J., & Nägerl, U. V. (2016). Dendritic Spines as Tunable Regulators of Synaptic Signals. *Frontiers in Psychiatry*, *7*, 101.

Toyoizumi, T., Kaneko, M., Stryker, M. P., & Miller, K. D. (2014). Modeling the dynamic interaction of Hebbian and homeostatic plasticity. *Neuron*, *84*(2), 497–510.

Trachtenberg, J. T., Trepel, C., & Stryker, M. P. (2000). Rapid extragranular plasticity in the absence of thalamocortical plasticity in the developing primary visual cortex. *Science (New York, N.Y.)*, *287*(5460), 2029–2032.

Tropea, D., Kreiman, G., Lyckman, A., Mukherjee, S., Yu, H., Horng, S., & Sur, M. (2006). Gene expression changes and molecular pathways mediating activity-dependent plasticity in visual cortex. *Nature Neuroscience*, *9*(5), 660–668.

van der Kooij, M. A., Fantin, M., Rejmak, E., Grosse, J., Zanoletti, O., Fournier, C., … Sandi, C. (2014). Role for MMP-9 in stress-induced downregulation of nectin-3 in hippocampal CA1 and associated behavioural alterations. *Nature Communications*, *5*, 4995.

Van Hooser, S. D. (2007). Similarity and Diversity in Visual Cortex: Is There a Unifying Theory of Cortical Computation? *The Neuroscientist*, *13*(6), 639–656.

Vandesompele, J., De Preter, K., Pattyn, F., Poppe, B., Van Roy, N., De Paepe, A., & Speleman, F. (2002). Accurate normalization of real-time quantitative RT-PCR data by geometric averaging of multiple internal control genes. *Genome Biology*, *3*(7), RESEARCH0034.

Ventura, A., Meissner, A., Dillon, C. P., McManus, M., Sharp, P. A., Van Parijs, L., … Jacks, T. (2004). Cre-lox-regulated conditional RNA interference from transgenes. *Proceedings of the National Academy of Sciences of the United States of America*, *101*(28), 10380–10385.

Vidal, G. S., Djurisic, M., Brown, K., Sapp, R. W., & Shatz, C. J. (2016). Cell-Autonomous Regulation of Dendritic Spine Density by PirB. *ENeuro*, *3*(5).

Wang, X.-D., Su, Y.-A., Wagner, K. V, Avrabos, C., Scharf, S. H., Hartmann, J., … Schmidt, M. V. (2013). Nectin-3 links CRHR1 signaling to stress-induced memory deficits and spine loss. *Nature Neuroscience*, *16*(6), 706–713.

Wang, X.-X., Li, J.-T., Xie, X.-M., Gu, Y., Si, T.-M., Schmidt, M. V, & Wang, X.-D. (2017). Nectin-3 modulates the structural plasticity of dentate granule cells and long-term memory. *Translational Psychiatry*, *7*(9), e1228.

Wang, Z., Gerstein, M., & Snyder, M. (2009). RNA-Seq: a revolutionary tool for transcriptomics. *Nature Reviews. Genetics*, *10*(1), 57–63.

Wehr, M., Hostick, U., Kyweriga, M., Tan, A., Weible, A. P., Wu, H., … Kentros, C. (2009). Transgenic silencing of neurons in the mammalian brain by expression of the allatostatin receptor (AlstR). *Journal of Neurophysiology*, *102*(4), 2554–2562.

Williams, M. E., Wilke, S. A., Daggett, A., Davis, E., Otto, S., Ravi, D., … Ghosh, A. (2011). Cadherin-9 regulates synapse-specific differentiation in the developing hippocampus. *Neuron*, *71*(4), 640–655.

Wong-Riley, M. T. T. (1989). Cytochrome oxidase: an endogenous metabolic marker for neuronal activity. *Trends in Neurosciences*, *12*(3), 94–101.

Wu, T. D., & Nacu, S. (2010). Fast and SNP-tolerant detection of complex variants and splicing in short reads. *Bioinformatics (Oxford, England)*, *26*(7), 873–881.

Yang, L., Pan, Z., Zhou, L., Lin, S., & Wu, K. (2009). Continuously changed genes during postnatal periods in rat visual cortex. *Neuroscience Letters*, *462*(2), 162–165.

Yokota, Y., Ring, C., Cheung, R., Pevny, L., & Anton, E. S. (2007). Nap1-Regulated Neuronal Cytoskeletal Dynamics Is Essential for the Final Differentiation of Neurons in Cerebral Cortex. *Neuron*, *54*(3), 429–445.

Yoshii, A., Murata, Y., Kim, J., Zhang, C., Shokat, K. M., & Constantine-Paton, M. (2011). TrkB and protein kinase Mζ regulate synaptic localization of PSD-95 in developing cortex. *The Journal of Neuroscience : The Official Journal of the Society for Neuroscience*, *31*(33), 11894–11904.

Zhang, Y., Chen, K., Sloan, S. A., Bennett, M. L., Scholze, A. R., O'Keeffe, S., … Wu, J. Q. (2014). An RNA-Sequencing Transcriptome and Splicing D1. Zhang, Y. et al. An RNA-Sequencing Transcriptome and Splicing Database of Glia, Neurons, and Vascular Cells of the Cerebral Cortex. J. Neurosci. 34, 11929–47 (2014).atabase of Glia, Neurons, and Vascular Ce. *The Journal of Neuroscience : The Official Journal of the Society for Neuroscience*, *34*(36), 11929–11947.

Ziv, N. E., & Smith, S. J. (1996). Evidence for a role of dendritic filopodia in synaptogenesis and spine formation. *Neuron*, *17*(1), 91–102.

Zuo, Y., Lin, A., Chang, P., & Gan, W.-B. (2005). Development of long-term dendritic spine stability in diverse regions of cerebral cortex. *Neuron*, *46*(2), 181–189.